Modeling Surfactant-Tuned Separation Processes for Carbon Nanotubes (CNT)

Submitted in partial fulfillment of the requirements for the

degree of

Doctor of Philosophy in

Department of Chemical Engineering

Yanxin Li

B.S., Chemical Engineering, Illinois Institute of Technology

Carnegie Mellon University
Pittsburgh, PA

August, 2021

Acknowledgments

First and foremost, I would like to thank my advisor Shelley Anna. Shelley has supported me through many difficult times when the research process seems to be stagnant. She trained and helped me pursue novel scientific ideas on my own throughout the five years of my Ph.D. Her encouragement during the COVID time gave me the confidence to transfer to computational-based work from entirely experimental. Her guidance is indispensable for this thesis work.

I would like to thank my thesis committee members, Professors Michael Domach, Aditya Khair, and Alan McGaughey. They have provided critical feedbacks for me to evaluate the work in this thesis from a more comprehensive perspective.

Dr. Jeffrey Fagan from NIST has provided the carbon nanotubes samples for the initial experiments. His in-depth knowledge of surfactant-tuned carbon nanotubes separation has helped me have an early understanding of the advantages and limitations of this technique. Dr. Christopher Nelson performed the experiments from which this model is developed. His work is greatly appreciated.

Members of the CMU chemical engineering complex fluids lab have helped me build up and troubleshoot the experimental setup. Drs. Junchi Ma and Blake Bleier shared their knowledge of the millifluidic devices, which makes fixing the bugs in my experimental design a much more efficient process. The colleagues in the complex labs have kept me company throughout all the emotional ups and downs and make the Ph.D. life much more enjoyable.

Lastly, I would like to thank my family and friends. My parents and grandparents had provided the strongest support and the clearest opinion when I encountered difficulties while progressing through research and life. My husband, Michael Ayers, has always been able to calm

me down and get a laugh out of me when I was stressed by all kinds of situations. Thank you to my friends for the trips for cultural performances and natural exploration. They have made the experience for the past five years much more memorable and enjoyable.

This work was partially supported by National Science Foundation CBET Grant # 1511016, Lawrence Livermore National Laboratory Sub-Contract #B621703, the Paul and James Wang-Sercomm Presidential Graduate Fellowship, the John E. Swearingen, CIT 1939, H 1981, Fellowship, the Neil and Jo Bushnell Fellowship, and the Carnegie Mellon University Provost Office GuSH Funding grant.

Abstract

Single wall carbon nanotubes (CNTs) were first discovered in the early 1990s. This new form of carbon material possesses remarkable thermal, mechanical, and electrical properties, positioning it as a promising candidate for a wide range of applications, including field-effect transistors, display technologies, hydrogen storage, and so on. The market value of CNTs was valued at $2.6 billion in 2019 and is expected to grow to $5.8 billion by 2027. These highly-anticipated qualities have made CNTs the focus of significant research efforts since their initial discovery.

The application of CNTs is far from realizing its full potential and is largely not commercially available in most cases. Methods for synthesizing nanotubes typically generate a carbonaceous soot-like powder containing a minority population of numerous different CNT species. These CNT species are uniquely identified by their diameter and chiral vector (a_1, a_2) and each species has different functionalities. To date, neither synthesis methods nor separation processes can produce a CNT sample containing only a single species. Using mixtures of distinct CNTs can significantly compromise their material properties and reduce their advantage compared with other newly-developed nanomaterials.

Isolating specific carbon nanotube species, however, is not trivial. Current separation methods are expensive to implement, require specialized equipment, offer low throughput, or present challenges to cost-effective scale-up. The lack of scalable technology for species-based CNT separation has prevented the widespread application of carbon nanotubes. A simpler and cheaper separation technique is thus called for to facilitate large-scale processing.

Aqueous two-phase systems (ATPSs), formed by mixing two polymers or a polymer and a salt, have been used as a separation and purification tool for more than 50 years. With nearly 80% water content, ATPS can achieve separations with minimal damage to particles with delicate structures such as CNTs. Because of its potential for continuous operation and process integration, ATPS is particularly promising to meet the downstream processing needs created by the fast-growing production rate of carbon nanotubes. The partitioning behavior involved, however, is complex and difficult to predict due to the large number of factors that can alter the process. The application of ATPS is therefore limited without the technology to easily optimize the desired partitioning behavior across a very large parameter space. Here, we develop and analyze a simplified model to systematically investigate the impact of various factors on the partitioning behavior of carbon nanotubes in an ATPS process. The model is based on high-resolution data previously obtained from droplet-based millifluidic experiments characterizing the partitioning behavior of CNT in PEG-DEX two-phase systems with added surfactant as the primary tuning factor. Using the model we developed, we have identified several dimensionless parameters that capture the salient features of the partitioning behavior of different CNT species, making this model an efficient and flexible tool for rapidly exploring separations over a large parameter space. In this thesis, we use the model to simulate one-stage and multi-stage aqueous two-phase separations between two CNT species. Yield and purity are reported as the separation performance metrics for both species after every stage. A threshold of 0.8 is proposed as the minimum requirement for both yield and purity to mimic the industrial operation process. For some types of CNT samples, only one-stage separation is needed to reach the threshold. Other types of samples require multi-stage processes. Under specific conditions, one CNT species can be concentrated 5000 times with a two-stage process, validating the purifying power of this separation technique.

Three key parameters in the model are varied to simulate a broader representation of different CNT species. One-stage separation results are reported for two CNT species under different parameter variations. Parameter variations that can make the partition coefficient curve of one CNT species more distinguishable than other species allow more experimental conditions to be used to reach the same separation performance.

Contents

List of Tables

List of Figures

Chapter 1: Introduction

1.1 Motivation

Single wall carbon nanotubes (CNT) are cylindrical carbon allotropes whose impressive thermal, mechanical, and electrical properties have made them the focus of significant research efforts since their initial discovery[1,2]. These unique, nearly one-dimensional materials exhibit a variety of interesting properties, such as ballistic transport of electrons and ultra-high thermal conductivity, with numerous potential applications[2] in advanced composite materials[3], field-effect transistors[4], display technology[5], and hydrogen storage[6]. Synthesis methods for nanotubes generate a carbonaceous soot-like hydrophobic powder containing a minority population of CNT[7]. The nanotubes often exist as dozens of different isomers or 'species', each with distinct electronic, thermal, and mechanical properties[8]. These nanotube species are uniquely identified by their diameter and chiral vector (n,m), which determines their properties, and whether they are semiconducting or metallic. From a given CNT sample, it is desired to separate and retain all of the minority species, since each has unique properties for potential applications.

Isolating specific carbon nanotube species, however, is a significant challenge[9]. Current separation methods primarily rely on high-speed ultracentrifugation in density gradient media[10–17] or chromatography-based methods[9,18–22], although other techniques have been demonstrated[23]. Generally, these approaches are expensive to implement, require specialized equipment, offer low throughput, or present challenges to cost-effective scale-up. The lack of scalable technology for species-based CNT separation has prevented the widespread application of carbon nanotubes. A simpler and cheaper separation technique is thus called for to facilitate large-scale processing.

Recent works demonstrate that aqueous two-phase systems[24,25] (ATPS), especially the system made from polyethylene glycol (PEG) and dextran (DEX), can effectively partition carbon nanotubes based on their diameter and degree of metallicity[22,26–33]. It has been shown that by varying temperature, solution pH, salt concentration, and surfactant concentration in ATPS, elective partitioning of carbon nanotubes can be achieved[27–29]. Specifically, surfactant-tuned CNT separation has received widespread attention because of the relatively low cost of the material, the ease of implementation, and the significant changes in partitioning behavior that a small amount of surfactants can induce. The usage of ATPS for CNT separations, however, is different from its traditional usage for separations of biomolecules. All CNT species are valuable and have unique functionality. Therefore, there is interest in purifying and collecting every species from a CNT raw sample. In contrast, separations of biomolecules, especially protein products, only value one single target. This singularity in product selection allows the rest of materials to be treated as waste, simplifying the search for optimal operating conditions and shortening the separation procedure.

Surfactant-tuned aqueous two-phase extraction is a highly scalable technique amenable to both continuous flow and batch processing. However, very little data exists currently regarding how the distribution of carbon nanotube species in an ATPS is affected by the composition of the ATPS. A rational design of large-scale separations requires information on how changes in the composition of the ATPS affect the partition coefficient for particular CNT species. Macroscale, bench-top techniques for measuring the distribution of analytes in an ATPS are poorly suited to exploring the vast operating parameter space controlling the partitioning behavior. This is primarily due to the low speed of testing, labor-intensive handling and detection procedures, and the high cost and scarcity of materials needed to perform these experiments. The lack of data relating the partition coefficient to experimental parameters continues to present a major roadblock

to the large-scale optimization of aqueous two-phase separations for carbon nanotubes and has restricted their widespread application. Compared to experimental approaches, computational approaches are more robust and can efficiently scan through the vast parameter space, allow exploration of model behaviors, and enable designs of more streamlined experiments. In this thesis, we develop an idealized model to map out the partition coefficient of carbon nanotubes as a function of composition and then use that model to develop a quantitative approach to designing a separation process.

1.2 Thesis Outline

In chapter 2, the background on ATPS extraction and the idealized model is discussed. Experimental data generated previously using a droplet-based approach in the Anna group are briefly explained. The salient features of these experimental data are summarized into four categories that become the main criteria for the model. The error function is chosen as the mathematical base function for the model. Three parameters *a*, *b*, and *c* are incorporated into the error function to add flexibility so that a wide variety of CNT species can be simulated, including those that have not been tested yet. By adjusting the values of *a*, *b*, and *c* combinations, the model successfully generates a series of figures that capture the salient features of the experimental data.

In chapter 3, the idealized model is used to simulate the separation process of two distinct CNT species. The model is used to calculate partition coefficients as a function of surfactant concentration, and subsequently, the yield and purity of the separation are computed. Yield and purity are conventional separation metrics that allow us to establish an approach for directly comparing the separation performance across all operating conditions as well as to other separation methods. Yield and purity are revealed to depend on two additional dimensionless parameters, the volume ratio, *R*, and the initial mass ratio of the two species, *m*. These two parameters are varied systematically along with the surfactant concentration when we investigate the influence of experimental conditions on the separation results. We select 80% yield and 80% purity as the minimum threshold for a successful separation to demonstrate a practical approach to separation.

In chapter 4, a multi-stage separation of two CNT species is investigated. When a single-stage process cannot meet the separation goal, additional separation steps are required. Because no experimental conditions can produce the yield and purity desired in the first stage, we first search for the highest-performing conditions in the first stage. The outputs from the first stage are

transferred to the second stage as inputs. Four multi-stage-specific guidelines are added to complement the use of yield and purity. A comparison of yield and purity is no longer sufficient to make operational decisions. After considering the real-life limitations imposed by the polymer and surfactant concentrations carried across different aqueous two-phase systems, the computed optimal experimental conditions are re-evaluated and amended. Yield and purity values are reported for the final separated product of each CNT species.

In chapter 5, three parameters *a*, *b*, and *c* in the model are varied to examine the partitioning behavior as a function of the sensitivity of the CNT species to surfactant concentration. The parameters are varied to allow for comparison with the two baseline species examined in chapters 3 and 4. A dimensionless analysis is used to examine the role of parameter *b*. The ranges of possible yield and purity values are reported and compared for each set of parameters. The surfactant concentration range that produces threshold-complying separation results is plotted as a function of volume ratio *R* and initial mass ratio *m*. Overall, the same approach used in chapter 3 is used to examine each set of CNT parameters.

In chapter 6, conclusions from each of the three projects are outlined. Potential future work is discussed, focusing on multi-stage separations of multiple CNT species.

Chapter 2: Background

2.1 Introduction

So far, experiment-based methods are the standards for studies of carbon nanotubes separation in aqueous two-phase systems[29,32,34–36]. Data reported in the literature are often at a few selected experimental conditions, while the available parameter space is vast[26,28,31,33]. To increase the efficiency of experiments and bridge the gap between what can be done and what needs to be done, the Anna group introduced a millifluidic droplet-based approach to study CNT separation. By using this droplet-based approach, the data resolution is increased by a factor of ten compared to traditional benchtop approaches. As a result, we have the capability to evaluate aqueous two-phase separations as a direct function of any compositional variables, including the surfactant concentration. For CNT separation studies, it is common to see absorbance data reported at a handful of surfactant concentrations[16,19,27]. However, absorbance is not a universal measurement of separation performance, and it has limited use in terms of assisting the design or optimization of a separation process. To systematically investigate the separation result, we choose to plot the partition coefficient as a function of surfactant concentration. Partition coefficients describe the current distribution of CNT species within an aqueous two-phase system. Partition coefficients can also be used to calculate yield and purity, which are conventional metrics used to evaluate separation performance. In order to find the surfactant concentration associated with the optimal separation result, a massive number of experimental conditions would need to be tested. Even with the more efficient millifluidic droplet-based platform, it still takes a whole day to generate about 80 data points. Therefore, it is necessary to adopt a more effective approach that can thoroughly scan all possible conditions and quickly compare the results. This is when the computational power is fully appreciated. Using models built to simulate the CNT separation

process, we can systematically and rapidly perform experiments at hundreds of thousands of conditions within seconds. Moreover, models allow us to independently vary any parameters and study their effect on the separation, which is difficult to achieve in the experimental setting when numerous physico-chemical parameters are involved.

2.2 Extraction using aqueous two-phase systems

Liquid-liquid extraction is a scalable, tunable technique for partitioning analytes between two immiscible fluid phases that share an interface. The technique was first used for separation purposes with organic-aqueous two-phase systems. For example, the distribution of compounds in an octanol-water system has been used to develop active pharmaceutical ingredients to simulate how compounds distribute throughout the body. In environmental science, octanol-water partitioning is used to predict how compounds will distribute in soil and ground water[37]. When an analyte is introduced into a liquid-liquid system, a net transfer or partition of the analyte from one liquid phase to another liquid phase occurs. The direction of this transfer is determined by the chemical potential. Once the transfer is complete or reaches equilibrium, one liquid phase becomes enriched with the analyte while the other phase is depleted from it, and the overall free energy of the system is lower than that in the initial state when the analyte is just introduced to the system[24,38]. Different compounds, polar or non-polar, partition into different phases, which provides the foundation for separating these compounds.

Liquid-liquid extraction can also be accomplished using two aqueous phases. When two structurally dissimilar polymers or a polymer and a salt are combined in water above a threshold concentration, the mixture will spontaneously decompose into two immiscible aqueous phases[24,38]. These two phases are physically connected but have distinct compartments separated by a clear interface. In aqueous two-phase systems, each phase is rich in one of the polymers or salt, while the other phase is rich in the other polymer or salt. Due to gravity, the heavier polymer/salt primarily occupies the bottom phase, while the lighter component occupies the top phase. For example, in a PEG and dextran DEX two-phase system, the PEG-rich phase is the top compartment while the DEX-rich phase is the bottom compartment. Both phases exhibit very high water content,

80-90 wt%, and very low interfacial tension, 1-1000 μN/m[39–41]. The predominantly aqueous environment and the low interfacial tension provide a suitable environment to prevent denaturing of macromolecules. Therefore, ATPS is particularly well suited to separate fragile water-soluble molecules. The partitioning preference to one phase in an ATPS is determined by the chemical potential of that molecule. The chemical potential can be described as the net effects of hydrophobic, electrostatic, steric, conformational, van der Waals attraction, and other molecular interactions between the analyte and the components of each phase[24,42]. The distribution of a molecule between the two phases reflects the surface properties of that compound since partitioning behavior is driven by surface properties[24] rather than density or hydrodynamic drag. The distribution of a dispersed species between two immiscible liquid phases, expressed as the partition coefficient, is a critical parameter for designing and evaluating the performance of laboratory and industrial-scale liquid-liquid separation processes. The partition coefficient of a molecule in an aqueous two-phase extraction is defined as the concentration ratio between the two phases,

$$K = \frac{c_t}{c_b} \tag{2.1}$$

where c is the concentration of the partitioning species, and the subscripts t and b refer to the 'top' and 'bottom' phases of an ATPS. Numerous factors can influence the partition coefficient in an aqueous two-phase extraction, such as the type, molecular weight, and composition of the phase-forming polymers or salts, the ionic composition, solution pH, hydrophobic affinity, and the size and properties of the molecules[24,43–47].

The mechanism of how surfactants control the partitioning of CNT is complex and not fully understood. However, it is generally believed that different surfactants competitively adsorb to and assemble on the intrinsically hydrophobic nanotube surface in a chirality-specific way[29,48–50], and then alter the hydrophobicity of carbon nanotubes that eventually drives different species into different phases. Changes in temperature, surfactant type, and salt concentration modify surfactant-surfactant and surfactant-nanotube interactions, for example, by screening interactions between the charged surfactant head groups[51]. For multi-surfactant systems in an aqueous two-phase extraction, it is found that nanotubes wrapped in SDS are slightly less hydrophilic than those wrapped in sodium deoxycholate[29] (DOC). The result is that the SDS-wrapped CNT partitions into the slightly less hydrophilic PEG-rich phase, while the DOC-wrapped nanotubes partition into the slightly more hydrophilic DEX-rich phase. The wrapping or binding affinity between different surfactants and different nanotube species is diameter and chirality specific. This characteristic lays the foundation for species-based carbon nanotubes separation in ATPS using surfactant concentration as the controlling parameter.

Within the Anna group, a droplet-based experimental approach was developed and applied to study CNT separations in aqueous two-phase systems. This new approach significantly improves the experimental capability to identify and optimize the critical parameters for aqueous two-phase extraction of carbon nanotubes while reducing sample consumption by up to two orders of magnitude compared to traditional procedures. However, even with this more powerful tool, very few experimental conditions have been tested due to difficulties obtaining analytical-grade CNT samples containing only a handful of species.

2.3 The separation results from droplet-based experiments

Using a millifluidic platform developed by Chris Nelson, an alumnus of the Anna group, we can perform controlled experiments in microliter-volume water droplets[52]. Less than one milliliter CNT samples are used for one experiment, and 60-80 data points are generated per experiment. All droplets generated by the platform are uniform in size, shape, and composition, ensuring homogeneity of the experimental conditions. The droplets are identical to each other except that the surfactant concentration varies from drop to drop. The surfactant concentrations are varied from drop to drop with an increment of around 0.02 wt%. The surfactant concentration is the independent variable in the experiment. The partition coefficient is the dependent variable, and it is measured as optical absorbance and converted to concentration using the Beer-Lambert equation. Combining these two variables, we obtain the partition coefficient curve in Figure 2.1.

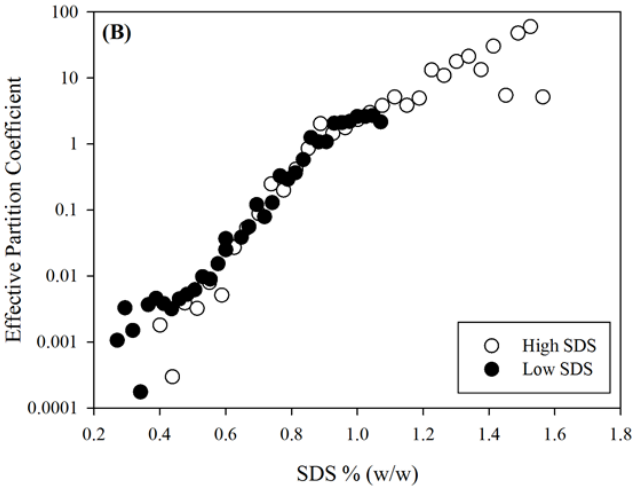

Figure 2. 1.A partition coefficient curve with SDS surfactant concentration plotted on the x-axis for a semiconducting CNT species. (Reproduced with permission from Figure 5.7[52]. Copyright Christopher Nelson (2016).

Using the droplet-based approach, we successfully generate partition coefficient plots at much higher resolution. Traditional benchtop approaches are limited to study five to ten data points due to the intensive labor and time required to create aqueous two-phase systems with various compositions[53,54]. Thanks to the high-resolution data, we can relate the partition coefficient to the

surfactant concentration as a continuous function other than a few sparsely located dots. This feature is the foundation of our modeling work. In Figure 2.1, the partition coefficient is plotted as a function of surfactant SDS concentration. Two data sets are presented, one for surfactant concentrations below 1 wt% and another for surfactant concentrations expanding up to 1.6 wt%. Partition coefficient k is defined as the concentration ratio between the top and bottom phases. Therefore, it should have a value greater than 0. When k is larger than 1, the top phase contains more CNT. When *K* is between 0 and 1, the bottom phase has more CNT. Because of this inherent symmetry around *K*=1, the partition coefficient curve is usually plotted on a log scale. As the surfactant concentration increases from 0.3 to 1.6 wt%, the partition coefficient increases by almost five orders of magnitude, from 0.001 to 100. This amount of change in partition coefficient indicates that the majority of CNT species are moved from the bottom to the top phase. This result is consistent with published data[26,28,30], where an almost complete transition from one phase to another is observed over a similar surfactant concentration range. It is worth noting that the semiconducting CNT sample used to generate Figure 2.1 is a mixture of various semiconducting species. Therefore, the partition coefficient curve shows the compounded effect of the partitioning behavior of all species in that sample. For individual CNT species in its pure form, the partition coefficient curve will increase more sharply and rapidly as a function of surfactant concentration compared with Figure 2.1

2.4 The design concepts of building a model that simulates the CNT separation process

The first step for this project is to create a model that captures the salient features of the partition coefficient curves. The model serves as a transcriber between surfactant concentration and separation performance, which produces an output immediately upon receiving an input. The model needs to be flexible enough to allow generalization to represent a wide variety of CNT species, including those that have not been tested yet. The model should have the ability to predict separation results and present them in a helpful format that can serve as design guidelines for practitioners. The goal of this project is not to precisely fit the experimental data. Instead, the goal is to build a model that can simulate the CNT separation process and reveal general trends on the various impact created by different types of experimental parameters. Such information is essential to assist experimentalists in locating the optimal surfactant concentration for their unique design purpose. However, with limited availability of experimental information in the literature, we turn to computational modeling to assist in better understanding the process.

2.5 Salient features of the partition coefficient curves

Before incorporating salient features of the experimental results into the model, we first need to summarize what they are. Thus, we refer back to the droplet-based experimental data. Besides the results in Figure 2.1, three more comparison experiments were carried out using the droplet-based approach by Chris Nelson[52] which are reported in Figure 2.2.

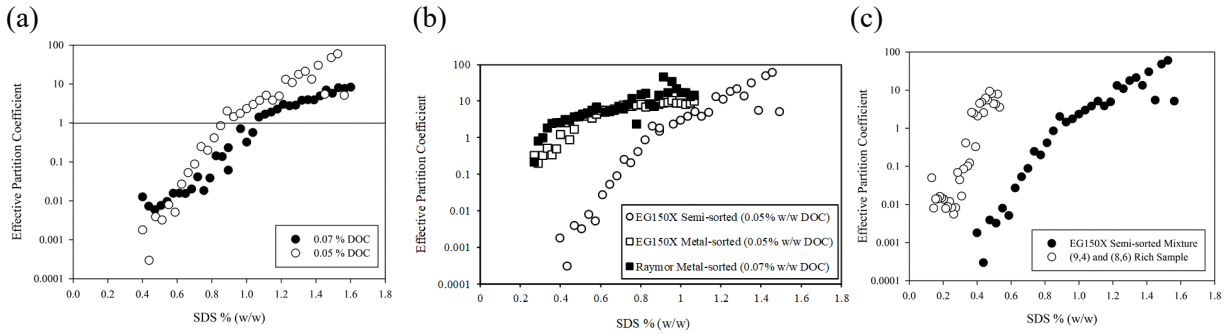

Figure 2. 2. Partition coefficient is plotted as a function of surfactant concentration under three different types of experimental parameters. (a) The concentration of a secondary surfactant is varied. (b) The type of carbon nanotubes samples are varied between semi-conducting and metallic CNT. (c) The purity of the carbon nanotube samples are varied between purified and raw samples. (a) and (c) are reproduced with permission[52]. Copyright Christopher Nelson (2016).

After examining the general trends in Figures 2.1 and 2.2, we conclude that four shared features of all partition coefficient curves should be built into the model.

1) The trajectory of all partition coefficient curves looks like the letter S centered around the crossover surfactant concentration on K=1 line. This observation is consistent with the literature results and the physics behind aqueous two-phase extractions. In literature, CNT species are always tuned from the bottom to the top phase, which an S-shape curve can imitate. The K values transit from 0−1 to above 1 when CNT species are tuned from the bottom to the top phase. Therefore, the S-shape curve should have symmetry around a point on the K=1 line. From the thermodynamics of partitioning behavior in an aqueous two-phase system, we know the partition coefficient curves should plateau at the two extremes of the surfactant concentration spectrum when the separation process reaches equilibrium.

2) The S-shape curve should have different slopes. The slope difference between the semiconducting and metallic CNT species is prominent. The slope of a partition coefficient curve is related to the sensitivity of a particular CNT species to a specific type of surfactant[55–58]. A higher sensitivity leads to a steeper slope. Different sensitivity shown by different CNT species to the same surfactant is one of the key elements for designing a successful separation process.
3) The third feature is the presence of different crossover points. The crossover point is the intercept of the partition coefficient curve and the K=1 reference line. This point reveals the surfactant concentration at which a CNT species is tuned from one phase to the other. Different species usually have different crossover points[59], which can be considered as unique barcodes. The essence of separating two CNT species using the surfactants-tuned aqueous two-phase extraction is to find out the crossover point of each species and operate with surfactant concentrations in between the crossover points. In this way, the CNT species with the lower crossover point stays in the bottom phase at the operating concentration, while the species with the higher crossover point is tuned into the top phase.
4) The maximum and minimum partition coefficients obtained at the two extremes of the surfactant concentration spectrum are different. In other words, the partition coefficients plateau at different magnitudes after reaching thermodynamic equilibrium at very low and very high surfactant concentrations. The magnitude of max and min partition coefficients varies for different species and different phases. This phenomenon could be the result of limitations in droplet-based experiments. However, adding the feature to alter the max and min values allows more flexibility in the model for broader species representation.

2.6 Error function is selected as the base function of the model

The error function is selected as the base function of our model, because the error function displays all four salient features discussed in the previous section. It is worth noting that many mathematical functions can satisfy these four criteria, and the error function is by no means the absolute best option for the separation processes considered. S-shaped functions or sigmoidal functions that have been considered include the logistic function, the hyperbolic tangent, the Hill–Langmuir equation, the Gompertz function, and the error function. The logistic function and the Hill-Langmuir equation have inflection points at half of the maximum y-axis values. In other words, the S-shape curve can be separated to one part above the half-maximum and another part below the half-maximum. Based on the experimental results, the inflection point should occur at K=1. Above K=1, the CNT species are found predominantly in the top phase. Below K=1 ($0< K <1$), the CNT species are found predominantly in the bottom phase. Therefore, the boundary of the top- and bottom-phase partitioning behavior should be aligned with y=1, not the half-maximum for the S-shape curve. Thus the logistic function and the Hill-Langmuir equation are less desired. The Gompertz function approaches the minimum and maximum asymptotes at different rates. We assume the partitioning of CNTs has the same rate in the top and the bottom phases, which makes the Gompertz function less desirable. The error function and the hyperbolic tangent function have similar behavior after being scaled, and both can serve as the base function for our model. In order to select a model function that more accurately captures the physical characteristics, we would need much more extensive experimental data with which to validate and compare. Thus, we emphasize that the selection of the error function here is primarily intended to qualitatively capture the main features of the known data and to provide a simplified avenue for exploring the role of those salient features on the separation process. The approach we outline in this thesis can be

applied with other choices of functions, including with empirical, interpolated data fit directly to experiments. This leaves open the possibility to replace the base function in future research as more experimental data becomes available and the functional dependencies on physico-chemical parameters becomes more clear.

2.7 Three important parameters and their values in the error function

Using a general error function to interpret the relation between partition coefficients and surfactant concentrations, we have the following formula,

$$\log_{10} K = erf(x) \tag{2.2}$$

where K is the partition coefficient, and x is the surfactant concentration. However, this basic form of the error function has a fixed symmetry around the origin and a fixed max/min value at +/-1. Thus, we need to add more parameters to this form so that all the four features discussed in Section 2.4 can be varied freely. In order to add more flexibility to the error function, we add parameters a, b, and c,

$$\log_{10} K = c * erf(\frac{x-b}{a}) \tag{2.3}$$

With these three parameters, we can adjust the slope, the crossover point, and the max/min values of the partition coefficient curves generated with an error function, which allows better representation or approximation of the experimental data. Parameter a controls the steepness of the slope. A larger a value creates a more gradual curve, while a smaller a value generates a steeper curve. Based on the experimental results, different types of CNT species, such as semiconducting and metallic, have distinct slopes. Highly enriched and mixed samples also have different slopes. Therefore, the parameter a can be related to the types and purity of CNT[60,61]. Parameter b represents the surfactant concentration at the crossover point on $K = 1$. Varying b moves the partition curve horizontally along the K=1 line. It has been reported that the crossover surfactant concentration varies for CNT species with different diameters and chiral vectors[59]. Thus, the parameter b captures the diameter, configurational, and chiral differences for various CNT species[62,63]. Parameter c determines the magnitude of the max/min values, which describes how

concentrated a species can become in one phase. When *c* increases, the maximum rises higher while the minimum falls lower. Diameter, chirality, electrical properties, and hydrophobicity can all determine the affinity of one CNT species to a particular phase[24,64]. Therefore, the parameter *c* represents several categories of differences among CNT species. It is critical to point out that parameters *a*, *b*, and *c* represent intrinsic properties, which are fixed for a given CNT species, selection of the phase-forming polymers, and the types of surfactant used to do the separation. In other words, once a system is selected, the shape of a partition coefficient curve is determined. We assume such knowledge about the partition coefficient curve is known prior to a separation procedure for all investigated systems.

To select a set of appropriate *a*, *b*, *c* values, we use Figures 2.1 and 2.2 as the blueprint. After adjusting the parameters to make the model-generated curves look closer to the experimental data, we decide to use the *a*, *b*, *c* combinations tabulated in Table 2.1 to model Figures 2.1 and 2.2. The model partition coefficient curves are plotted in Figure 2.3.

Figure 2.1			Figure 2.2 (a)			Figure 2.2 (b)			Figure 2.2 (c)		
a	*b*	*c*	low secondary surfactant			semiconducting sample			highly purified semiconducting sample		
			a	*b*	*c*	*a*	*b*	*c*	*a*	*b*	*c*
0.4	0.8	2	0.4	0.8	2	0.4	0.8	2	0.05	0.4	1
			high secondary surfactant			metallic sample			raw semiconducting sample		
			a	*b*	*c*	*a*	*b*	*c*	*a*	*b*	*c*
			0.6	1.0	2	0.1	0.3	1	0.4	0.8	2

Table 2. 1. Values of parameters *a*, *b*, and *c* used to generate partition coefficient curves using the error-function-based model for different experimental conditions.

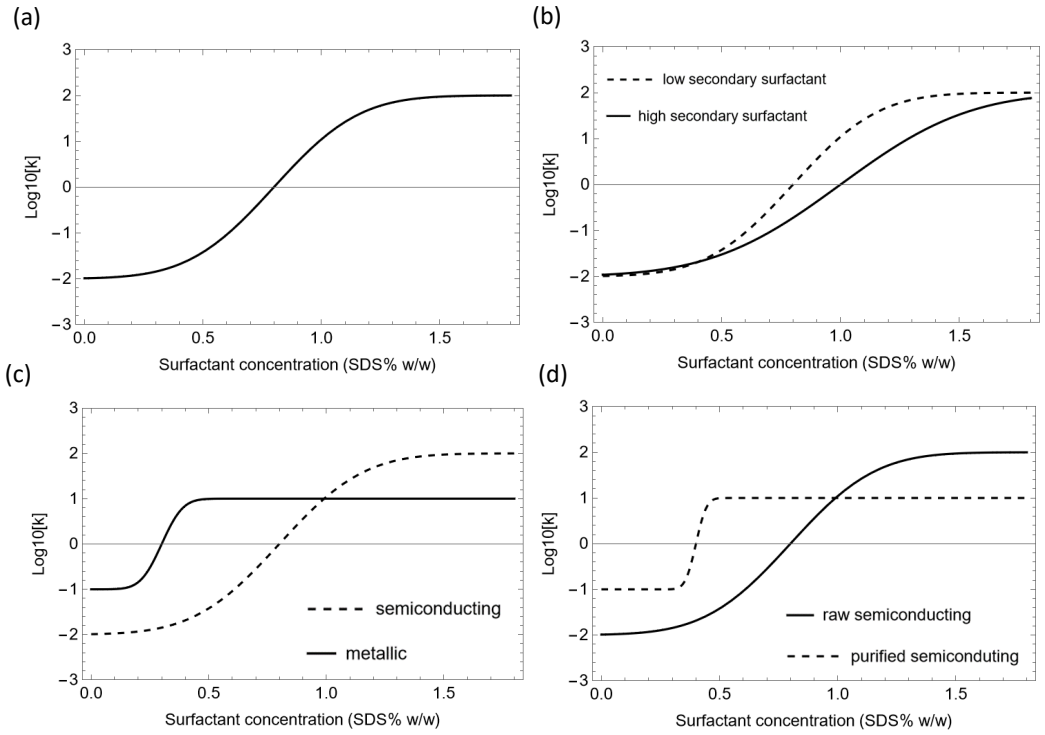

Figure 2. 3. Model capturing behavior shown in the experimental data of Figures 2.1 and 2.2, using error function as the base function. (a) Estimating the values of *a*, *b*, and *c* to simulate the curve in Figure 2.1. (b) Varying *a* and *b* to reflect the use of a different surfactant. (c) Varying *a*, *b*, and *c* to reflect difference observed in semiconducting and metallic samples. (d) Varying *a*, *b*, and *c* to reflect observed differences between polydisperse and pure samples.

Using Figure 2.3, we demonstrate the ability of the model to simulate partition coefficient curves that represent a wide range of CNT species and experimental conditions. Later in Chapter 5, we will systematically investigate how each parameter influences the separation results.

Chapter 3: Building a model to simulate one-stage separation of two CNT species

3.1 Introduction

As-synthesized CNT samples often contain dozens of species which requires multiple stages of separation. This complex process involves a large number of parameters. To quickly assess the model's ability to predict separation performance without spending too much time deciding how to set up different initial parameters, we start the analysis with a one-stage separation process between two species only. To further simplify this problem, we decide only to vary parameter *b* in the model while keeping parameters *a* and *c* the same and constant for these two species. Parameter *b* indicates the crossover point, the surfactant concentration at which a CNT species is tuned from one phase to another. Locating a crossover point for a specific species is key to a species-based separation[30,59]. Surfactant concentration is also believed to induce the most drastic effect on CNT partitioning behavior, compared to other experimental factors, such as polymers concentration[29,31,65]. Therefore, in our model, parameter *b* will be the focus of our investigation.

3.2 The simplified scenario of CNT separation

The first step in approximating a separation process using the model is to plot the partition coefficient curves for each species. This allows us to see how each individual species reacts differently to surfactant concentration. This difference will be the basis of selecting the proper experimental conditions to achieve the maximum separation between any two CNT species.

(a)

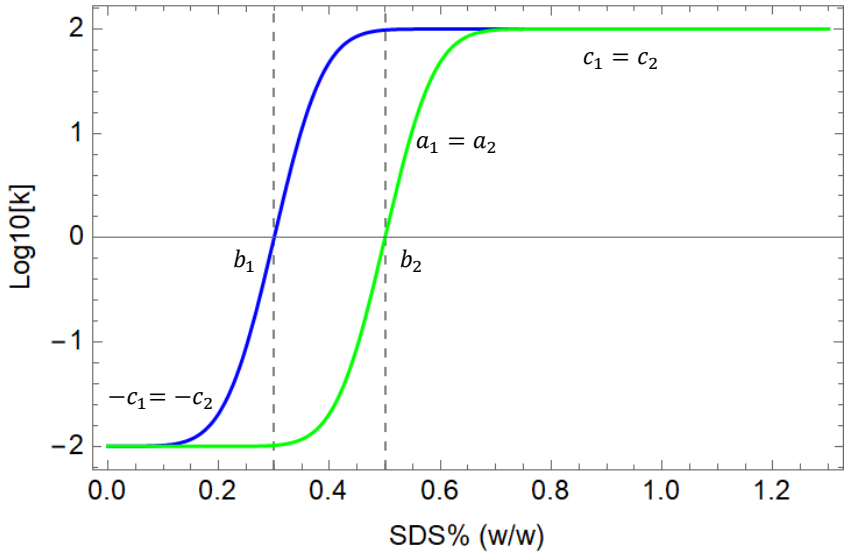

(b)

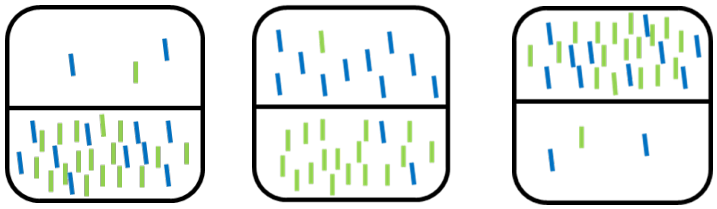

Figure 3. 1. One-stage separations between two CNT species. (a) A model simulation of the partition coefficient curves for two species. These two species have *a* and *c* parameters the same, which gives them identical slopes and maximum and minimum *K* values. The blue curve has a smaller *b*, and hence, we name it species 1. The green curve has a larger *b*, and hence, it is named species 2. (b) Three cartoon images help illustrate the same physical process of two species separation demonstrated as partition coefficient curves in (a). The left image mimics the situation when surfactant concentration is low, and the majority of both species stay in the bottom phase. The middle image mimics medium surfactant concentration when species 1 (blue) is tuned into the top phase, while species 2 (green) still stays in the bottom phase. The right image mimics high surfactant concentration when both species are tuned into the top phase.

In Figure 3.1 (a), partition coefficient curves of two different species are simulated by the model. These two curves have identical a and c values, where a_1=a_2=0.1 and c_1=c_2=2. The *b*

values are 0.3 and 0.5 for the blue and green curves, respectively. The blue curve, which has a smaller *b*, will be called species 1 for discussions in the entire thesis, and the green curve will be called species 2. The values of *a* and *c* are selected so that the general shape of these two curves mimics the experimental data of a semi-conducting CNT species. The values of *b* are selected arbitrarily but are kept within the surfactant range (0.1-1.8 wt%) explored in previous experiments. At low surfactant concentration (<0.2 wt%), both species 1 and species 2 have *K* values around 0.01. Partition coefficient *K* is defined as the concentration ratio between the top and bottom phases. A very small *K* ($K \ll 1$) indicates that the majority of CNT is stored in the bottom phase. As surfactant concentration increases from 0.2 to 0.4 wt%, *K* values for species 1 increase from 0.01 to 100. When the surfactant concentration increases further from 0.4 to 0.6 wt%, *K* values for species 2 have the same increment. A *K* value much greater than 1 ($K \gg 1$) implies that the majority of such species is stored in the top phase. Therefore, both species can be tuned from almost entirely in the bottom phase to almost entirely in the top phase as surfactant concentration increases, except that species 1 finishes the transformation at a lower concentration. At both low and high surfactant concentrations (<0.2 or >0.6 wt%), species 1 and 2 have very similar *K* values, and as a result, they stay in the same phase, which is not helpful for separation. However, within the surfactant range 0.3-0.5 wt%, species 1 has a much higher *K* value than species 2. In other words, most species 1 is the top phase while most species 2 is in the bottom phase within this surfactant range. This difference is the key to achieve the goal of separation. When the two species are tuned separately into the top and bottom phases, the whole system can be physical taken apart into two compartments. The top compartment can be further processed to remove the polymers and extract highly-concentrated species 1, while the bottom compartment yields highly-concentrated species 2.

In Figure 3.1 (b), three schematics are drawn to help visually describe the same physical process of CNT partitioning with an increasing surfactant concentration, as shown in Figure 3.1 (a). The schematic on the left illustrates when both species 1 (blue) and 2 (green) stay in the bottom phase at low surfactant concentration (<0.2wt%). The middle schematic illustrates when the bulk of species 1 is tuned into the top phase while most of species 2 is still left in the bottom phase, which corresponds to the medium surfactant concentration range of 0.3-0.5 wt%. The right schematic shows that both species are eventually tuned into the top phase as surfactant concentration keeps increasing (>0.6 wt%).

3.3 Use yield and purity as the separation performance evaluation metrics

It is shown in the previous sections that the model can be used to generate partition coefficient curves that approximate experimental data for different types of CNT. However, the generated curves can only describe the partitioning behavior of an individual species as a function of surfactant concentration in a two-phase system. It does not quantify the performance of a separation process or the quality of final products. To quantitatively measure how much one species is separated from the other species, we introduce yield and purity as the evaluation criteria. Yield and purity have been widely accepted as the standards to measure the performance of two-phase extraction processes [38,64,66]. Similar examples have been seen in a few cases for carbo nanotubes separation[15,34,67–69].In short, yield compares how much useful materials are left in the final product to how much are there in the original sample. It can also be understood as a measurement of how much waste is created due to the separation or purification processes. Purity reports how pure the final product is. In general, for both yield and purity, the higher, the better. High yield suggests very few materials are wasted during the separation process, and the majority of desired products are preserved from the initial sample to the final product. High purity suggests minimal traces of other unwanted molecules in the final product besides the desired molecule. There is usually a threshold for both yield and purity for an industrial separation process, such as 95% for protein separation and 99.9% for gas purification[70–72]. Even though higher yield or purity might be achieved by adding more processes or steps, a separation is considered complete when the threshold is met. Applying this concept to the model, we decide to set a threshold of 80% for both yield and purity. Instead of chasing after the exact surfactant concentration that gives the absolute optimal result, we aim to explore all surfactant concentrations that can meet the threshold.

Mathematically yield is defined as,

$$Y = \frac{m_p}{m_i} \tag{3.1}$$

where m_p denotes the remaining mass of the desired product after separation , and m_i is the initial mass of such product before separation.

For a two-species separation in an aqueous two-phase system, each species has two yields, one in the top phase and one in the bottom phase. For species 1, the yields are shown below,

$$Y_{1,top} = \frac{m_{1,top}}{m_{1,i}} \tag{3.2}$$

$$Y_{1,bot} = \frac{m_{1,bot}}{m_{1,i}} \tag{3.3}$$

For species 2, the yields are

$$Y_{2,top} = \frac{m_{2,top}}{m_{2,i}} \tag{3.4}$$

$$Y_{2,bot} = \frac{m_{2,bot}}{m_{2,i}} \tag{3.5}$$

After separation, each CNT species is either in the top phase or in the bottom phase. Given the mass conservation, the sum of mass of each species in the top and the bottom phase should equal to the initial mass of such species in the original sample. So we have the following relations,

$$m_{1,i} = m_{1,top} + m_{1,bot} \tag{3.6}$$

$$m_{2,i} = m_{2,top} + m_{2,bot} \tag{3.7}$$

Dividing $m_{1,i}$ on both sides in Equation 3.6 and dividing $m_{2,i}$ on both sides in Equation 3.7, we obtain the following equations for yields,

$$Y_{1,top} + Y_{1,bot} = 1 \tag{3.8}$$

$$Y_{2,top} + Y_{2,bot} = 1 \tag{3.9}$$

From Figure 3.1, we can see that species 1 has a bigger *K* value than species 2 across the entire middle surfactant concentration range (0.3-0.5 wt%), where these two species start to separate. Furthermore, the *K* values of species 1 are constantly bigger than 1 ($\log_{10} K > 0$), whereas the *K* values of species 2 are constantly smaller than 1. This big contrast in *K* values shows that the two species are well separated into two different phases within this surfactant range, with species 1 predominantly in the top phase and species 2 predominantly in the bottom phase. After physical separation of the top and bottom phases, species 1 and 2 can be extracted from the corresponding phase. Because the final product of species 1 will only come from the top phase and the final product of species 2 will only come from the bottom phase, we will proceed with all future calculations like the following,

$$Y_1 = Y_{1,top} = \frac{m_{1,top}}{m_{1,i}} \tag{3.10}$$

$$Y_2 = Y_{2,bot} = \frac{m_{2,bot}}{m_{2,i}} \tag{3.11}$$

where Y_1 is the final yield of species 1, and Y_2 is the final yield of species 2. According to the mass conservation, Y_1 and Y_2 should be a value between 0 and 1.

The definition of purity is given below,

$$P = \frac{m_p}{m_{tot}} \tag{3.12}$$

Where m_p is the remaining mass of the desired product after separation, and m_{tot} is the total mass of all CNT species after separation. Along the same logic shown for the calculation of yield, purity for species 1 and species 2 are calculated as the following,

$$P_1 = P_{1,top} = \frac{m_{1,top}}{m_{top}} \tag{3.13}$$

$$P_2 = P_{2,bot} = \frac{m_{2,bot}}{m_{bot}} \tag{3.14}$$

where m_{top} is the total mass of all CNT species in the top phase, and m_{bot} is the total mass of all CNT species in the bottom phase. Because we only consider the separation between two species for this chapter, the purity can be written as,

$$P_1 = P_{1,top} = \frac{m_{1,top}}{m_{1,top} + m_{2,top}} \tag{3.15}$$

$$P_2 = P_{2,bot} = \frac{m_{2,bot}}{m_{1,bot} + m_{2,bot}} \tag{3.16}$$

Given that all masses will be larger than zero, purity for both species should be a value between 0 and 1 as well.

In order to compute yield and purity using the model, the derived formulas are not enough. So far, both yield and purity are written in the form of mass ratios. However, the model is built to simulate partition coefficient curves using a language consisted of parameters *a*, *b*, c, *K*, and *x*, as we introduced before. We need to relate mass to partition coefficients using the same parameters, which we accomplish by applying mass balances and mass conservation.

After separation, the sum of masses of a CNT species in each phase should be the same as its initial mass before separation. We can re-write mass as the product of concentration multiplies volume. The initial mass and the mass in the top phase of species 1 can be shown as,

$$m_{1,i} = c_{1,top}V_{top} + c_{1,bot}V_{bot} \tag{3.17}$$

$$m_{1,top} = c_{1,top}V_{top} \tag{3.18}$$

where V_{top} and V_{bot} are the volumes of the top and bottom phases after separation. $c_{1,top}$ and $c_{1,bot}$ are the concentrations of species 1 in the top and bottom phases. The concentrations of species 1 in different phases can be substituted by the partition coefficient, whose definition is the concentration ratio between the top and the bottom phases. Equation 3.13 becomes,

$$m_{1,i} = c_{1,top}V_{top} + \frac{c_{1,top}}{K_1}V_{bot} \tag{3.19}$$

where K_1 is the partition coefficient of species 1. The volume of each phase can also be substituted by a new parameter, the volume ratio. We name the volume ratio, *R*, and its definition is given below,

$$R = \frac{V_{top}}{V_{bot}} \tag{3.20}$$

Now we introduce the volume ratio into the mass balance equation,

$$m_{1,i} = c_{1,top}V_{top} + \frac{c_{1,top}}{K_1}\frac{V_{top}}{R} = c_{1,top}V_{top}\left(\frac{K_1R + 1}{K_1R}\right) \tag{3.21}$$

By substituting Equation 3.14 and Equation 3.17 into Equation 3.6, yield of species is rewritten as,

$$Y_1 = \frac{c_{1,top}V_{top}}{c_{1,top}V_{top}\left(\frac{K_1R + 1}{K_1R}\right)} = \frac{K_1R}{K_1R + 1} \tag{3.22}$$

In this way, the yield of species 1 is expressed in partition coefficient and volume ratio only, the same language of the model. The model can compute a value for yield directly as long as parameters *x*, *a*, *b*, and *c* are given.

Volume ratio is another parameter that can be altered during an experiment besides *x* the surfactant concentration. Unlike parameters, *a*, *b*, and *c*, volume ratio *R* is not an intrinsic property determined by the type of CNT species. Therefore it can be changed freely during an experiment.

The volume ratio of an aqueous two-phase system is regulated by the composition of the two phase-forming polymers, PEG and DEX, in this case. The compositions of these two polymers can also govern other experimental phenomena, such as the time needed to reach equilibrium and the system's viscosity. To guarantee the system reaches equilibrium in a reasonable time, is easy to handle during separation, and has enough volume to extract the final CNT product, we decide that volume ratio *R* should stay within the range of 0.1 to 10. In other words, the volume ratio between the two phases is no more than 10. In the next chapter, we will discuss the relation between volume ratio and phase systems in more detail.

Repeating the steps taken to derive Equation 3.22, we can obtain the yield for species 2 in a similar manner,

$$Y_2 = \frac{1}{K_2 R + 1} \tag{3.23}$$

It is worth pointing out that we make an interesting discovery when rewrite $Y_{2,top}$ and $Y_{1,bot}$ by following the same derivation steps through Equation 3.17 to 3.22. It is found that yield of all species in the top phase share the same form as Y_1, and yield of all species in the bottom phase share the same form as Y_2. That means,

$$Y_{2,top} = \frac{K_2 R}{K_2 R + 1} \tag{3.24}$$

$$Y_{1,bot} = \frac{1}{K_1 R + 1} \tag{3.25}$$

Adding Equation 3.22 and 3.24, we generate the same result shown in Equation 3.8, and adding Equation 3.23 and 3.25, we obtain Equation 3.9. Even though we will not actively calculate $Y_{2,top}$ and $Y_{1,bot}$ throughout the separation process for reasons discussed before, such findings do validate the derivation for Y_1 and Y_2 mathematically.

In the same way, purity of species 1 can be expressed as,

$$P_1 = P_{1,top} = \frac{c_{1,top}V_{top}}{c_{1,top}V_{top} + c_{2,top}V_{top}} = \frac{c_{1,top}}{c_{1,top} + c_{2,top}} \tag{3.26}$$

To compare the concentration between species 1 and 2, we introduce another parameter, *m*. The definition of *m* is given as the following,

$$m = \frac{m_{1,i}}{m_{2,i}} \tag{3.27}$$

where $m_{1,i}$ and $m_{2,i}$ are the initial masses of species 1 and 2 in the original sample. Parameter *m* is an initial condition, which is determined by the CNT synthesis process. The compositions of CNT species are unique to the sample and cannot be altered during the separation process. Based on values reported in the literature, *m* can vary between 0.001 and 1000 for commercially available samples[73–75]. Therefore, we choose to examine *m* values within this range. Plugging Equation 3.21 and its equivalent formula for species 2 into Equation 3.27, we obtain,

$$m = \frac{c_{1,top}V_{top}\left(\frac{K_1R+1}{K_1R}\right)}{c_{2,top}V_{top}\left(\frac{K_2R+1}{K_2R}\right)} = \frac{c_{1,top}\left(\frac{K_1R+1}{K_1R}\right)}{c_{2,top}\left(\frac{K_2R+1}{K_2R}\right)} \tag{3.28}$$

$$\frac{c_{2,top}}{c_{1,top}} = \frac{\left(\frac{K_1R+1}{K_1R}\right)}{m\left(\frac{K_2R+1}{K_2R}\right)} \tag{3.29}$$

Now we divide both sides of Equation 3.26 by $c_{1,top}$ and plug Equation 3.29 into 3.26, the following equation can be derived,

$$P_1 = \frac{1}{1 + \frac{c_{2,top}}{c_{1,top}}} = \frac{1}{1 + \frac{\left(\frac{K_1 R + 1}{K_1 R}\right)}{m\left(\frac{K_2 R + 1}{K_2 R}\right)}} = \frac{\frac{mK_1}{K_1 R + 1}}{\frac{mK_1}{K_1 R + 1} + \frac{K_2}{K_2 R + 1}} \tag{3.30}$$

Following the same steps, purity for species 2 is calculated as,

$$P_2 = \frac{\frac{1}{K_2 R + 1}}{\frac{m}{K_1 R + 1} + \frac{1}{K_2 R + 1}} \tag{3.31}$$

With both yield and purity expressed in the same language as the model, we can now proceed and use the model to study how surfactant concentration affects the overall separation performance.

3.4 Effect of surfactant concentration on yield and purity

It has been shown in the previous section that yield is a function of partition coefficient K and volume ratio R, whereas purity is a function of partition coefficient K, volume ratio R, and initial mass ratio m. Partition coefficient K can be converted to surfactant concentration x using the error-function-based model. Considering both yield and purity, x, R, and m are the three determining parameters. Out of these three parameters, x and R can be altered by changing experimental conditions. Initial mass ratio m is directly related to the sample and cannot be altered by experimental conditions. In an experiment, x is controlled by adding or removing surfactant to the solution. Variation of volume ratio R is done by adding or removing polymers. Because the main goal of this section is to study how surfactant concentration affects the separation performance, we will fix m and R at several exemplary values within their possible ranges and let surfactant concentration vary freely.

The first m and R pair we pick is m=2 and R=0.1. Using the model, we plot yield and purity as a function of surfactant concentration x at the given m and R values. We choose to investigate the surfactant concentration range between 0.1 and 1.3 wt%, where the experimental tests are performed.

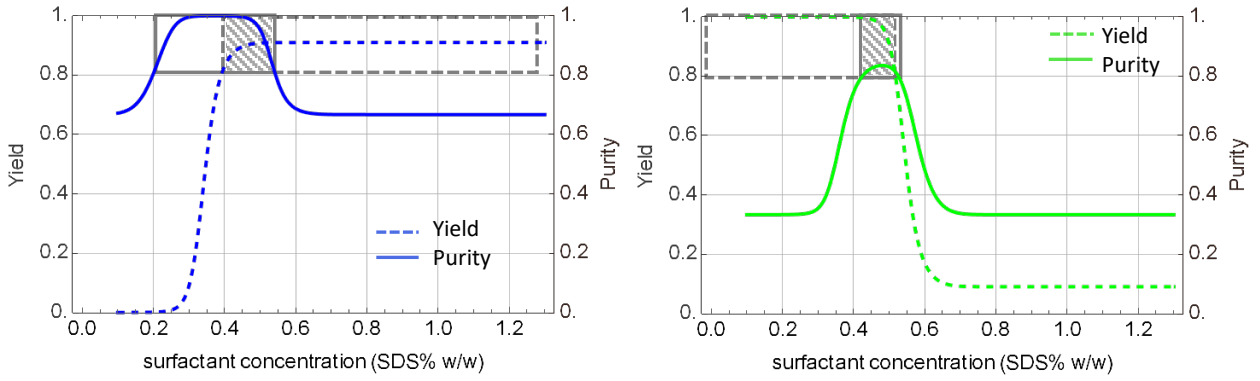

Species 1 (m=2, R=0.1) Species 2

Figure 3. 2. Yield and purity are plotted as a function of surfactant concentration at m=2 and R=0.1. Species 1 and 2 are designated by the color blue and color green, respectively. This color scheme will remain consistent throughout the thesis. Each plot consists of two y-axes, with the yield on the left axis and purity on the right axis. The x-axis is surfactant concentration. Dashed curves represent yield, and solid curves represent purity. For both species, the yield shows a monotonic change with increasing surfactant concentrations. However, the monotonic changes differ in direction for the two species. Yield for species 1 increases with surfactant concentrations, while yield for species 2 decreases. The purity curves for both species share a similar trend. They increase first, reach a peak, and then decrease with surfactant concentration increasing from 0.1 to 1.3 wt%, forming a volcano shape.

For species 1, the yield plateaus at low (<0.3 wt%) and high surfactant concentrations (>0.5 wt%). In the middle surfactant range, yield increases from 0 to 0.9 as surfactant concentration increases from 0.3 to 0.5 wt%. The purity for species 1 also increases with a growing surfactant concentration and reaches a peak around x=0.4 wt%. After peaking, it gradually decreases and eventually plateaus around 0.7 for x>0.6 wt%. These results agree with the general trend shown in Figure 3.1 (a) where the partition coefficient K grows significantly from 0.01 to 100 over the surfactant range 0.2-0.4 wt%. Both figures describe the same physical process, where the majority of species 1 is tuned from the bottom phase to the top phase by a small fraction of surfactant. Comparing the surfactant concentrations at which yield and purity peak, we notice that they don't coincide. This leads us to conclude that maximum yield and maximum purity do not occur simultaneously, and therefore, a trade-off exists in deciding which separation conditions are most beneficial.

The yield of a CNT species is defined as the ratio between the mass in the final phase and the initial mass. The initial mass does not change. According to Figure 3.2, the mass in the final phase (top phase) for species 1 increases with increasing surfactant concentration, while the mass in the final phase (bottom phase) for species 2 decreases with increasing surfactant concentration. As a result, we can predict that the maximum yield occurs at the highest surfactant concentration for species 1 and the lowest surfactant concentration for species 2. Purity is defined as the mass of one species divided by the total mass in the final phase. Rearranging Equation 3.15 and 3.16, we obtain the following formulas,

$$P_1 = P_{1,top} = \frac{1}{1 + \frac{m_{2,top}}{m_{1,top}}} \tag{3.32}$$

$$P_2 = P_{2,bot} = \frac{1}{\frac{m_{1,bot}}{m_{2,bot}} + 1} \tag{3.33}$$

According to Figure 3.2, the mass ratio of species 2 and 1 in the top phase decreases as surfactant concentration increases from low to moderate values, reaches a minimum, and then increases as the surfactant concentration continues to increase. The purity of species 1 reaches a maximum when the mass ratio between species 2 and 1 in the top phase is at a minimum. Following the same logic, the purity of species 2 also reaches the maximum at a moderate surfactant concentration. Comparing the surfactant concentrations that produce the maximum yield and purity, we confirm that yield and purity will not be maximized at the same condition.

At the beginning of Section 3.3, we introduce the concept of a threshold used to determine where the end-point is for a separation process. Here, we arbitrarily assume a threshold of 80% or 0.8 for yield and purity. The goal of separation becomes finding surfactant concentrations that allow both yield and purity have a value greater than 0.8. This includes situations where such

surfactant concentrations is a range, a single point, or do not exist. This process can be accomplished easily with plots featured in Figure 3.2. In the figure, we use rectangular lines to outline regions where yield and purity are greater than 0.8. Dashed lines are for yield and solid lines for purity. For example, for species 1, the dashed lines square out a region where the yield is above 0.8, and the corresponding surfactant range is x>0.4 wt%. Utilizing the plot helps us quickly locates the boundary surfactant concentration at 0.4 wt%. Similarly, the surfactant concentrations that satisfy the purity threshold for species 1 are between 0.2 and 0.55 wt%. If we need the threshold for both yield and purity simultaneously met, we look for the area where the dashed and solid rectangles overlap, shaded in grey in Figure 3.2. In this shaded area, the corresponding surfactant concentrations are approximately 0.4<x<0.55 wt%.

The yield and purity for species 2 share similar trends to species 1. The yield plateaus at the two ends of the surfactant concentration spectrum. When x<0.5 wt%, the yield stays near 1 stably. As the surfactant concentration increases, yield decreases sharply until it reaches another plateau of 0.1 around x>0.7 wt%. These changes of yield are in the opposite direction of those for species 1. This is due to the difference in the definition of Y_1 and Y_2. Yield for species 1 is defined as the mass in the top phase divided by the initial mass. However, for species 2, yield is the mass in the bottom phase divided by the initial mass. We have discussed the reasons behind this decision in the previous section. At low surfactant concentration, the majority of both species are in the bottom phase. Thus, Y_2 is very large and is Y_1 is very small. At high surfactant concentration, the majority of both species are in the top phase. So, Y_1 becomes very large and Y_2 becomes very small. Neither of those two situations has a good separation. Good separation occurs in the middle surfactant concentration range, where both Y_1 and Y_2 are relatively high. This is an important point throughout the thesis. An isolated high yield for species 2 does not warrant good separation. The

purity of species 2 also has a volcano shape, which starts at 0.35, then reaches a peak of 0.85 near x=0.5 wt%, and eventually decreases to 0.35 again for x>0.7 wt%. The volcano shape of the purity plot can be explained by Figure 3.1 (b). The purity is low at both lower and higher surfactant concentrations because both species 1 and species 2 are in the same phase under those conditions, shown by the left and right cartoons in Figure 3.1 (b). There is no separation in either case. However, in the medium surfactant range, species 1 is tuned into the top phase while species 2 is still left in the bottom phase. In this case, the separation is maximized, and each phase only consists of primarily one species, which is the definition of high purity. Following the same analysis we have done for species 1, we find that the surfactant concentrations that meet the standards of both yield and purity for species 2 are $0.45<x<0.55$ wt%. This is a rather small interval to allow errors in surfactant concentrations. In an experiment, we cannot guarantee the surfactant solutions made have the exact concentration we design. In the droplets experiment, the concentration interval between data points is approximately 0.02 wt%. In a traditional benchtop experiment setting, the surfactant concentration interval is usually set at 0.1 wt% increments[55,76,77]. Figure 3.2 shows that a concentration shifts 0.1 wt% away from the shaded region can result in a change as much as 0.2 in yield and purity. However, at high surfactant concentration x>0.8 wt%, yield and purity stay stable regardless of surfactant concentration. Hence, we conclude the sensitivity in surfactant concentration is highly dependent on which region the concentration belongs to.

It is worth pointing out that all values of yield, purity, and surfactant concentration given in the discussions above are visual estimations obtained directly by reading Figure 3.2. This process only serves as an example, which aims at demonstrating how the figure is used. Exact values require further computation by the model. Nevertheless, Figure 3.2 helps us quickly discover the surfactant concentrations needed to meet the separation threshold for both species,

$0.4<x<0.55$ wt% for species 1 and $0.45<x<0.55$ wt% for species 2. If the goal is to collect both species that have yield and purity greater than 0.8, the surfactant range is further narrowed down to $0.45<x<0.55$ wt%. This result is only valid when the initial mass ratio m=2 and volume ratio R=0.1. As we discussed in the previous section, m can be any value between 0.001 and 1000, whereas R can be anywhere from 0.1 to 10. In the next section 3.5, we will investigate how m and R impact the separation and whether or not a threshold surfactant concentration range exists for all m and R pairs. In section 3.6, we will take one step further and compute the threshold surfactant concentration for exemplary m and R pairs.

3.5 Effect of *m* and *R* on yield and purity

Given the wide range of possible values of *m* and *R*, we carefully choose several exemplary values to investigate. *m* is a continuous function that can vary from 0.001 to 1000. A specific type of CNT species might be abundant or scarce in an as-synthesized sample. If such a species is desirable for its functionality, we therefore may encounter a large variety of *m* values depending on the sample. For this section, we characterize the initial mass ratio *m* into three situations. For small *m*, when the concentration of species 1 is significantly less than that of species 2 in the original sample, we select m=0.02. For medium *m*, when the concentration of species 1 and species 2 are comparable, we select m=2. For large *m*, when the concentration of species 1 is much greater than that of species 2, we select m=200. To systematically examine the effect of volume ratio *R*, we choose multiple *R* values from three groups. When the top phase volume is smaller than the bottom phase volume (R<1), we select R=0.1, 0.2, 0.3, 0.5. When the top phase and the bottom phase have equal volume, we have R=1. When the top phase is bigger than the bottom phase (R>1), we select R=3, 5, 10. We should emphasize again that *m* is an initial condition and cannot be altered by experimental conditions. We vary the values of *m* only to study how different samples react to the same set of conditions. On the contrary, R is an experimental parameter and can be varied between 0.1 and 10 during experiments.

To have a more direct view of how *m* and *R* affect separation results, we plot yield vs. purity as a function of surfactant concentration for different *m* and *R* pair, shown in Figure 3.3. In this series of plots, purity is on the x-axis, and yield is on the y-axis. The opposite C-shape curves are obtained by calculating the yield and purity for all surfactant concentrations ranging from 0.1 to 1.3 wt% at any given *m* and *R* values. Each curve contains all the data points for one *R* value, and different curves or different *R* values are distinguishable by the various spacing of the dashed

lines. The blue arrows in Figure 3.1 (a) and the green arrows in (b) are guidelines indicating the direction of increasing surfactant concentrations. Reference lines at 0.8 are marked for both yield and purity so that we can easily decide whether the curve passes the performance threshold or not.

(a)

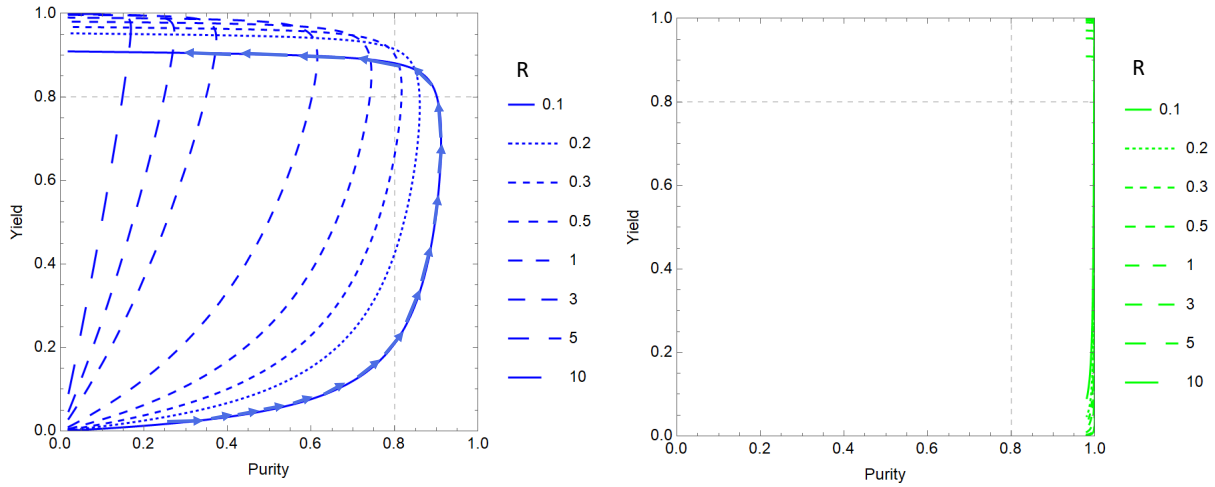

Species 1 (m=0.02) Species 2

(b)

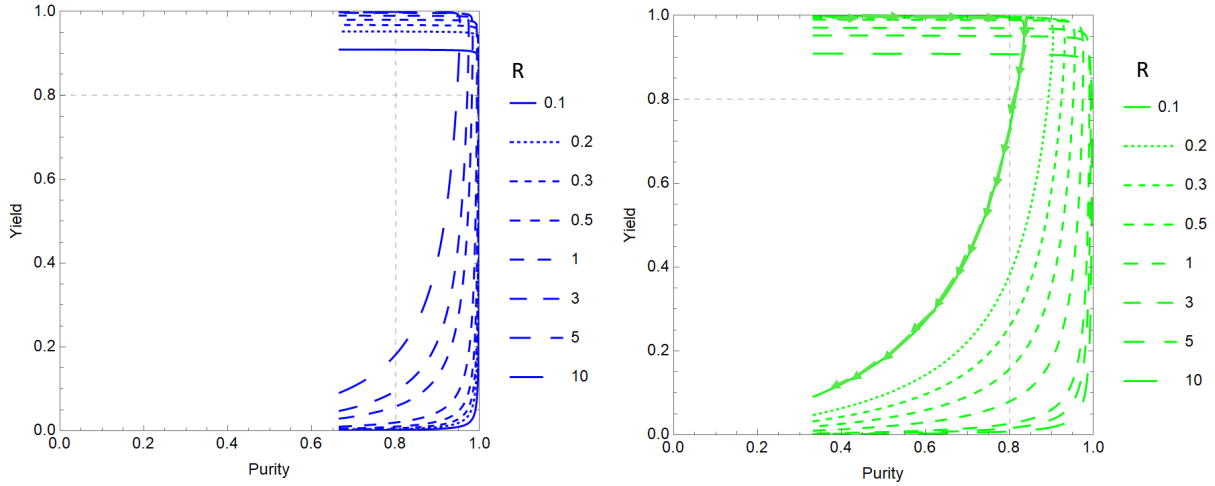

Species 1 (m=2) Species 2

(c)

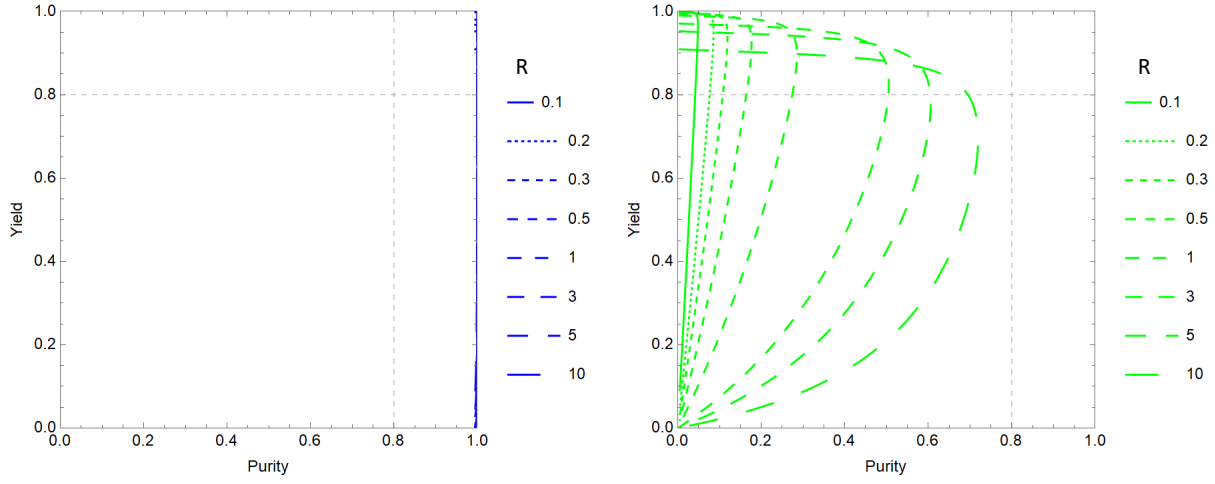

Species 1 (m=200) Species 2

Figure 3. 3. Yield and purity are plotted as a function of surfactant concentration for chosen *m* and *R* values. Using Equations 3.24-3.25 and 3.30-3.31, yield and purity are calculated for all surfactant concentrations between 0.1-1.3 wt%. The computed yield and purity are then plotted as the y and the x values for each data point, respectively. On the solid blue curve in (a) and the solid green curve in (b), the arrows indicate the direction of an increasing surfactant concentration. The different spacing between dashed lines is used to distinguish *R* values, with narrow spacing corresponds to smaller *R* and wide spacing corresponds to bigger *R*. The grey dashed lines at 0.8 for both yield and purity are guidelines for making easy judgement on meeting the separation threshold. (a) Yield-purity plots for *m*=0.02. (b) Yield-purity plots for *m*=2. (c) Yield-purity plots for *m*=200.

To further explain these plots, we use the solid blue and green curves at *m*=2 and *R*=0.1 in Figure 3.3 (b) as an example. The experimental conditions for these two particular curves are identical to those in Figure 3.2. We first examine the blue curves for species 1. At low surfactant concentration, species 1 has a yield almost to 0 and a purity slightly larger than 0.65. As the surfactant concentration increases, the yield remains near 0, yet the purity starts to increase from 0.65 to almost 1. In the middle surfactant concentration range, the purity stays stable around 1 as the yield grows sharply from 0 to 0.9. As the surfactant concentration rises into the high range, the yield remains unchanged at 0.9, whilst the purity drops back to 0.65. For species 2, yield begins with a value of 1, and purity starts around 0.35. With an increasing surfactant concentration, the purity climbs to a peak value of 0.8, while the yield continues to stay at 1. At even higher surfactant concentrations, both yield and purity monotonically decrease. Yield decreases to 10% of its original level, reaching 0.1, and purity shrinks back to its initial value at 0.35. Comparing this series of changes of yield and purity in this plot to Figure 3.2, we verify that both figures are equivalent to each other. However, it needs to be mentioned that all the adjectives used for surfactant concentrations, low, middle, and high, are only relative because Figure 3.3 does not report the exact surfactant concentration corresponding to each point on the plot.

Using the reference lines at Y=0.8 and P=0.8, we can decide if a certain *m* and *R* pair can provide a separation performance that meets the threshold by observing whether or not the C-shape curve passes the small square region at the upper-right corner. In the case of *m*=2 and *R*=0.1, the

solid blue curve does pass through this region. Hence, there are surfactant concentrations that can produce a yield>0.8 and a purity>0.8. Nevertheless, by reading Figure 3.3 alone, we do not know what those surfactant concentrations are. Applying the same type of analysis to Figure 3.3 (a), we find that at m=2, separation for species 1 can meet the threshold when $R \leq 0.3$, but cannot when $R \geq 0.5$. As a result, a boundary value exists in the range of $0.3 < R < 0.5$. The threshold for species 2 can be met with all R values at m=2.

The yield vs. purity curves for species 2 in Figure 3.3 (a) look like straight lines regardless of R values. These straight lines suggest that the purity of species 2 is close to 1 at all surfactant concentrations under every R. In this section, we first explain this with a simple argument. In the next section, we will discuss it in more detail. Purity for species 2 is defined as the mass ratio between species 2 and all CNT species in the bottom phase. When m=0.02, the sample starts with an initial mass ratio of species 2:species 1=50:1 in the bottom phase. Species 2 is already in abundance before separation. If we calculate the purity for species 2 using Equation 3.16, it turns out to be 0.98. The separation is designed to improve purity further. As a result, the purity of species 2 is always high at approximately 1 regardless of x or R values when m=0.02. The same concept also applies to the blue curves in Figure 3.3 (c), where m=200 and species 1 is in abundance before separation.

In Figure 3.3 (b), the yield vs. purity curves for both species passes through the threshold-satisfying region for all R values. This is good news because a practitioner will not need to worry about which volume ratio to choose from when performing the separation process. However, it needs to be kept in mind that the ranges of surfactant concentrations that allow sufficient separation are different for different R values; they can be narrow or wide. We will discuss this in more detail in section 3.7.

In Figure 3.3 (c), none of the green curves passes through the upper-right region. This result reveals that no volume ratio between 0.1 and 10 can lead to a separation with both yield and purity greater than 0.8 for species 2, regardless of the surfactant concentrations used. At this point, one-stage separation is not sufficient to produce a result that satisfies the threshold. If the threshold must be met for both species 1 and species 2, more separation steps have to be taken. This particular situation prompts the discussion of multi-stage separation for two species in chapter 4.

3.6 The maximum and minimum yield and purity can be achieved at given *m* and *R* values

In the previous section, we have shown that for a given *m* value, the separation threshold can be achieved with 1) a small number of *R* values, 2) all *R* values, or 3) none of the available *R* values. By analyzing Figure 3.3, we can answer the yes or no question if the pre-selected separation threshold can be met at a couple of chosen *m* and *R* values. However, we cannot answer the question of what the exact level of yield and purity are at all *R* values. Volume ratio *R* is one of the two model parameters that can be altered freely during an experiment, and we have assumed its possible range is 0.1-10. In this section, a different type of plot will be used when we compare yield and purity for all *R* values at three chosen *m* values. We choose just a few *m* values that represent the extremes of the wide range of possible values. Since *m* depends on the synthesis conditions and cannot be controlled freely during an experiment, we examine representative values that exemplify scenarios in which species of interest are abundant (large *m*), comparable (*m* near unity) and scarce (small *m*). Because the separation metrics, yield, and purity, are continuous functions of *m*, these three boundary scenarios are expected to capture the predominant effects of *m* on the separation results.

From Figure 3.3 and 3.2, we have seen that yield always change monotonically as a function of surfactant concentration. For species 1, yield increases from approximately 0 to approximately 1 when surfactant increases from 0.1 to 1.3 wt%. For species 2, yield decreases the same amount over the same range. The interval between the minimum and the maximum yield is relatively constant, although the exact values shift up and down. Looking for surfactant concentrations that can produce a yield>0.8, we realize that such concentrations will be above a certain value for species 1 and below a certain value for species 2. Let's call this certain concentration x_Y. Mathematically, the surfactant concentration range that meet the yield threshold

is x_Y-1.3 wt% for species 1 and 0.1-x_Y wt% for species 2. This observation helps us make quick decisions on whether or not a specific *m* and *R* pair can produce a threshold-meeting yield. For any given *m* and *R* pair, we only need to assess if the maximum yield is greater than 0.8. If the maximum yield>0.8, then a x_Y exists. If the maximum yield<0.8, no surfactant concentrations can satisfy the yield threshold. Based on this conclusion, we decide only to track the maximum yield as we vary initial mass ratio *m* and volume ratio *R*.

On the contrary, purity increases and then decreases with an increasing surfactant concentration. The values of purity vary widely depending on the specific *m* and *R* pair. Some *m* and *R* combinations have purity completely below 0.8 regardless of the choices of surfactant concentration, as shown by the green curves in Figure 3.3 (c). Some *m* and *R* pairs have purity past the 0.8 reference line over a range of surfactant concentrations, as shown in Figure 3.2 (b). For the rest of *m* and *R* sets, purity stays above 0.8 across the entire surfactant concentration range, as shown by the green curves in Figure 3.3 (a) and the blue curves in Figure 3.3 (c). Considering the dramatic variation in purity, we will track both the minimum and maximum purity for any *m* and *R* combination. This allows a practitioner to quickly identify the entire purity range, even if it might not meet the threshold.

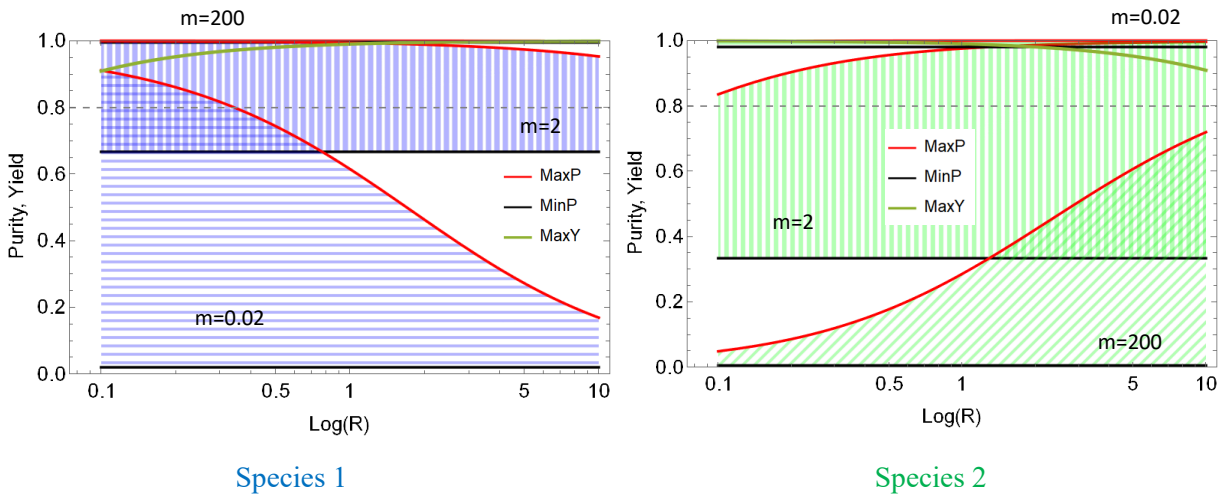

Figure 3. 4. The purity and yield are plotted as a function of volume ratio *R* at three different *m* values. Each *m* value consists of two lines for purity, red and black, outlining the boundary of possible purity values, and one green line for the maximum yield values. The red and black curves represent the maximum and minimum purity recorded for each *R* value. For a specific *m* value, the region between the MaxP and MinP is filled with hatching lines, horizontal for *m*=0.02, vertical for *m*=2, and at a 45-degree angle for *m*=200. Because yield is not a function *m*, the MaxY lines for these three *m* values are identical. The MaxP (red) and MinP (black) curves are not visibly clear at *m*=200 for species 1 and at *m*=0.02 for species 2, because they are stacked with the upper boundary of the plot where purity is equal to 1. This result agrees with the earlier observation for the green curves in Figure 3.3 (a) and the blue curves in (c). A grey dashed line at 0.8 is also included for easy reference of the separation threshold.

To generate Figure 3.4, we compute the maximum yield (MaxY), the minimum (MinP), and maximum purity (MaxP) for any given *m* and *R* pair using the model. The calculation of yield and purity is carried out for all surfactant concentrations from 0.1 to 1.3 wt%, but only the MaxY, MinP, and MaxP are recorded. After this process is done for one pair of *m* and *R*, the computational program moves on to the next *m* and *R* pair. As discussed at the beginning of this section, we consistently vary *R* across the entire possible range, but only three exemplary *m* values are studied.

For species 1 and *m*=0.02, the purity range becomes narrower as *R* increases. Starting with a maximum purity around 0.9 at *R*=0.1, it drops to 0.2 at *R*=10. This monotonic change reveals that a top phase with a smaller volume is advantageous to produce higher purity for species 1-abundant samples. The maximum purity line (red) intersects with the threshold reference line between 0.3 and 0.4, reinforcing the finding of a boundary *R* value we make in Figure 3.3 (a). At *m*=2, species 1 has a maximum purity greater than 0.8 across all *R* values. This means that there

are always some surfactant concentrations that can induce a separation that passes the threshold for species 1 at any volume ratio between 0.1 and 10. Though the exact ranges of surfactant concentrations are different for different *R* values. We will discuss this in detail in the next section. At *m*=200, the minimum purity is above 0.8 for all volume ratios, which means any surfactant concentrations (0.1-1.3 wt%) can be chosen at any *R* value.

For species 2, the entire purity range is above 0.8 at *m*=0.02, indicating satisfactory separation at any surfactant concentrations at any *R* values. At *m*=2, the maximum purity is constantly greater than 0.8 for all *R* values, while the minimum purity line is below the threshold. As a result, only specific surfactant concentrations can create a separation that passes the threshold. At *m*=200, the purity range grows wider with an increasing volume ratio. Starting with a maximum purity around 0.05 at *R*=0.1, it increases to almost 0.75 at *R*=10. This change reveals that a bottom phase with a smaller volume should be used to produce higher purity for species 2-abundant samples. The maximum purity line lies below the threshold reference line for all *R* values, supporting the same conclusion we make in Figure 3.3 (c).

The goal of Figure 3.4 is to serve as a map that shows all the possible ranges of purity and yield for the entire parameter space. With such information, a practitioner can make a knowledgeable assessment of where the threshold should be made and how many experimental conditions can achieve such threshold.

3.7 The surfactant concentrations that can satisfy the threshold at given *m* and *R* values

In the previous section, we mapped out all the possible ranges of yield and purity for all *R* values and three exemplary *m* values. Using Figure 3.4, one can quickly detect if a specific experimental condition can produce a desirable separation result. In this section, we continue to apply 0.8 as the threshold for both yield and purity to species 1 and 2. After realizing whether or not the threshold can be met, the next question one usually asks is what sets of experimental conditions can achieve this goal.

In this section, we plot the threshold-satisfying surfactant concentration as a function of volume ratio. Mathematically, we first calculate the surfactant concentrations that satisfy the threshold for yield or purity separately. Then we compare these two ranges and select the part where they overlap with each other, which essentially is a repentance of the same process used in Figure 3.2 to find the shaded area.

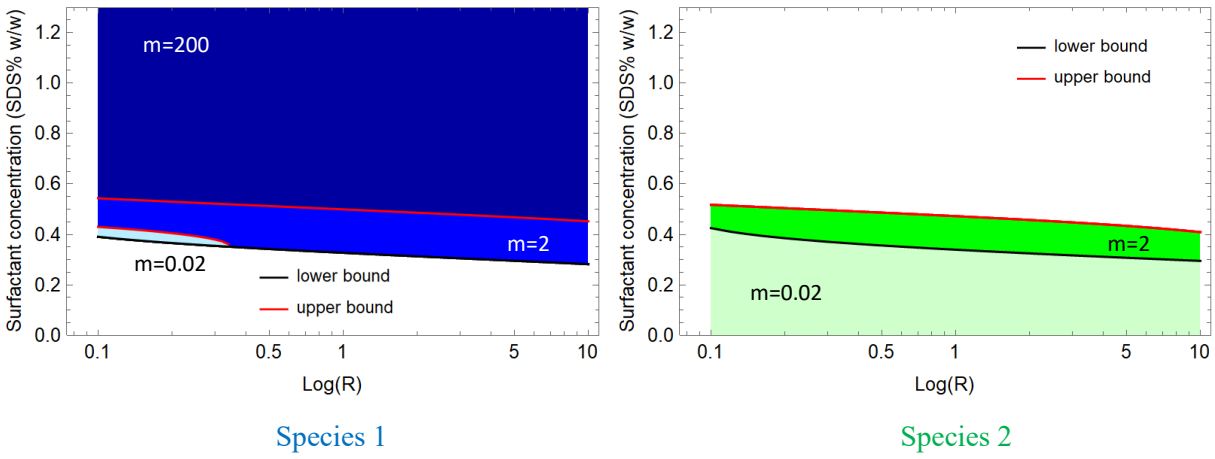

Figure 3. 5. The surfactant concentrations that can produce yield>0.8 and purity>0.8 are plotted as a function of volume ratio. For each *m* value, the highest and the lowest surfactant concentration that satisfies the threshold are outlined as red and black curves. The region between the highest (upper bound) and the lowest concentration (lower bound) are filled with the color blue for species 1 and the color green for species 2. The intensity of the color is an indication of the *m* value. The lightest color is used for the smallest *m*, whereas the darkest color is used for the largest *m*. At *m*=200 for species 1, all surfactant concentrations greater than the lower bound can meet the threshold. Therefore, an upper bound is not specified. At *m*=0.02 for species 2, all surfactant concentrations below the upper bound can meet the threshold. Hence, a lower bound is not specified.

In Figure 3.5, all surfactant concentrations that can provide a separation result exceeding the 0.8 thresholds for yield and purity are mapped out. For each m value, the highest and the lowest threshold-satisfying surfactant concentrations are plotted in red and black as a function of volume ratio. The red and black curves are called the upper and the lower bound, respectively. At a specific *R* value, any surfactant concentrations between the red and black points can produce a yield>0.8 and purity>0.8. However, the exact values of yield and purity are not reported in Figure 3.5. The region between the red and black curves is filled with blue for species 1 and green for species 2. The intensity of the color corresponds to the magnitude of *m*. For species 1, the lower bound is always dictated by the surfactant concentration that satisfy the yield threshold. Because yield is not a function of initial mass ratio *m*, all three scenarios with different *m* values share the same lower bound (black curve) for species 1. On the contrary, for species 2, the upper bound is controlled by the yield-threshold satisfying concentration. Therefore, all three scenarios with different *m* values have the same upper bound (red curve) for species 2. At *m*=200, all surfactant

concentrations above the lower bound can meet the requirement for both yield and purity for species 1. Thus an upper bound is not plotted. At *m*=0.02, the same rule applies to the lower bound for species 2.

Figure 3.5 directly summarizes the surfactant concentration ranges that fulfill the 0.8 requirements at all experimental conditions. For species 1, the smaller the *m* value, the narrower this range. In other words, larger *m* values make it easier to achieve high yield and high purity for species 1. At *m*=0.02, the surfactant range is quite narrow, from slightly below to slightly above 0.4. The volume ratio *R* also has a tight range, from 0.1 to somewhere between 0.3 and 0.4. For species 2, the story is the opposite. The smaller the *m* value, the more experimental conditions are allowed to achieve high yield and purity. When *m* increases to 200, there is no surfactant concentration or volume ratio that can meet the threshold for species 2. Figure 3.5 helps represent the possible conditions for achieving thresholds for each species individually. However, the goal of separation is usually high yield and purity for all species simultaneously since each species has its unique functionality and is highly valuable. To help practitioners decide for both species at the same time, we transform Figure 3.5 into Figure 3.6.

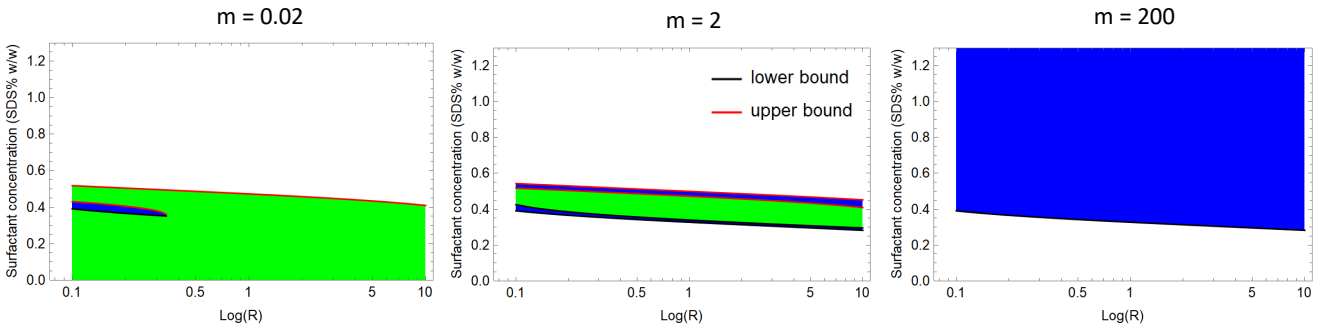

Figure 3. 6. A re-make of Figure 3.5. Figure 3.6 is plotted based on the value of *m* instead of species types, using the same data in Figure 3.5. The intensity of the blue or green color is removed as *m* is already labeled on the graph.

Figure 3.6 shows the threshold-satisfying surfactant ranges for species 1 and 2 on the same plot while using the same data as Figure 3.5. The plots are now categorized by the values of m

instead of the species type. The same *m* value represents the same initial condition or the same original sample. In this way, one can quickly locate what the operating conditions are for different samples.

At *m*=0.02, the range of appropriate conditions for species 1 (blue region) is significantly smaller than that for species 2 (green region). Because the separation goal is to have both species passing the 0.8 threshold, the surfactant concentration and the volume ratio should be selected from the region where blue and green overlap. In this case, it is the blue region outlined for species 1. At *m*=2, the blue region is larger, and it surrounds the green region. Hence, the appropriate conditions for species 2 are more limiting than those for species 1. The final experimental conditions should be chosen from the green region. At *m*=200, there is no green region in the plot, indicating no experimental condition can produce the desired result, and more separation stages must be performed.

3.8 Summary

In this chapter, we use the model to approximate one-step separation processes between two CNT species. In the first step, partition coefficient curves of different CNT species are generated, and they resemble the experimental data. Then yield and purity are rewritten in a model compatible language, adding volume ratio R and initial mass ratio m to the parameters list. The parameters tuned for each CNT species are fed into the model to compute yield and purity. The concept of a threshold is introduced to incorporate the industrial standard of setting up a separation goal. Applying an arbitrary threshold, we use the model to screen through a large parameter space and select a small range of threshold-satisfying experimental conditions. Such experimental conditions are summarized and plotted in a compact format to help practitioners easily identify the appropriate operating range based on their unique separation needs. In one special case (m=200), there is no experimental condition that can meet the proposed threshold. This scenario leads to the discussion in chapter 4.

Chapter 4: Modifying the model to simulate multi-stage separation of two CNT species

4.1 Introduction

In the previous chapter, we have seen that for samples starting with m=200, there is no experimental condition that can produce a separation result that meets the 0.8 thresholds for both species 1 and 2. This limitation of one-stage separation leads to the introduction of multi-stage separation. Multi-stage vs. one-stage separation in aqueous two-phase extraction is analogous to multi-tray vs. one-tray for distillation. After one stage or one tray, the products are re-fed into the system to go through the same separation process in order to achieve higher purity. In aqueous two-phase extraction, multi-stage processes involve physically pulling apart the top and bottom phases after the previous stage and treating each phase as a new sample. Polymers and surfactants are added to these two new samples to undergo another phase separation and extraction process. As a result, the total number of compartments or phases after n-stage separation is 2^n, i.e., two phases for one-stage and four phases for two-stage. For easy tracking, each phase is assigned a label T (top) or B (bottom) for each stage it goes through. For example, a two-stage separation will produce four phases, TT and TB from the top phase in the first stage and BT and BB from the bottom phase in the first stage.

In reality, the overall separation process is most likely multi-stage among dozens of species. However, we only take one step further in this chapter by discussing multi-stage separation between two species.

4.2 Keeping yield and purity as the performance evaluation metrics

In the previous chapter, we use yield and purity to measure the separation performance for one-stage processes. In this chapter, we continue this practice. However, there are also some differences coming along. One big decision we make in chapter 3 is only tracking yield and purity in the top phase for species 1 and those in the bottom phase for species 2. This decision is justified because the partition coefficient curves predict the top phase will be the destination phase for species 1 while the bottom phase will be the target spot for species 2 for one-stage separation. In multi-stage separation, however, we have to know the yield and purity in both phases from the previous stage to be able to calculate a new set of parameters for the next stage. Because of that, we need to compute yield and purity for both species in both phases, which mounts to eight parameters for each two-phase system. By following the same steps shown in section 3.3, the following parameters are computed,

$$Y_{1,top} = \frac{k_1 R}{k_1 R + 1} \tag{4.1}$$

$$Y_{1,bot} = \frac{1}{k_1 R + 1} \tag{4.2}$$

$$P_{1,top} = \frac{\frac{mk_1}{k_1 R + 1}}{\frac{mk_1}{k_1 R + 1} + \frac{k_2}{k_2 R + 1}} \tag{4.3}$$

$$P_{1,bot} = \frac{\frac{m}{k_1 R + 1}}{\frac{m}{k_1 R + 1} + \frac{1}{k_2 R + 1}} \tag{4.4}$$

$$Y_{2,top} = \frac{k_2 R}{k_2 R + 1} \tag{4.5}$$

$$Y_{2,bot} = \frac{1}{k_2 R + 1} \tag{4.6}$$

$$P_{2,top} = \frac{\frac{k_2}{k_2R+1}}{\frac{mk_1}{k_1R+1} + \frac{k_2}{k_2R+1}} \tag{4.7}$$

$$P_{2,bot} = \frac{\frac{1}{k_2R+1}}{\frac{m}{k_1R+1} + \frac{1}{k_2R+1}} \tag{4.8}$$

By the definitions of yield and purity, these eight parameters should also fulfill the relations listed below.

$$Y_{1,top} + Y_{1,bot} = 1 \tag{4.9}$$

$$Y_{2,top} + Y_{2,bot} = 1 \tag{4.10}$$

$$P_{1,top} + P_{2,top} = 1 \tag{4.11}$$

$$P_{1,bot} + P_{2,bot} = 1 \tag{4.12}$$

Plugging Equation 4.1-4.8 into the left sides of Equations 4.9-4.12, the equality of each equation is verified. Consequently, the formulas for each term in Equation 4.1-4.8 are all valid. These eight equations apply to any stage since no assumption of stage number is made during the derivation. Each stage is considered a brand new system with a given set of inputs. Even though the equations are universal across stages, the inputs or the initial conditions vary stage by stage. The outputs from the previous stage become the inputs for the current stage, and then the outputs from the current stage become the inputs for the next stage. Abstractly speaking, the yield and purity both carry information from an earlier stage. However, how the passage of information is facilitated forward is unclear yet.

So we return to the definition of yield and purity. Within each stage, yield is calculated as the mass ratio of the product in the destination phase to the initial input. For a one-stage process,

the initial input is the mass of such product in the original sample. But, for a multi-stage process, the initial input is the output mass from the earlier stage. Writing this logic into equation format,

$$Y_{i,p} = \frac{m_{i,p}}{m_{i,p-1}} \tag{4.13}$$

where i specifies the types of species, p identifies the phase the species is currently in, and p-1 tells the phase this product is in from the previous stage. For a two-stage example, the initial input mass of species 1 in the TT phase is the output mass of species 1 from the T phase. Writing into equation format,

$$Y_{1,TT} = \frac{m_{1,TT}}{m_{1,T}} \tag{4.14}$$

For a one-stage separation, Equation 4.14 is still valid,

$$Y_{1,T} = \frac{m_{1,T}}{m_{1,O}} \tag{4.15}$$

where O stands for the original sample. Combining Equation 4.14 and 4.15, we obtain the following,

$$Y_{1,TT} * Y_{1,T} = \frac{m_{1,TT}}{m_{1,O}} \tag{4.16}$$

Because the value of $m_{1,O}$ is independent of stage, using it as the denominator to calculate the mass ratio for yield can provide a more consistent comparison across different stages. Thus, we introduce a new concept of yield called the overall yield, which is defined as,

$$Y_{i,O\_p} = \frac{m_{i,p}}{m_{i,O}} = Y_{i,p} * Y_{i,p-1} \tag{4.17}$$

Going forward, we will only report the overall yield as the final yield for a species in any given phase. Translating the overall yield into the model language, we can substitute one of Equations

4.1, 4.2, 4.5, and 4.6 for $Y_{1,p}$ depending on the species type and its final phase. $Y_{1,p-1}$ is obtained from the calculations done for the previous stage. According to mass conservation, the overall yields for one species within the same stage should add up to 1. Using species 1 in a two-stage separation as an example again,

$$Y_{1,O\_TT} + Y_{1,O\_TB} + Y_{1,O\_BT} + Y_{1,O\_BB} = 1 \tag{4.18}$$

Now we move on to purity. The purity of a CNT species in any phase can be written as,

$$P_{i,p} = \frac{m_{i,p}}{m_{tot,p}} \tag{4.19}$$

For a two-species separation, which is the focus of our investigation in this chapter, Equation 4.19 becomes,

$$P_{i,p} = \frac{m_{i,p}}{m_{1,p} + m_{2,p}} \tag{4.20}$$

Because Equation 4.20 only contains terms within the same stage, Equations 4.3, 4.4, 4.7, and 4.8 are still applicable. One thing that changes for multi-stage separations is the initial mass ratio *m*. For stages later than the first one, *m* is no longer the mass ratio in the original sample. Instead, it becomes the output mass ratio from the previous stage. Suppose we treat any two-phase system as an isolated stage. Then, *m* can still be considered the initial mass ratio, except the initial input *m* is updated from stage to stage and is different from the value in the original sample. Therefore, it is essential to report the *m* values for both the top and bottom phases after a separation. The ratio of an output *m* to the initial *m* in the original sample is called enrichment. Comparing enrichment across stages helps evaluate the concentrating power of each separation process. In line with the definition of *m*, a high enrichment value (>>1) means species 1 is the dominating species, while a low enrichment (<<1) means species 2 is dominating.

4.3 Aim for the best possible in the first stage for samples require multi-stage separation

In the previous section, we set up the foundations for yield and purity calculation in multi-stage separations. In this section, we will discuss how to choose the experimental conditions in the first stage in preparation for the later stages to reach the pre-determined separation threshold. In this case, we keep using 0.8 for the following discussions.

It has been found that when m=200 in the original sample, there is no surfactant concentration or volume ratio that can produce a separation result where both yield and purity are greater than 0.8. Therefore, more separation steps are necessary. Before proceeding to the second stage, one must finish the first-stage separation first. However, what experimental conditions should we choose given that the threshold requirement cannot be met in any way? To answer that questions, we adopt a principle to pursue the best possible results. This leads to another question—what is the best possible. The general guidelines are that the higher, the better for both yield and purity. But, we have mentioned in chapter 3 that yield and purity do not peak simultaneously, and a trade-off decision has to be made.

Before going further on the conceptual route, we turn to re-analyzing the data in chapter 3 to look for constraints that help limit options for the best possible separation. From Figure 3.4, we can conclude that at m=200, the purity of species 1 is near 1 constantly at all surfactant concentrations under any volume ratio. So, we do not need to worry about the purity of species 1 in search of the best possible separation. The yield for species 1 has a similar story where it can always rise above 0.8 at any R value with specific surfactant concentrations, which makes it not the limiting factor either. The purity of species 2, on the contrary, is the limiting factor. Figure 3.4 shows that the maximum purity of species 2 occurs at R=10. But, we have no knowledge of the

exact surfactant concentration that can achieve this maximum from Figure 3.4. This leads us to plot Figure 4.1.

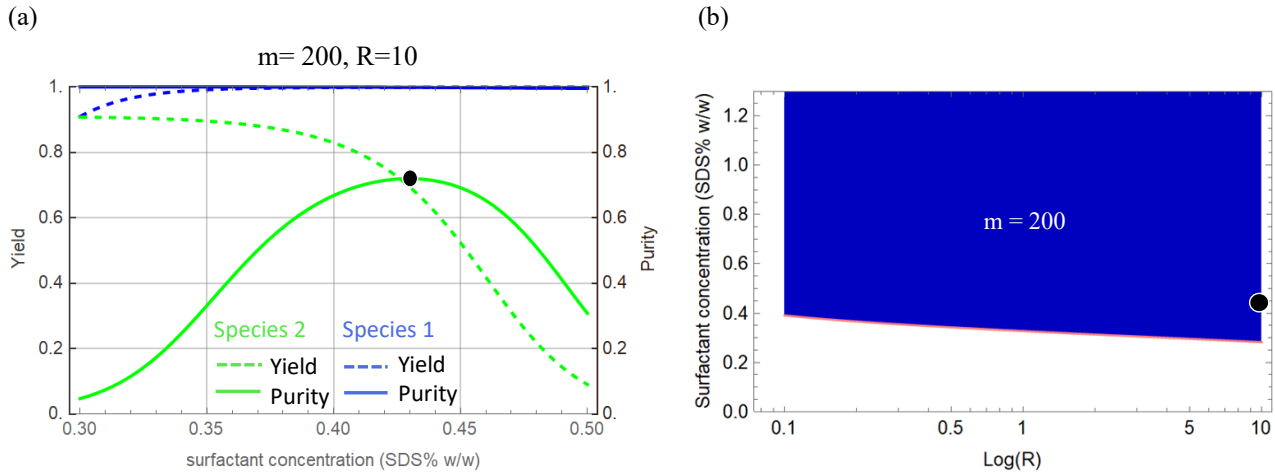

Figure 4. 1. The location of the best possible condition for the first stage at m=200. (a) Yield and purity are plotted as a function of surfactant concentration at m=200 and R=10. Yield is on the left y-axis, depicted by dashed curves. Purity is on the right y-axis, depicted by solid curves. The surfactant concentration is on the x-axis. Species 1 and species 2 are colored blue and green, respectively. The black dot is used to demonstrate the location of the chosen best possible point and its corresponding yield and purity. (b) A reprint of Figure 3.6. A black dot is added to the original plot to illustrate the surfactant concentration and volume ratio at best possible point and its relevant location compared to other threshold-satisfying experimental conditions.

In Figure 4.1, the two blue curves for species 1 are near 1 at all surfactant concentrations, which verifies our conclusion about the yield and purity of species 1 drawn earlier in this section. For species 2, the yield decreases with an increasing surfactant concentration and the purity peaks at a surfactant concentration near 0.43 wt%. Using the model, we calculate the exact surfactant concentration of this maximum-purity point to be x=0.4297, which can be rounded to 0.43 wt%. Plugging this number back into Equation 4.1 through 4.8, we compute the following table.

Experimental conditions		Phase	Top (T)		Bottom (B)	
Surfactant concentration (x)	0.43 wt%	Species type	Species 1	Species 2	Species 1	Species 2
Volume ratio (R)	10	Yield	0.9986	0.3041	0.0014	0.6959
		Purity	0.9985	0.0015	0.2806	0.7194
		Output mass ratio (m)	656.69 (m_T)		0.39 (m_B)	

Table 4. 1. Experimental conditions and separation results at the best possible point in the first stage for m=200.

In Table 4.1, the experimental conditions are shaded in grey, while the separation results are shaded in green. Once again, we see that species 1 achieves a very high yield and purity in the top phase. Species 2 achieves a relatively high yield and purity in the bottom phase, which does not pass the 0.8 thresholds. It is worth pointing out that the yield for species 2 in the top phase is around 0.3, which means 30% of species 2 will go to waste if only one-stage separation is performed. The output mass ratio in the top phase m_T is much higher than m_B in the bottom phase, indicating the first-stage operation is very efficient at concentrating and purifying species 1 while not so efficient for species 2. Going into the second stage, we will use the separation results in Table 4.1 as the inputs or the initial conditions for the next step.

4.4 Some rules to aid decision making at the second stage

The top (T) phase and the bottom (B) phase from the first stage are now two physically separated compartments. The experimental conditions applied to one phase do not interfere with those applied to the other phase. Decisions on what experimental conditions are the best for the second stage are made independently for the T and B phases. When a second stage separation is performed, the T-phase compartment goes through a phase separation process and forms TT and TB phases. The TT and TB phases do share the same experimental conditions because they are still physically connected. This process is also valid for the B-phase compartment, which eventually separates into BT and BB phases.

Another rule is that the same phase cannot be selected as the final phase for both species. For example, if the TT phase is selected as the final phase for species 1, this phase can only be counted towards the final product of species 1. Even though there might be traces of species 2, we do not count the mass of species 2 in the TT phase as a contributor to the final product of species 2. This rule applies to one-stage separation as well. If the separation stops after the first stage for the m=200 example, the T phase becomes the final phase for species 1 while the B phase is picked for species 2. Although there is about 30% of species 2 in the T phase, we do not count it. We only count the other 70% from the B phase and say this separation has a yield of 0.7 for species 2. We would not sum up the 30% and 70% and say the final product of species 2 has a yield of 1. This rule might seem quite obvious now, but adding more phases makes it easier to lose sight.

The third rule is a logical deduction from the second rule. Because once phase A is selected as the final phase for species x, it cannot be counted towards species y. We want phase A to have as little species y as possible. This rule can help select the more rewarding experimental conditions.

The fourth rule summarizes what we have done in the first stage of a multi-stage separation process for samples with m=200. In chapter 3, we seek a surfactant concentration range that permits the yield and purity for both species to pass the threshold. At the beginning of this chapter, we switch to looking for the best possible point, knowing that the threshold can never be met simultaneously for both species. To summarize, we opt to search for a point instead of a range of experimental conditions. Given that no range can satisfy the threshold reaching for an optimal point at this particular separation stage is more practical. It also ensures the best input parameters for the next stage.

4.5 Selecting the operating conditions at the second stage for a specific volume ratio

At the second stage, we have two sets of experiments to run in parallel, one for the T phase and another for the B phase. After the separation, each phase evolves into two new phases, which contributes to a total of four phases at the end of the second stage. This means we need to analyze and make decisions about two sets of experimental conditions and report the separation results for four phases. The computation workload doubles compared to the one-stage process. For n-stage separation, the parameter space grows exponentially, which explains why building a model to assist decision-making is essential for the development of CNT separation, which has been largely studied by experiments only.

The initial conditions for the second stage are listed in Table 4.1. The two experimental parameters we have control over are surfactant concentrations x and volume ratio R. We will follow the same steps as in chapter 3 to explore the large parameter space. First, we plot yield and purity as a function of surfactant concentration at a specific R value as an example to demonstrate how surfactant concentration influences the separation results. We use R=1 to plot Figure 4.2.

The TT and TB phases are physically connected and generated by the T phase, which contains more than 99% of species 1 and about 30% of species 2. When the surfactant concentration x is less than 0.2 wt%, the TT phase has the majority of species 1. When x>0.4 wt%, the TB phase is dominating for species 1. Without other constraints, both the TT and the TB phases can be selected as the final phase for species 1. According to the third rule in section 4.4, if a phase is chosen for species 1, we want as little species 2 as possible in that phase. If choosing the TT phase, the ideal operating surfactant concentration will be 0.4 wt%, which provides a yield of species 1 at almost 1 and a yield of species 2 at 0. This way, a minimum amount of species 2 is wasted in the final product of species 1. If choosing the TB phase, the optimal operating surfactant

concentration is x<0.2 wt%. Under this range, the yield of species 1 is approximately 1, which is desirable for the final phase. However, under the same condition, species 2 also has a yield of 0.3, which means 30% of species 2 will be wasted in the final product of species 1. This comparison between the two phases leads us to conclude that the TT phase is better suited as the final phase of species 1 when operating at R=1.

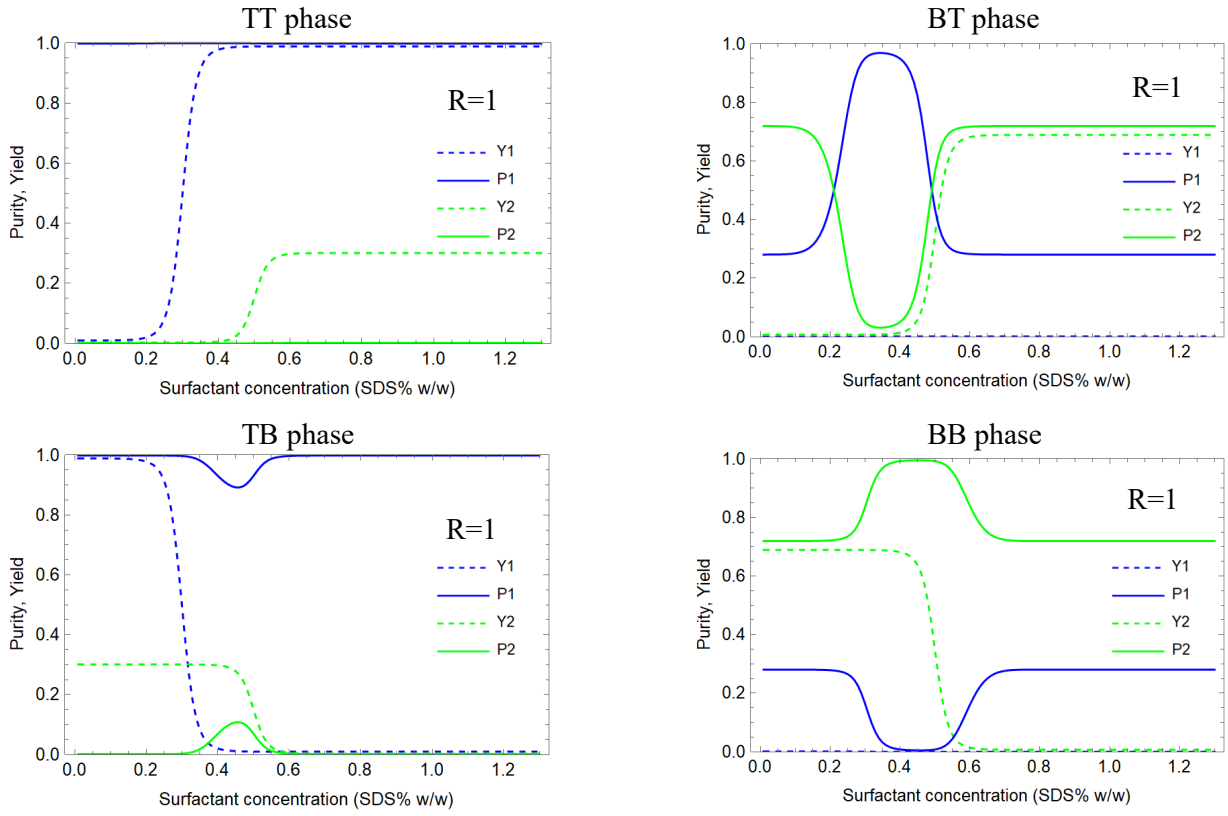

Figure 4. 2. Yield and purity are plotted as a function of surfactant concentration at R=1 for each phase in the second stage separation. The second-stage separation produces four phases, TT, TB, BT, and BB. The first two phases belong to the same aqueous two-phase system, which has one set of experimental conditions (x and R). The latter two phases belong to another two-phase system, with a different set of surfactant concentrations and volume ratio. The experimental conditions of each two-phase system are independently evaluated. Species 1 is colored in blue, and species 2 is in green. The solid curves denote purity, while the dashed curves denote yield. The yield reported here is overall yield, which compares the mass of a species in one phase to the mass of such species in the original sample. The overall yield is not calculated in the same way as the yield we use in chapter 3.

In the BT and BB phases, we prioritize achieving higher yield and purity for species 2. If the BT is chosen as the final phase for species 2, the preferable operating surfactant concentration is x>0.6 wt%, which results in both yield and purity reaching 0.7. Comparing this result to the

output values from the B phase in Table 4.1, neither yield nor purity for species 2 experiences a significant change in the second stage. In this case, operating a second-stage operation under this particular experiment condition does not help get closer to the separation goal. If the BB phase is chosen for species 2, the more suitable operating surfactant concentration is $0.35<x<0.45$ wt%. Within this range, the yield for species 2 is still around 0.7, but the purity rises up to the proximity of 1. Therefore, at R=1, we choose the BB phase as the final phase for species 2. Because more than 99% of species 1 is already tuned into the TT phase, the amount of species 1 left in either the BT or BB phase is negligible. As a result, we do not need to consider this aspect when selecting the operating conditions for those two phases.

4.6 Compare the second–stage results; at all *R* values for the T-phase compartment

In the previous section, we walked through the entire process of selecting a more advantageous experimental condition for the second-stage separation at one *R* value. In this section, we expand the volume ratio to the entire 0.1-10 range. Because the T-phase and the B-phase compartments are considered two different systems, we will first study the T-phase system in this section and then the B-phase system in the next section. Following the same approach we take in Chapter 3, the range of all possible purity and the maximum yield is plotted against the volume ratio for both species in each phase. From the analysis in the previous section, we learn the importance of the yield difference between species 1 and 2 and how it narrows down the choices of experimental conditions. Thus, we also plot $Y_1 - Y_2$ as a function of surfactant concentration for multiple values of volume ratio *R*.

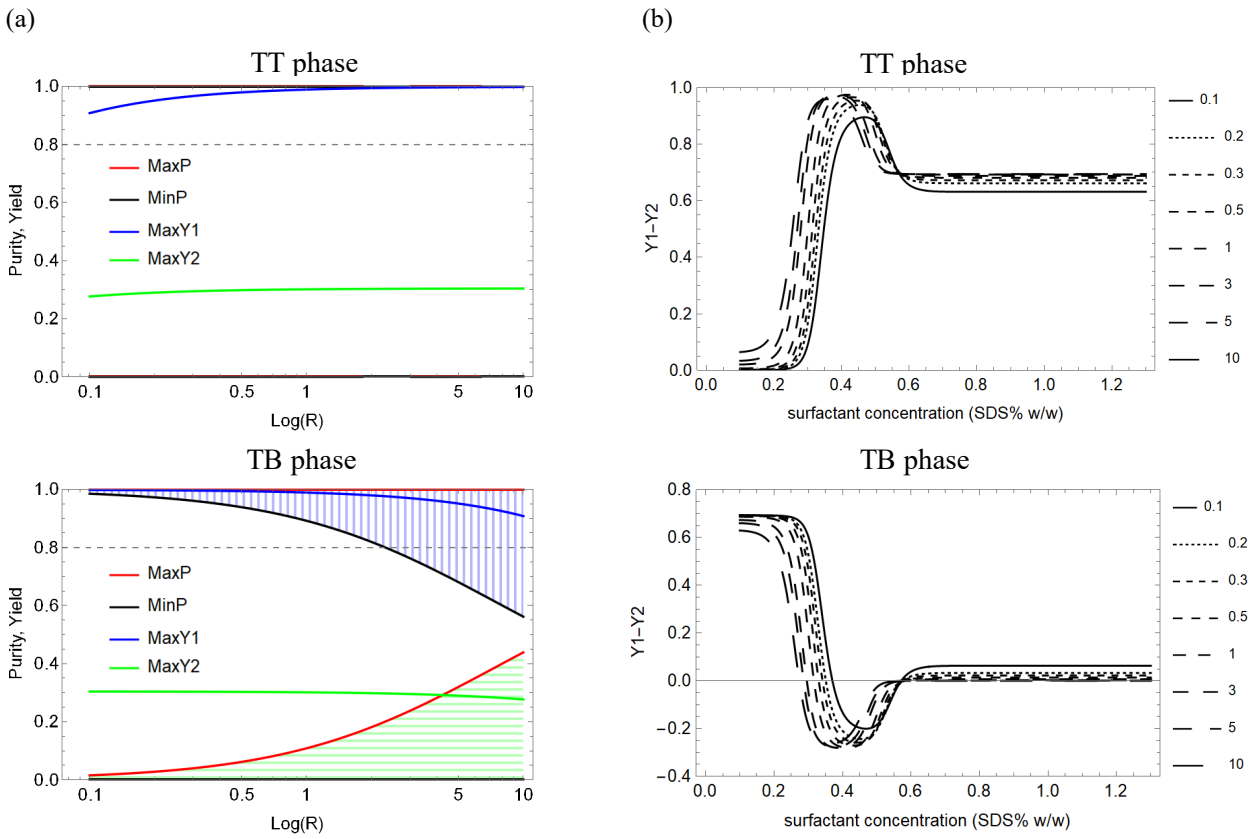

Figure 4. 3. The separation results for all *R* values in the TT and TB phases. (a) The maximum and minimum purity and the maximum yield are plotted as a function of the volume ratio *R* for both species 1 and 2 in each phase. The maximum purity is depicted by red lines, and the minimum purity is depicted by black lines. The spacing between the maximum and minimum purity is shaded with hatching lines, blue and vertical for species 1 and green and horizontal for species 2. The maximum yield for species 1 is the blue line, and the maximum yield is the green line. A dashed grey line is also plotted as a guideline for the 0.8 threshold. (b) The yield difference between species 1 and 2 is plotted against the surfactant concentration at eight exemplary *R* values. The spacing between the dashed lines corresponds to the *R* value. The narrower the spacing, the smaller the *R* value.

Focusing on Figure 4.3 (a), we realize the maximum yield and purity for species 1 stay close to 1 in both TT and TB phases at all *R* values. This finding is also supported by Figure 4.2. For species 2, however, the maximum yield is no more than 0.3 in both phases, and the maximum purity is almost 0 in the TT phase and less than 0.45 in the TB phase. Based on the fourth rule in section 4.4, when analyzing and comparing all experimental conditions, we need to work towards finding a point with the optimal separation outputs instead of a range that can satisfy the 0.8 thresholds for both species.

Both the TT and TB phases can be selected as the final product phase for species 1, given their high yield and purity. However, it should be noted that not all surfactant concentrations can produce the maximum purity and yield plotted in Figure 4.3. The maximum-achieving surfactant concentration is different in different phases and at different *R* values. Thus, we still need to compare other separation outputs produced by these maximum-achieving surfactant concentrations before making the final decision. Following the third rule in section 4.4, the TT phase is the better option because it provides a more considerable yield difference between species 1 and 2. The two plots in Figure 4.3(b) show that the yield difference between the two species can rise above 0.8 at all volume ratios in the TT phase but is less than 0.7 in the TB phase. Selecting the TT phase for species 1 allows two species to be more separated into two different phases and saves more species 2 from being wasted in the final product of species 1. The yield difference in the TT phase grows larger with increasing *R* values, and the largest yield difference occurs when surfactant concentration is 0.4 at *R*=10. In the TB phase, the experimental condition at *x*=0.4 and *R*=10 offers the smallest negative value of $Y_1 - Y_2$, indicating good preservation of species 2 with the minimum trace of species 1. Speaking only from the yield perspective, *x*=0.4 and *R*=10 seem to be the best operating point for both species 1 and 2.

However, besides pursuing a high yield, we also want to obtain a high purity for species 2 in the TB phase. From Figure 3.4, we know that the highest purity can be achieved occur at *R*=10. To help us further investigate the exact surfactant concentrated needed to achieve this high purity, we plot Figure 4.4

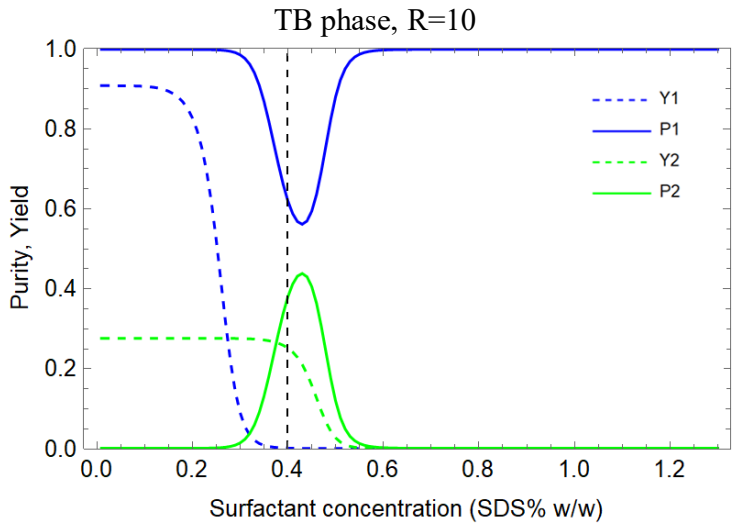

Figure 4. 4. The purity and yield vs. surfactant concentration plot at *R*=10 for the TB phase. Species 1 is plotted with blue curves, and species 2 is plotted with green curves. The solid curves are purity, while the dashed curves are yield. The *x*=0.4 line is added for easy comparison.

Figure 4.4 shows that the maximum purity of species 2 is produced at a surfactant concentration around *x*=0.45. However, at this surfactant concentration, the yield drops to half of its maximum value. This observation proves our conclusion in chapter 3 that yield and purity do not peak simultaneously, and a trade-off has to be made. At *x*=0.4, the best operating concentration from the yield perspective, the purity for species 2 is only slightly below the maximum value. After weighing the pros and cons for both yield and purity for both species, we decide the best operating condition for the T-phase compartment is at *x*= 0.4 and *R*=10. Applying this experimental condition to the T-phase compartment, we get the following output parameters.

Experimental conditions		Phase	TT		TB	
Surfactant concentration (*x*)	0.4 wt%	Species type	Species 1	Species 2	Species 1	Species 2
Volume ratio (*R*)	10	Yield	0.9966	0.0520	0.0021	0.2521
		Purity	0.9997	0.0003	0.6200	0.3800
		Output mass ratio (*m*)	3831.21 (m_{TT})		1.63 (m_{TB})	

Table 4. 2. The separation outputs in the second stage from the T-phase compartment at *x*=0.4 and *R*=10.

4.7 Compare the second–stage results at all *R* values for the B-phase compartment

After picking out the optimal operating conditions for the T-phase compartment, we move on to the B-phase compartment and run the same analysis. An equivalent plot to Figure 4.3 is generated for the BT and BB phases.

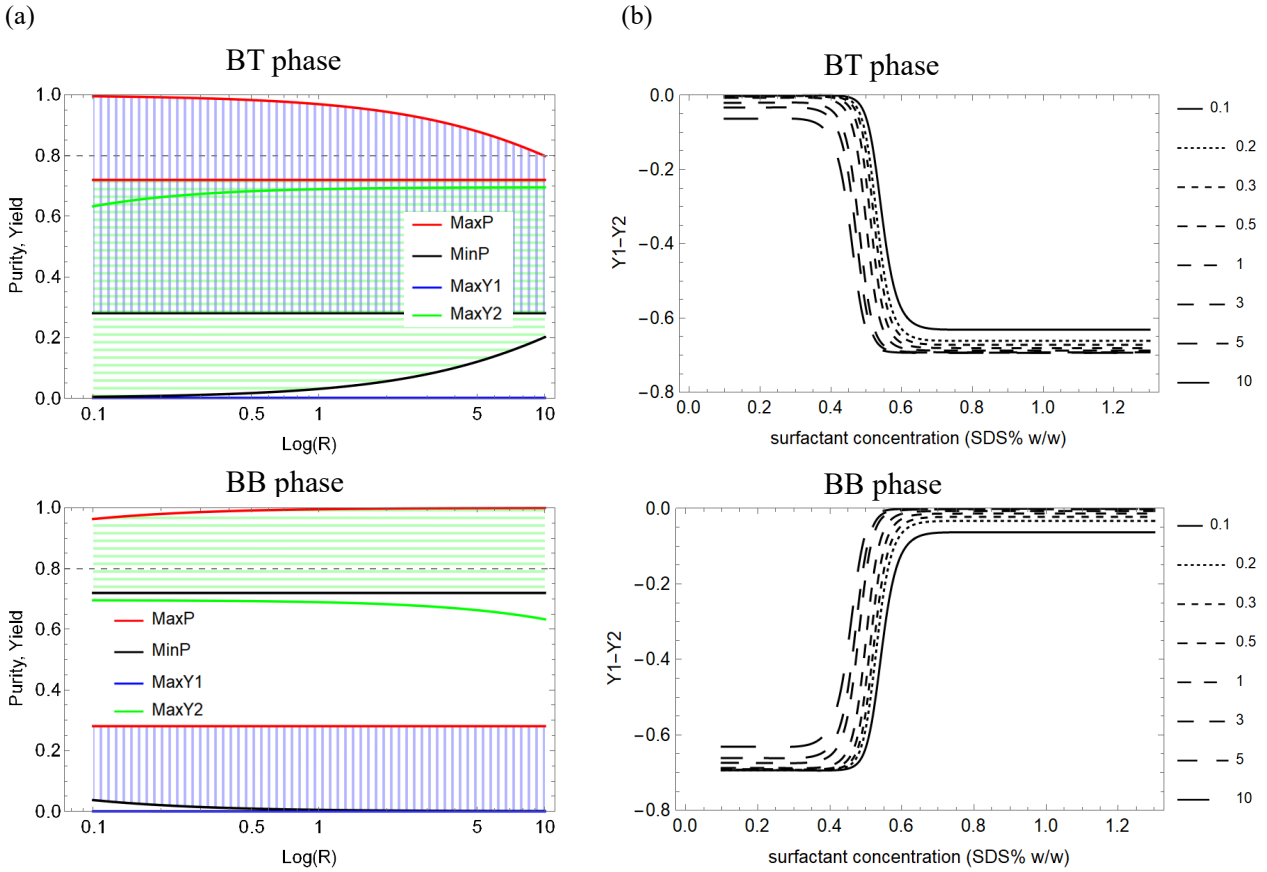

Figure 4. 5. The separation results for all *R* values in the BT and BB phases. (a) The maximum and minimum purity and the maximum yield are plotted as a function of the volume ratio *R* for both species 1 and 2 in each phase. The maximum purity is drawn with red lines, and the minimum purity is drawn with black lines. The spacing between the maximum and minimum purity is shaded with hatching lines, blue and vertical for species 1 and green and horizontal for species 2. The maximum yield for species 1 and 2 is the blue and the green line, respectively. A dashed grey line is added as a guideline for ease reference to the 0.8 threshold. (b) The yield difference between species 1 and 2 is plotted against the surfactant concentration at eight exemplary *R* values. The length of the dashed segment corresponds to the *R* value. The shorter the segment, the smaller the *R* value.

Since species 1 already has the TT phase as its final phase, we need to focus on deciding which phase is the most appropriate for concentrating species 2. Hence, in this section, a higher yield and purity of species 2 will be prioritized when comparing the experimental conditions.

In Figure 4.5 (a), the maximum purity for species 2 is constantly below 0.8 in the BT phase, while in the BB phase, it is close to 1 at all volume ratios. A second-stage separation has to be performed because the purity of species 2 cannot reach the 0.8 thresholds in the first stage. Therefore, we should only consider the experimental conditions that can produce a purity greater than 0.8 for species 2. Following this reason, the BB phase is selected as the final phase for species 2. Because the maximum purity for species 2 is above the 0.8 threshold at all *R* values, we know that there is always a range of surfactant concentrations that can achieve this goal at any given *R*. Though, the exact location of the surfactant range varies for different *R* values. We can now narrow down the choices of experimental conditions by considering the limitations on yield since the purity threshold is met at all volume ratios. In the BB phase, the maximum yield of species 2 decreases as the volume ratio increases, and it is always smaller than 0.8. At this point, one might notice that it is still not possible for the yield and purity of species 2 to pass the 0.8 thresholds simultaneously even after doing one more separation stage. We will discuss this in more detail in the next section. In this section, we stay focused on finding the optimal experimental conditions within the possible range. Since yield decreases with volume ratio, we can obtain the highest yield possible at the smallest R=0.1. To find out the exact surfactant concentration that produces this highest yield, we plot Figure 4.6.

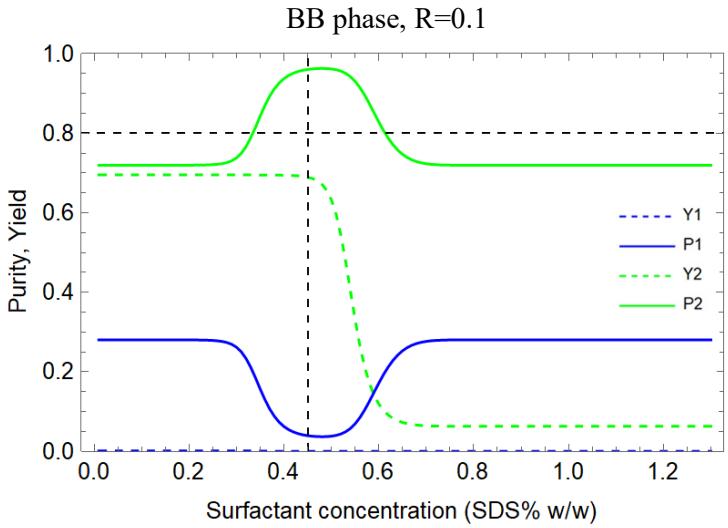

Figure 4. 6. The purity and yield vs. surfactant concentration plot at R=0.1 for the BB phase. Species 1 is plotted in blue, and species 2 is plotted in green. The solid curves are purity, and the dashed curves are yield. The x=0.45 and y=0.8 lines are added for easy comparison.

The highest yield occurs for x<0.45 wt%. Based on the fourth rule in section 4.4, we seek an optimal operating point instead of a range when it is proven that yield and purity cannot pass the threshold at the same time. Therefore, we look for a surfactant concentration and volume ratio combination that produces the highest possible yield and purity. The highest purity occurs between x=0.45 wt% and x=0.5 wt%. Once again, the yield and purity do not peak at the same time. Considering that the difference in purity between x=0.45 and the maximum point is smaller than the difference in yield at these two points, we choose x=0.45 wt% and R=0.1 as the best operating condition for the B-phase compartment. Applying this experimental condition to the B-phase compartment, we get the following output parameters in Table 4.3.

Experimental conditions		Phase	BT		BB	
Surfactant concentration (x)	0.45 wt%	Species type	Species 1	Species 2	Species 1	Species 2
Volume ratio (R)	0.1	Yield	0.0012	0.0063	0.0001	0.6896
		Purity	0.9748	0.0252	0.0396	0.9604
		Output mass ratio (m)	38.72 (m_{BT})		0.04 (m_{BB})	

Table 4.3. The separation outputs in the second stage from the B-phase compartment at x=0.45 and R=0.1.

4.8 Alternatives when no separated phase can meet the threshold for one species

To summarize the two-stage separation that we study, the following cartoon is drawn.

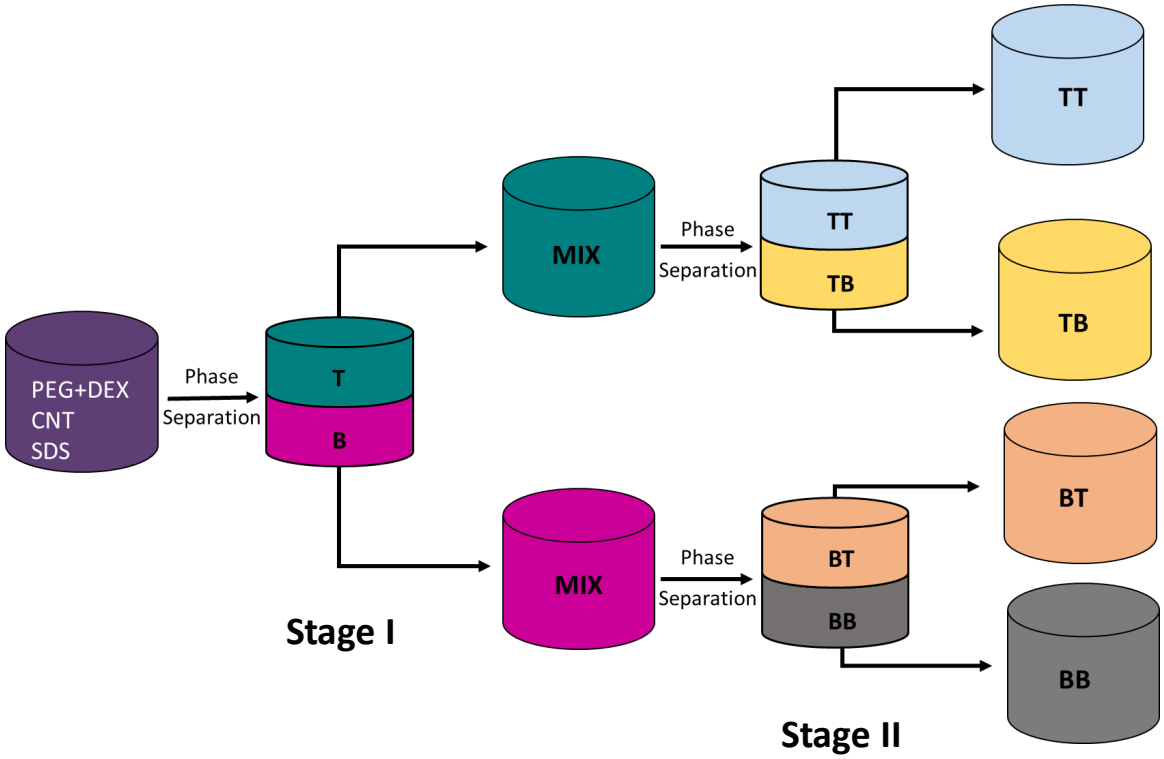

Figure 4. 7. A schematic of a two-stage aqueous two-phase separation process.

In Figure 4.7, the drawing stops at the second-stage separation. In reality, each of the four compartments at the end of the second stage can form a new two-phase system and go through more separation steps if polymers and surfactants are added. If the separation stops at the second stage, our analysis shows that the TT phase should be used to extract the final product of species 1, and the BB phase should be used for species 2. However, we also realize that the yield and purity for species 2 still cannot pass the 0.8 separation threshold concurrently even after performing the second stage. The purity does improve significantly from 0.7 in the B phase to 0.96 in the BB phase. This improvement, however, is at a small expense of yield, which decreases from 0.6959 in the B phase to 0.6896 in the BB phase. It is reasonable to expect the values of yield to decrease as more separation stages are performed, since each additional separation stage results in

additional compartments in which CNT species will migrate. However, the total mass of a given CNT species does not change. With additional stages, the constant total mass of a given CNT species is distributed into more compartments, which naturally leads to a smaller yield for each compartment. Purity is expected to increase with the number of separation stages since each stage of the two-phase extraction process is designed to concentrate each CNT species into a different compartment.

Because the yield for species 2 is still less than 0.7, we try to think of another way to recover more materials during the entire separation process. Besides the BB phase, the TB phase contains most species 2, about 25% of the total mass. The purity in the TB, however, is relatively low at 0.38. Since the purity in the BB phase is much higher than the 0.8 thresholds, we think combining the TB and BB phase might lead to a new system that has both yield and purity passing the threshold. The idea is illustrated in Figure 4.8.

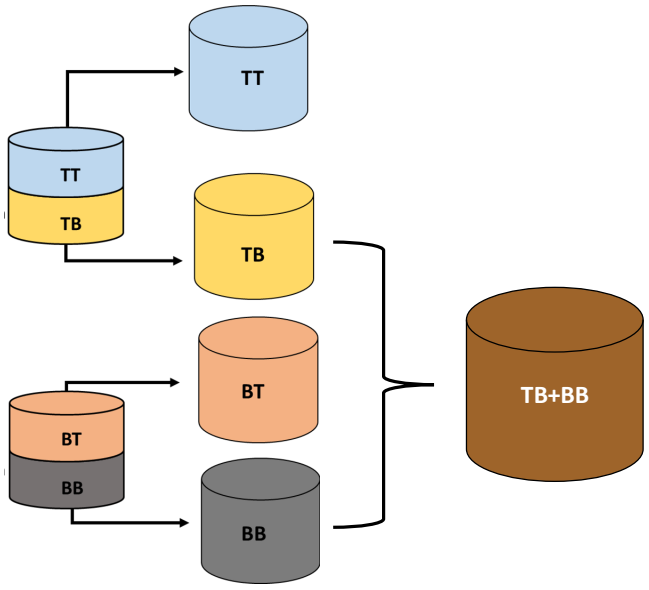

Figure 4. 8. Illustration of combining the TB and BB phase.

The yield of species 2 increases to 0.95 in the TB+BB compartment. Yield can be obtained by simple addition because the reported yields are overall yield, defined as the mass in the final

phase divided by the mass in the original sample. The purity of species 2 decreases to 0.68 in the combined compartment. Purity is calculated using the mass ratio *m* and purity reported for each of the four phases (T, TB, B, and BB). Comparing the results of species 1 after a two-stage separation, we also notice a slight decrease in yield with a small gain in purity from the first stage to the second stage. As a result, we conclude that doing more separation stages can significantly increase either yield or purity, but it cannot increase both. Consequently, a trade-off has to be made between yield and purity, which is a conclusion consistently made under different circumstances in our analysis.

Overall, performing a two-stage separation helps improve the mass ratio between species 1 and species 2 from 200 in the original sample (m) to 3831 in the TT phase (m_{TT}) and 0.04 in the BB phase (m_{BB}). The ratio of *m* is called enrichment. For species 1, the enrichment is 19.2, which means the final product of species 1 is more than 19 times more concentrated than the original sample. For species 2, the enrichment is 4855, which is quite impressive. Large enrichment for both species proves the two-stage separation process is very efficient at separating and purifying different types of CNT species.

4.9 Limitations on reaching the computed experimental conditions

So far, we have assumed that all volume ratios (0.1-10) and surfactant concentrations (0.1-1.3 wt%) can be reached freely in real-life experiments. This is true for the first-stage separation, where any amount of surfactant and polymers can be added to the original sample. However, the feasibility of creating any surfactant concentration or volume ratio becomes questionable at the second stage and beyond.

We examine the real-world situation for the surfactant concentration first. One assumption we make is that the surfactant is uniformly distributed within any two-phase system. This assumption requires the same surfactant concentration within each of the following phase pairs: T-B, TT-TB, and BT-BB. We also assume that the physical separation of two phases does not alter the surfactant concentration in each phase. In reality, surfactants stick to the interface, contributing to a lower surfactant concentration in the phase compartment than the total surfactant added to the system[31,78]. We neglected this effort in our analysis. We assume no water is added to the system after the first stage to avoid diluting the CNT species. As a result, the volume of each phase remains the same throughout the separation process. This also means that concentrations in any phase can only increase, for both surfactants and polymers, starting from the second stage. Revisiting the surfactant concentrations used in the second stage, we suggested x=0.4 for the T phase and x=0.45 for the B phase. In the first stage, the optimal surfactant concentration is 0.43 wt%, which permits the conditions in the B phase but denies the conditions in the T phase. In other words, the lowest surfactant concentration that can be used for the T-phase is 0.43 wt%, with no extra surfactant added during the second stage. Even without changing surfactant concentration, a new separation can still be performed for the T-phase by adding more polymers and re-establishing a new two-phase system. From Figures 4.3 and 4.4, it can be found that the surfactant concentration at 0.43

wt% produces a slightly higher purity and lower yield for species 2 and almost has no effect on the results for species 1, compared to the proposed optimal of x=0.4.

Next, we examine the possibility of all volume ratios used. Volume ratios are determined by the composition of the phase-forming polymers, PEG, and DEX in our case. Volume ratio can be predicted using a phase diagram and tie lines.

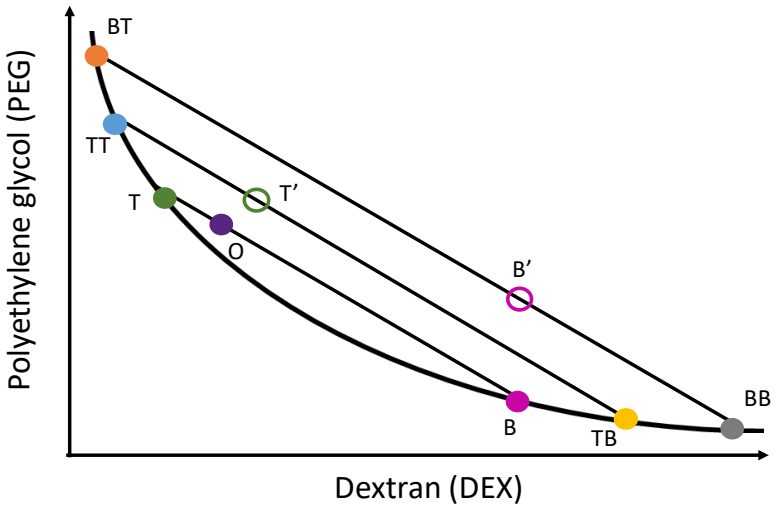

Figure 4. 9. A schematic of the phase diagram for a PEG-DEX system. The composition of DEX is on the x-axis, and the composition of PEG is on the y-axis. The color of the dots corresponds to the phase color in Figure 4.7: purple-original sample, green-T phase, magenta-B phase, blue-TT phase, yellow-TB phase, orange-BT phase, and gray-BB phase. The hollow dots are the T phase (green) and the B phase (magenta) after adding polymers but before forming a new two-phase system.

A phase diagram is composed of a binodal curve and multiple tie-lines[38,79–81]. The binodal curve, also called the co-existence curve, specifies the boundary compositions needed to form a two-phase system. Solutions with polymer compositions below the curve remain as one phase. Once the compositions of two polymers rise above the curve, the solution forms a two-phase system. The tie-lines predict the polymer compositions in the top and bottom phases after a two-phase solution reaches equilibrium. For the first-stage CNT separation process, the amount of PEG and DEX added to the original sample is shown by the purple dot (O). The two polymers spontaneously undergo a phase separation process and form a two-phase system. The new top and

bottom phases have polymer compositions indicated by the green (T), and magenta (B) intercepts of the tie line and the binodal curve. The length ratio between O-B and O-T is the volume ratio between the top and bottom phases, defined as *R* in our model. To achieve a volume ratio of 10 in the first stage, we can move the location of the purple dot along the same tie-line until the O-B:O-T=10:1. In the second stage, we need volume ratios of 10 for the T phase and 0.1 for the B phase. For the T phase, we can achieve this volume ratio by adding more DEX until the compositions of two polymers arrive at a new tie-line with T'-TB:T'-TT equals 10. Similarly, for the B phase, we can add more PEG until the polymer compositions reach a B' point which has B'-BB:B'-BT=1:10. By utilizing the phase diagram, we confirm that all volume ratios needed for the two-stage operation can be realized in experiments by varying the PEG and DEX compositions.

After considering the limitations imposed by other experimental parameters, we adjust the proposed optimal operating conditions for the T phase shown in Table 4.2. The new sets of conditions and separation outputs are tabulated below. The results for the B phase listed in Table 4.3 remain unchanged.

Experimental conditions		Phase	TT		TB	
Surfactant concentration (x)	0.43 wt%	Species type	Species 1	Species 2	Species 1	Species 2
Volume ratio (R)	10	Yield	0.9974	0.0930	0.0013	0.2110
		Purity	0.9995	0.0004	0.5615	0.4385
		Output mass ratio (m)	2498.75 (m_{TT})		1.28 (m_{TB})	

Table 4.4. The separation outputs in the second stage from the T-phase compartment at x=0.43 and R=10.

4.10 Summary

In this chapter, we use the model to simulate a multi-stage separation process between two CNT species. Before going into the second stage, the CNT sample with m=200 is processed in the first stage with a surfactant concentration that facilitates the highest possible outcome of yield and purity. Four additional separation rules are clarified to guide decision-making when more complex situations arise. After the first stage, the original aqueous two-phase system divides into two new phase systems. Each phase system is analyzed independently. At the most desirable operating conditions, species 1 is concentrated nearly 20 times, and species 2 is concentrated almost 5000 times, speaking loudly for the capability of a two-stage aqueous two-phase extraction process. It is also found that an increase in purity is always at the expense of a yield reduction and vice versa. Despite that performing more stages cannot improve yield and purity concurrently, it can increase one of them significantly. Lastly, the possibility of reaching the calculated optimal conditions in experiments is reviewed. As a result, the proposed surfactant concentration in the second stage is adjusted, which lowered the overall performance slightly.

Chapter 5: Vary three species-specific parameters *a*, *b*, and *c* in the model

5.1 Introduction

In the previous two chapters, we study and compare the separation results between one-stage and two-stage operations. These separations only involve two CNT species. Moreover, the only difference between these two species is their *b* values, the crossover surfactant concentration. We purposely limit the number and the types of CNT species to quickly adapt the model to simulate an entire separation process and obtain general trend information. In this chapter, we will expand the representations of CNT species by varying parameters *a*, *b*, and *c* in the model. Different *a*, *b*, and *c* values are used to describe the unique partitioning behavior shown by different carbon nanotubes. Only one-stage separation results are computed for easy comparison to results in the earlier chapters.

The first parameter we will vary is *b*. There are two *b* values for two different CNT species, b_1 for species 1 and b_2 for species 2. Instead of individually changing b_1 or b_2, we will treat the interval between them as the variable. Previous results show that the optimal separation surfactant concentration lies between b_1 and b_2. Thus, we will vary the width and location of the interval between b_1 and b_2, and call it $b_1 - b_2$ in the following discussions. For parameters *a* and *c*, we will examine the effect of an increase and a decrease for each parameter. Because the effect of parameter changes on species 1 and species 2 are not interchangeable, we will individually adjust the *a* and *c* parameters for species 1 and species 2 separately.

5.2 Vary parameter *b* in the model

There are many ways to vary the $b_1 - b_2$ range. In this section, we categorize all possibilities into five different groups. A schematic is drawn to show the relativity among these five groups. However, the location and the width of the $b_1 - b_2$ interval is not up to scale and only serve for illustration purposes.

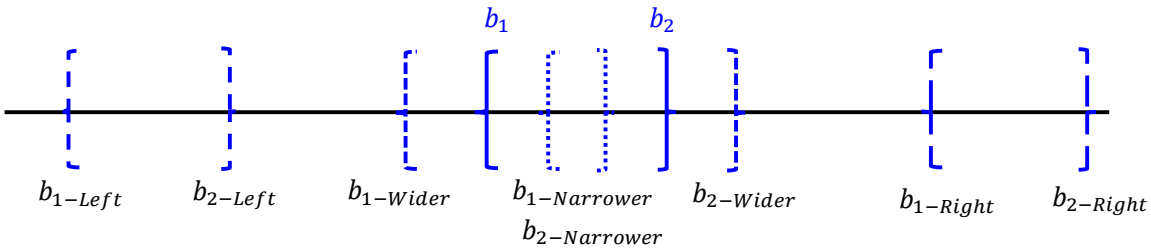

Figure 5. 1. A schematic of five different ways to vary the $\boldsymbol{b_1 - b_2}$ interval. Two examples vary the width of the interval while keeping the middle point of $\boldsymbol{b_1}$ and $\boldsymbol{b_2}$ the same. The $\boldsymbol{b_1 - b_2}$ interval can be varied wider and narrower than the original example. Another two examples vary the location of the interval while keeping the width consistent. The $\boldsymbol{b_1 - b_2}$ interval can be on the left or the right of the original location.

To study how changes of the $b_1 - b_2$ interval affect the separation results, we follow the same approach used in the previous two chapters. Purity is plotted as a function of volume ratios. The maximum and minimum purity are reported to help visualize the range of all possible purity values at a given *R* value. The maximum yield is not plotted here because it does not change when varying the $b_1 - b_2$ interval. Yield is a function of partition coefficient *K* and volume ratio *R*. The maximum yield at a specific *R* is obtained at the asymptotes of the partition coefficient curve. The asymptotes of partition coefficient curves only change when parameter *c* is altered. Besides plotting the purity vs. volume ratio, we also plot the surfactant concentration ranges that satisfy the 0.8 thresholds for both purity and yield as a function of the volume ratio. The exact *b* values used to generate the plots are tabulated in the following table.

b_1	b_2	$b_{1-Wider}$	$b_{2-Wider}$	$b_{1-Narrower}$	$b_{2-Narrower}$	b_{1-Left}	b_{2-Left}	$b_{1-Right}$	$b_{2-Right}$
0.3	0.5	0.2	0.6	0.35	0.45	0.15	0.35	0.6	0.8

Table 5. 1. Values of $\boldsymbol{b_1}$ and $\boldsymbol{b_2}$ for five different variations of the $\boldsymbol{b_1 - b_2}$ interval.

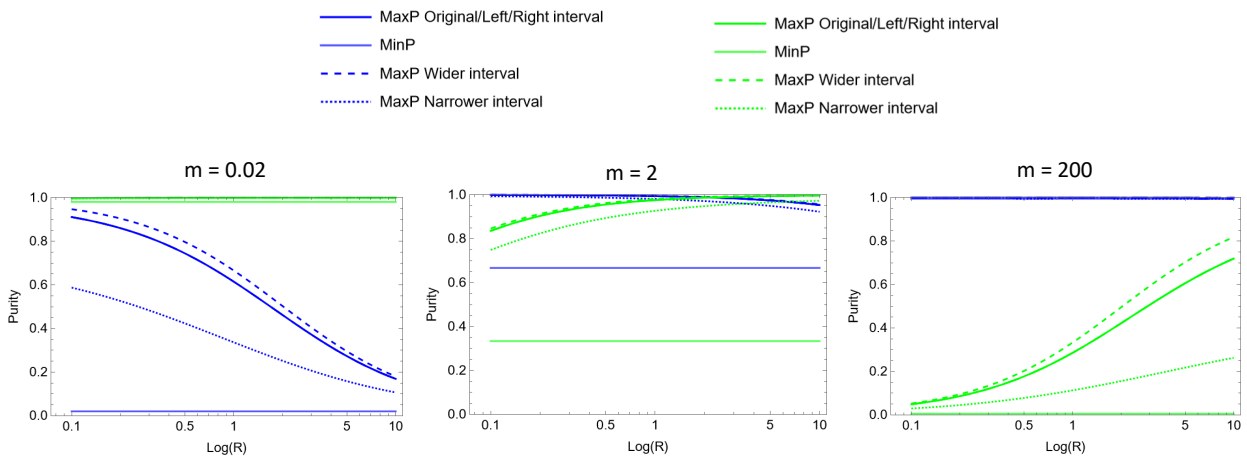

Figure 5. 2. The maximum and minimum purity of species 1 and 2 are plotted as a function of volume ratio at three different *m* values. Data of species 1 are plotted in blue, and data of species 2 data are plotted in green. The data for the original $\boldsymbol{b_1 - b_2}$ interval is plotted using solid lines. The wider $\boldsymbol{b_1 - b_2}$ interval is drawn with longer dashed lines, while the narrower $\boldsymbol{b_1 - b_2}$ interval is drawn with shorter dashed lines. The purity values for the original, shifted-left, and shifted-right variations are numerically the same, and therefore, they are illustrated by the same solid

The numerical values of the maximum purity are the same for the original, shifted-left, and shifted-right variations. Thus, they are shown by one single line. This similarity will be discussed later in this section. At a fixed *m* value, the minimum purity values are the same for all five variations of the $b_1 - b_2$ interval. This can be explained by examining the experimental condition that generates the minimum purity. The goal of separation is to concentrate or purify CNT species. Consequently, we expect the purity to increase along a separation process. The minimum purity, therefore, occurs at the initial condition, which is characterized by the initial mass ratio *m*. When the value of *m* is fixed, the minimum purity should remain the same as well. The general trends of the purity in Figure 5.2 are analogous to those in Figure 3.4. At *m*=0.02, the purity range of species 1 shrinks with an increasing volume ratio. Species 2 has purity close to 1 regardless of volume ratio and surfactant concentration due to the low initial mass ratio (specie 1:species 2=1:50). The situation for species 1 and 2 are reversed at *m*=200 when species 1 replaces species 2 to become the dominating species. At *m*=2, both species can meet the purity threshold with some surfactant concentrations for any given volume ratio. A new trend shown in Figure 5.2 is that a wider $b_1 -$

b_2 interval can provide a wider purity range while a narrower $b_1 - b_2$ interval leads to a narrower purity range. In comparison, the original, shifted-left, and shifted-right variations have the same purity values. The wider and narrower variations adjust the width of the $b_1 - b_2$ interval, while the shifted-left and shifted-right examples move the location of the $b_1 - b_2$ interval on the x-axis in a partition coefficient plot. Comparing the results generated by these two types of adjustments, it is found that changes in the location of the interval do not affect the maximum and minimum purity. However, changes in the width of the interval do impact the purity values. In other words, any two CNT species, whose $b_1 - b_2$ intervals have the same width, will have the same separation results.

In order to know the exact surfactant concentrations needed to pass the separation threshold (yield>0.8 and purity>0.8), we plot the threshold-meeting surfactant concentrations as a function of volume ratio at three different m values in Figure 5.3. Figure 5.3 is equivalent to Figure 3.5, except that five variations of $b_1 - b_2$ are discussed instead of one. There are two schemes to help identify these five variations, 1) different-spaced dashed lines to outline the upper and lower boundaries of surfactant concentrations and 2) different-colored shaded regions that fill between the surfactant concentration boundaries. If the shading for one variation does not obstruct the boundaries for other variations, the color scheme is prioritized. Otherwise, the dashed lines are used without filling with color.

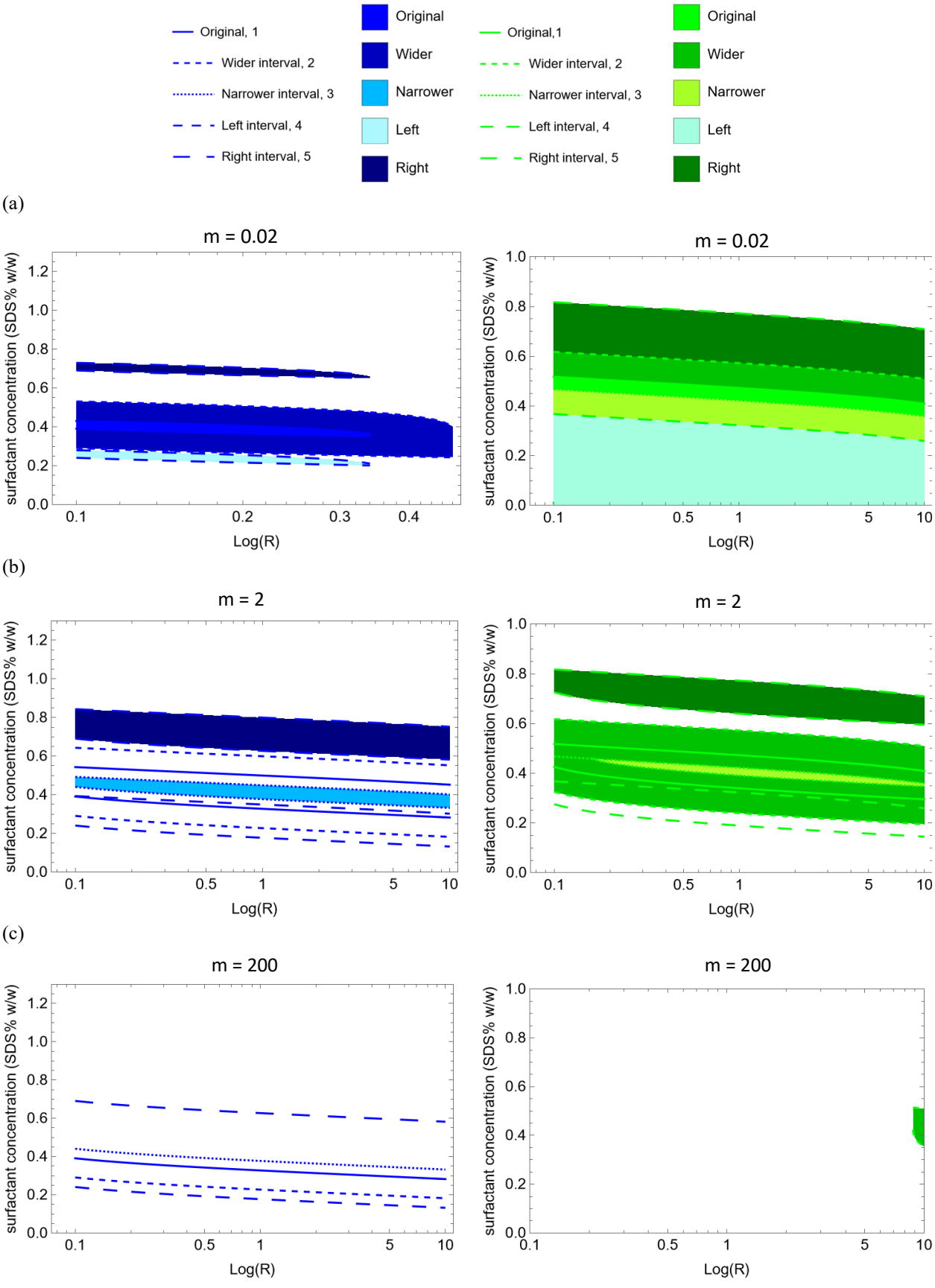
Original, 1
Wider interval, 2
Narrower interval, 3
Left interval, 4
Right interval, 5
Original
Wider
Narrower
Left
Right
Original,1
Wider interval, 2
Narrower interval, 3
Left interval, 4
Right interval, 5
Original
Wider
Narrower
Left
Right
(a)
m = 0.02
surfactant concentration (SDS% w/w)
Log(R)
m = 0.02
surfactant concentration (SDS% w/w)
Log(R)
(b)
m = 2
surfactant concentration (SDS% w/w)
Log(R)
m = 2
surfactant concentration (SDS% w/w)
Log(R)
(c)
m = 200
surfactant concentration (SDS% w/w)
Log(R)
m = 200
surfactant concentration (SDS% w/w)
Log(R)

Figure 5. 3. The threshold-satisfying surfactant concentration is plotted as a function of volume ratio at three different *m* values. Color blue is used for species 1, and color green is used for species 2. The upper and lower boundaries are outlined with dashed lines. The original situation has solid lines. For the rest, the space between the dashed lines are given in the following order: narrower<wider<left<right. To help identify the dashed lines in future discussions, they are also numbered as Original=1, Wider=2, Narrower=3, Left=4, Right=5. The intensity of the color shading is given in the following order from the lightest to the darkest: left<narrower<original<wider <right.

Figure 5.3 summarizes all the surfactant concentrations that satisfy the yield and purity threshold at any *m* and *R* values. At *m*=0.02, the surfactant concentration boundaries for species 1 enclose a region that is thin and long. For the shifted-right variation, the enclosed region moves upward to a higher concentration but maintains the same shape as the original example. For the shifted-left variation, the shape and size of the enclosed region are also consistent with the original example, except the location of this region shifts to a lower surfactant concentration region. The enclosed region for the wider-interval variation has a similar shape but expands in all directions compared to the original example. The narrower-interval example does not have surfactant concentrations that can satisfy the threshold. However, it can also be understood as the enclosed region is reduced to a point with zero areas. Similar trends are observed for species 2 in Figure 5.3(a). In general, the shaded region is the entire area below a certain upper surfactant concentration boundary. For the shifted-left variation, the shaded region shifts downward, contributing to a lower upper boundary than the original example. The shifted-right variation shifts upwards, hence, a higher upper surfactant concentration boundary. The narrower and wider interval variations are expected to have a smaller and a larger area, respectively, which converts to a lower and a higher upper boundary.

At *m*=2, only the narrower and shifted-right variations are filled with their corresponding colors for species 1. Dashed lines are used to illustrate the rest variations. Compared to the original example (line #1), the enclosed region for the narrower-interval variation (line #3) shrinks to a smaller size. The enclosed region for the wider-interval variation (line # 2) almost doubles in size

compared to the original example. The enclosed region of the shifted-right variation (line #5) shifts upward, reaching outside the wider-interval variation. The left interval example (line #4) shifts downward but still overlaps with the bottom part of the original example. For specie 2, the narrower-interval, wider-interval, and shifted-right variations are shaded with the appropriate colors. Comparing the two plots of both species, the relations among these five $b_1 - b_2$ variations are identical for species 1 and 2.

At *m*=200, the plot for species 1 is a reciprocal of Figure 5.3 (a) for species 2. No shading is added to illustrate a parallel comparison between dashed lines and color shades when describing the same type of plot. The dashed lines are the lower boundaries that specify the surfactant concentrations that satisfy the threshold for both yield and purity. The entire area above this lower boundary complies with the separation threshold. Once again, the shifted-right (line #5) and the narrower-interval (line #3) variations have a higher lower boundary than the original example. The shifted-left and wider-interval variations have a lower boundary lower than the original example. For species 2, the only situation that has a threshold-complying surfactant concentration is the wider-interval variation. This can also be verified using the purity plot in Figure 5.2.

Because the shifted-left, shifted-right, and the original examples all have an enclosed region that shares the same shape, we seek to compile these individual regions into a master plot. This is achieved by introducing a dimensionless surfactant concentration *S*. The definition of *S* is given below,

$$S = \frac{x - \frac{b_1 + b_2}{2}}{b_2 - \frac{b_1 + b_2}{2}} \tag{5.1}$$

where x is the surfactant concentration, and b_1 and b_2 are the crossover surfactant concentrations for species 1 and 2. By converting all x to S, we generate Figure 5.4.

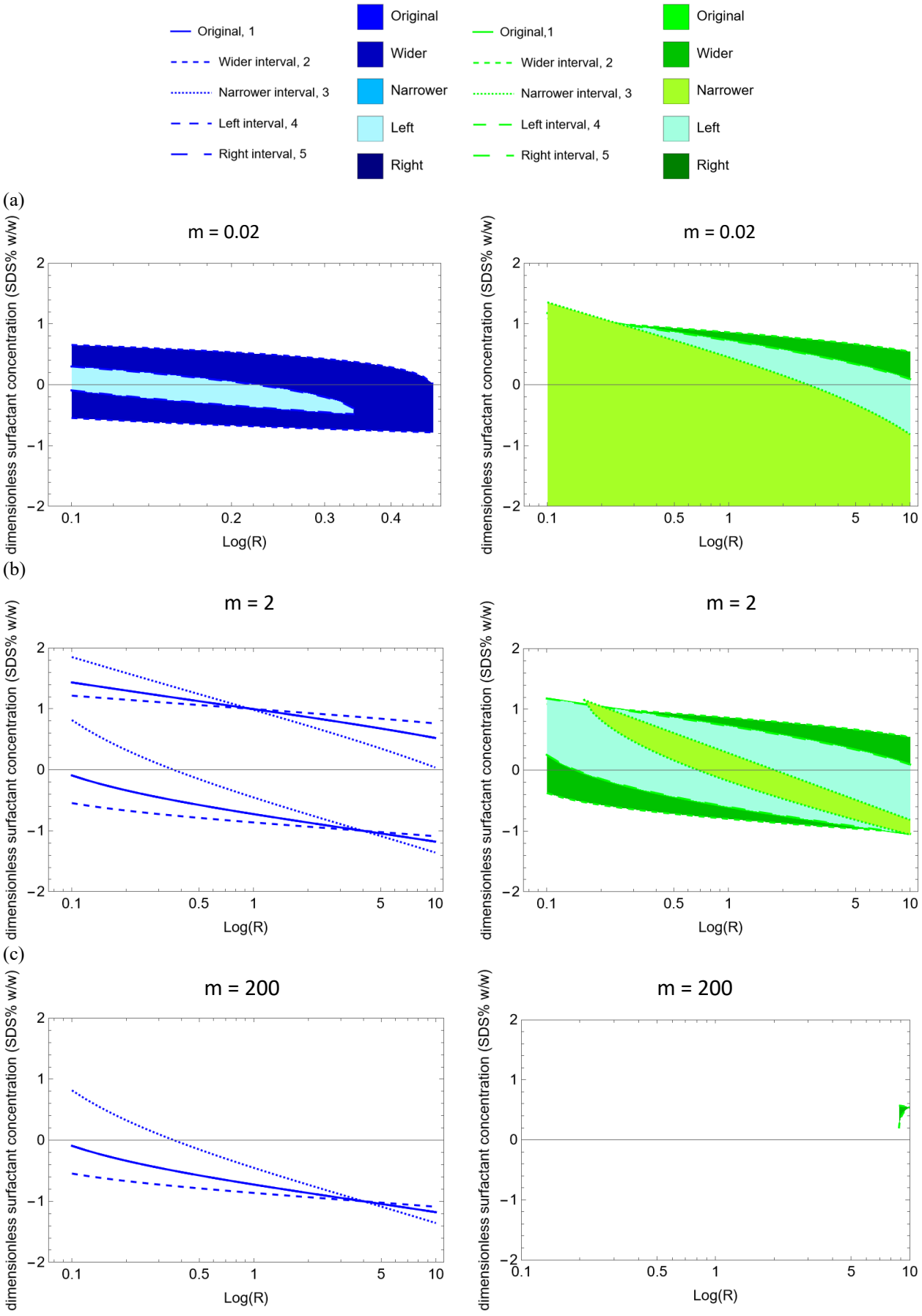

Figure 5. 4. A remake of Figure 5.3 using dimensionless surfactant concentration *S*.

In Figure 5.4, the shifted-left, shifted-right, and the original examples are compounded into one group. In the color scheme, the shaded region of the shifted-left variation is plotted on top of the original and the shifted-right variations. As a result, only the shifted-left variation is visible. Similarly, only the boundaries of the original example are visible because solid lines are used for the original example, while dashed lines are used for other variations.

Besides the compounding effect, the dimensionless analysis also reveals another trend among the five b variations. The slopes of the surfactant concentration boundaries increase in the following order: wider <original=shifted-left=shifted-right <narrower. A steeper slope means the surfactant concentration boundary is more sensitive to the volume ratio. This result is consistent with experimental observation. When two species have very different crossover surfactant concentrations, they are easier to separate than those with very similar crossover points. Crossover concentration is converted to the location of b in our model. CNT species with a smaller b value respond to the addition of surfactant faster and are tuned from the bottom to the top at a lower surfactant concentration. When the $b_1 - b_2$ interval is wide, species 1 is tuned into the top phase at a much lower surfactant concentration than species 2. As a result, a large operation window of surfactant concentrations can be used to separate species 1 and 2. Volume ratio becomes less relevant when the operating condition provided by the surfactant concentration is highly favorable. In contrast, when the $b_1 - b_2$ interval is narrow, very few surfactant concentrations can provide a favorable separation environment. In order to reach the separation goal, the volume ratio has to play a more significant role, even though it is much less effective than the surfactants. As a result, in Figure 5.4, we observe that the steepness of the slopes decreases from the narrower-interval variation to the original example then down to the wider-interval variation.

5.3 Vary parameter *a* in the model

The next parameter we vary to simulate the diverse behavior of different CNT species is *a*. Parameter *a* controls the slope of the partitioning coefficient curves. A CNT species with a small *a* value is highly sensitive to surfactant concentration and completes the transformation from the bottom to the top phase within a narrow surfactant concentration range. To systematically vary *a*, we increase and decrease the value of a_1 (species 1) and a_2 (species 2) individually. In total, there are five scenarios, original, a_1 up, a_1 down, a_2 up, and a_2 down. When *a* is changed for one species, the *a* value of the other species remains the same as in the original example. The exact values of *a* are tabulated in Table 5.2. a_1 and a_2 are equal to each other in the original example.

a_1	a_2	a_{1-up}	a_2	a_{1-down}	a_2	a_1	a_{2-up}	a_1	a_{2-down}
0.1	0.1	0.2	0.1	0.05	0.1	0.1	0.2	0.1	0.05

Table 5. 2. The values of a_1 and a_2 for five variations for parameter *a*.

The resulted partition coefficient curves for each *a* value is shown in Figure 5.5.

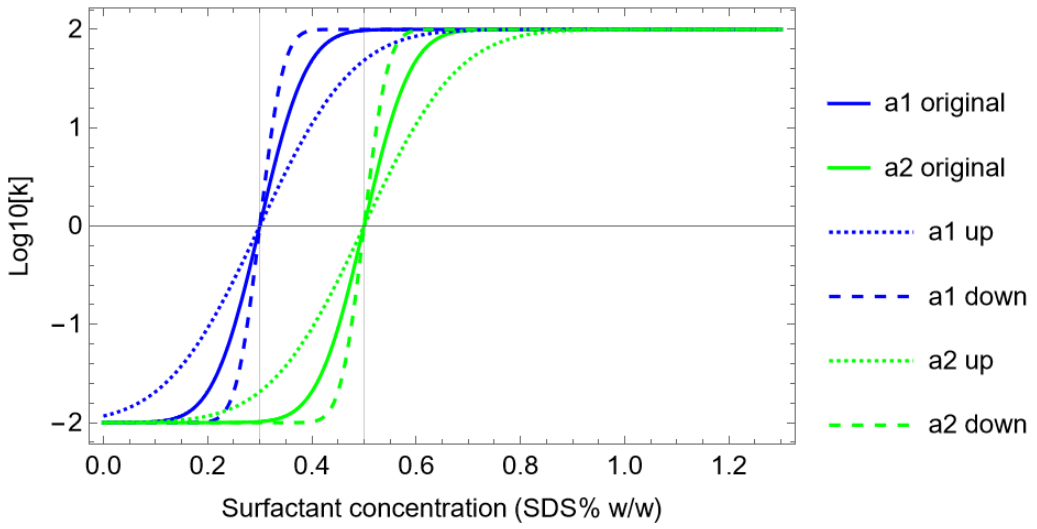

Figure 5. 5. The partition coefficient curves for the five variations of *a* value.

It is worth noting that an increase in *a* value causes the slope of a partition coefficient curve to become flattered, and a decrease in *a* value leads to a steeper partition coefficient curve.

Repeating the same analysis run in previous chapters, we generate the purity vs. volume ratio curves for each *a* variation at three different *m* values.

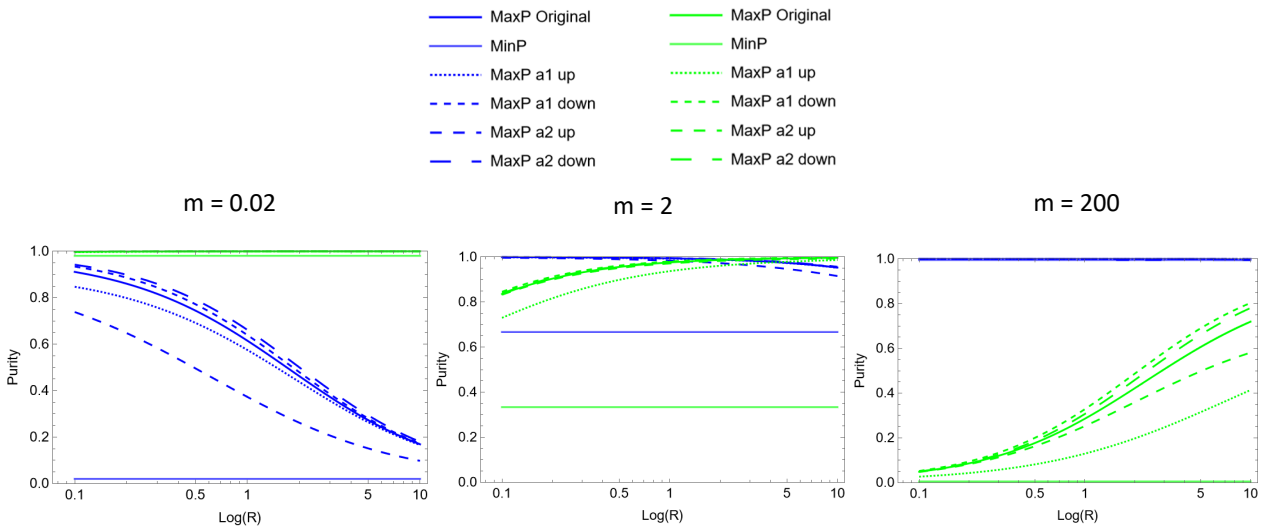

Figure 5. 6. The maximum and minimum purity of species 1 and 2 are plotted as a function of volume ratio at three different *m* values. Data of species 1 are plotted in blue, and data of species 2 are plotted in green. The data for the original example is plotted using solid lines. The rest are plotted with dashed lines. The spacing between the dashed lines increases in the following order: $\boldsymbol{a_1}$ up<$\boldsymbol{a_1}$ down<$\boldsymbol{a_2}$ up<$\boldsymbol{a_2}$ down.

Comparing the scenarios with *a* variations to the original example, the general trends of purity are the same. At *m*=0.02, the purity range of species 1 decreases with volume ratio, while the purity range of species 2 is close to 1 regardless of volume ratios. At *m*=2, both species have a range of surfactant concentrations that can produce a purity higher than the 0.8 thresholds at any given *R* value. At *m*=200, the purity range of species 2 increases with volume ratio while the purity range of species 1 is near 1 at all possible R values.

The effect of *a* variations shown in Figure 5.6 is supported by our previous analysis of slope steepness and surfactant sensitivity. The "up" variations shift the maximum purity curves down below the original example, shrinking the overall purity range for both species 1 and 2. When the value of *a* goes up for one species, its partition coefficient curve becomes flatter. As a result, it requires more surfactant to induce the same amount of partitioning behavior. This

situation leads to less separation when an equivalent amount of surfactant is added, and therefore is not ideal for reaching high purity. The "down" variations shift the maximum purity curve up above the original example, boosting the maximum purity for both species. The purity changes induced by "up" variations are more significant than the "down" variations, even though both types of variations see the magnitude of a changes by a factor of two. It seems the change in absolute value instead of the change in magnitude determines how much effect a a variation can generate. When the a value changes for species 1, the purity curve of species 2 shows a more significant change than the purity curve of species 1. For example, a_1 up almost halves the maximum purity of species 2 while only produces a slight drop for maximum purity of species 1.

Even though the general shape of purity curves in Figure 5.6 is comparable to that in Figure 5.2, a fundamental change is brought up by a variations instead of b variations. Figure 5.6 is plotted to help demonstrate this point. The purity and yield curves are plotted as a function of surfactant concentration under a specific experimental condition for the "a_1 up" variation. The purity curve becomes noticeably asymmetric compared to the original example. The left side of the volcano

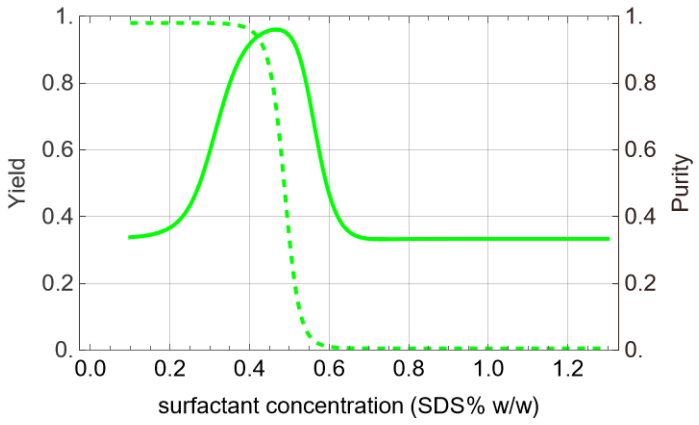

Figure 5. 7. The purity and yield curves are plotted for species 2 at m=2, R=2, $\boldsymbol{a_1}$=0.2, and $\boldsymbol{a_2}$=0.1.

shape is more gradual than the right side, which supports the conclusion that "up" variations make a CNT species require more surfactant to induce the same amount of partitioning behavior. The *a* variation is for species 1, and it is the left side of the purity curve that gets altered. A "down" type variation can also create an asymmetrical purity curve, except the curve will become steeper.

To further analyze how *a* variations affect the separation results, we plot the surfactant concentration ranges that allow both yield and purity to pass the separation threshold as a function of volume ratios at three different *m* values in Figure 5.8. Figure 5.8 has the same format as Figure 5.3.

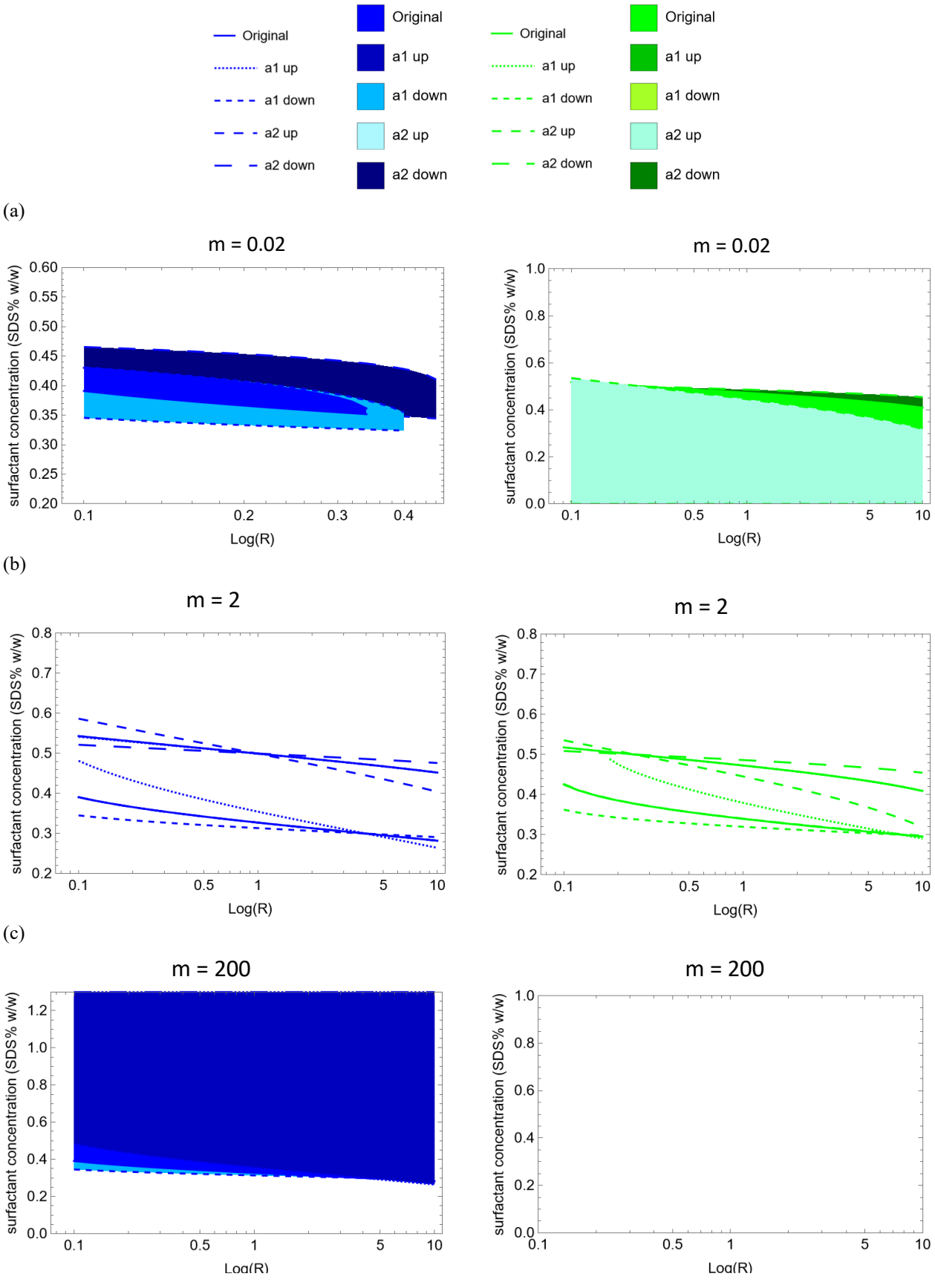
Original
a1 up
a1 down
a2 up
a2 down
Original
a1 up
a1 down
a2 up
a2 down
Original
a1 up
a1 down
a2 up
a2 down
Original
a1 up
a1 down
a2 up
a2 down
(a)
m = 0.02
surfactant concentration (SDS% w/w)
Log(R)
m = 0.02
surfactant concentration (SDS% w/w)
Log(R)
(b)
m = 2
surfactant concentration (SDS% w/w)
Log(R)
m = 2
surfactant concentration (SDS% w/w)
Log(R)
(c)
m = 200
surfactant concentration (SDS% w/w)
m = 200
surfactant concentration (SDS% w/w)

Figure 5. 8. The threshold-satisfying surfactant concentration is plotted as a function of volume ratio at three different *m* values for five different *a* variations. The color blue is used for species 1, and the color green is used for species 2. The upper and lower surfactant boundaries are outlined with dashed lines. The original situation has solid lines. For the rest, the spacing between the dashed lines increases in the following order: $\boldsymbol{a_1}$ up<$\boldsymbol{a_1}$ down<$\boldsymbol{a_2}$ up<$\boldsymbol{a_2}$ down. The intensity of the color scheme is given in the following order from the lightest to the darkest: $\boldsymbol{a_2}$ up<$\boldsymbol{a_1}$ down<original<$\boldsymbol{a_1}$ up <$\boldsymbol{a_2}$ down.

Figure 5.8 shares similar trends with Figure 5.3. At *m*=0.02, the threshold-satisfying surfactant concentrations for species 1 enclose a thin and long region. Only three enclosed regions are visible. They are for the original, a_1 down, and a_2 down variations. The other two "up" variations do not have surfactant concentrations that can meet the separation threshold. Based on our earlier analysis, the "up" variations shrink the purity range and make the CNT species more difficult to separate. Although "a_1 up" has purity values greater than 0.8 at the lower spectrum of volume ratios, it does not satisfy the yield threshold within this range. Therefore, no surfactant concentration is plotted for the "a_1 up" variation in Figure 5.8 (a). The "down" variations expand the surfactant concentration range and cause the enclosed region to have a larger size. A decrease in *a* value makes the partition coefficient curves steeper, and therefore, helps the separation process reach equilibrium faster. For species 2, all surfactant concentrations below a certain upper boundary can satisfy the separation threshold. The upper boundaries for the original example and the two a_1 variations overlap, and only the shaded region of the original example is visible because it is plotted on top of the other two. For species 1, some variations also have overlapping boundaries with the original example, and we will use Figure 5.8 (b) to discuss it in more detail. The "a_2 up" variation lowers down the upper boundary, while the "a_2 down" variation shifts up the upper boundary. As a result, the "a_2 up" variation shrinks the overall size of the shaded region while a_2 expands it. So far, we find it is generally true that the threshold-satisfying surfactant range shrinks for any variation that makes it harder for separation. On the contrary, any variation that promotes easier separation expands the size of the shaded region. This finding applies to both *a*

and *b* variations. Parameters *a* and *b* are intrinsic and are determined by the properties of the CNT species. Experimental conditions cannot alter them. A change in either *a* or *b* indicates a change in the type of CNT species. When the variations in *a* or *b* make the two CNT species easier to separate, it makes sense that the separation threshold becomes more achievable, which allows a broader range of experimental conditions.

At *m*=2, the upper boundary is only visible for the original, "a_2 up", and "a_2 down" variations. Conversely, the lower boundary only shows the original, "a_1 up", and "a_1 down" variations. This observation is true for both species 1 and 2. The upper and lower boundaries are not shown as five pairs because the upper boundary for the original, "a_1 up", and "a_1 down" variations are stacked together. Similarly, the lower boundaries are stacked for the original, "a_2 up", and "a_2 down" variations. In other words, when a_1 is altered, the upper boundary remains unchanged, and when a_2 is altered, the lower boundary remains the same. One possible explanation for this phenomenon is that the location of the upper boundary is determined by the properties of species 2 while the location of the lower boundary is determined by the properties of species 1. Species 1 and 2 have crossover surfactant concentrations at b_1 and b_2 (b_1<b_2). In previous sections, we mention that most separation occurs at surfactant concentrations within the b_1-b_2 range, and the operating surfactant concentration is usually selected from this range. Thus, it is reasonable to believe the upper surfactant concentration boundary is influenced by b_2, and the lower surfactant concentration boundary is influenced by b_1. More study needs to be done to verify this hypothesis.

At *m*=200, any surfactant concentration above a certain lower boundary can produce threshold-satisfying yield and purity for species 1. However, only the boundaries for original, "a_1 up", and "a_1 down" variations are showing. Once again, this is due to the overlapping boundaries

of the original and two a_2 variations. For species 2, no surfactant concentration meets the separation threshold.

5.4 Vary parameter *c* in the model

Parameter *c* in the model controls the maximum and minimum partition coefficient values when they plateau at the low and high extremes of the surfactant concentration. To study *c* systematically, we increase and then decrease the value of *c* for both species individually. In total, there are five types of scenarios, tabulated in the following Table 5.3. We name these five scenarios: original, "c_1 up", "c_1 down", "c_2 up", and "c_2 down". Using these new *c* values, we generate the corresponding partition coefficient curves in Figure 5.9.

c_1	c_2	c_{1-up}	c_2	c_{1-down}	c_2	c_1	c_{2-up}	c_1	c_{2-down}
2	2	3	2	1	2	2	3	2	1

Table 5. 3. The values of c_1 and c_2 for five variations of *c* values.

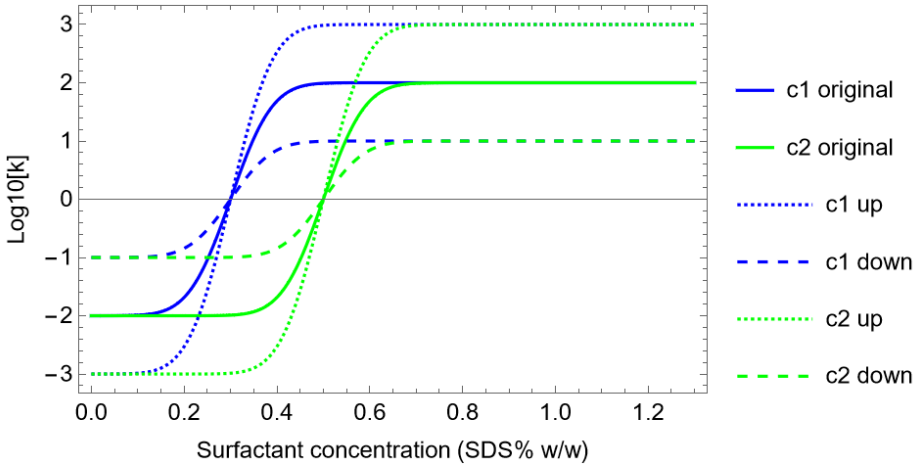

Figure 5. 9. The partition coefficient curves for five variations of *c*.

When *c* is increased, the magnitude of both the maximum and minimum increases. The maximum *K* value becomes more positive on a log scale, while the minimum *K* value becomes more negative. Besides the changes in maximum and minimum, a change in *c* value also affects the slope of the partition coefficient curves. A larger *c* value contributes to a steeper slope. Both steeper slopes and larger max/min magnitudes make a CNT species easier to separate. A steep slope indicates high sensitivity, which helps reach the separation goal with less surfactant needed. A larger max/min

magnitude allows a CNT species to become more concentrated in one phase, which eventually leads to a higher purity. Unlike parameters *a* and *b*, a change in *c* also alters the maximum yield, which will be discussed after purity.

Following the same steps taken in the previous section, we plot purity as a function of volume ratios at different *m* values for all five variations of *c* in Figure 5.10.

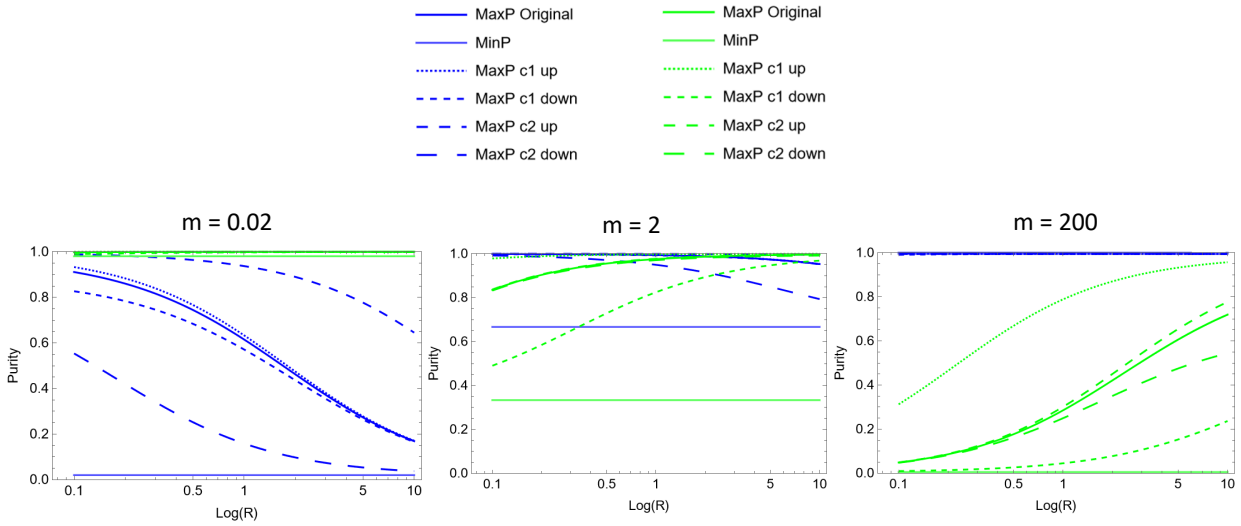

Figure 5. 10. The maximum and minimum purity of species 1 and 2 are plotted as a function of volume ratio at three different *m* values. Data of species 1 is plotted in blue, and data of species 2 is plotted in green. The data for the original example is plotted using solid lines. The rest are plotted with dashed lines. The spacing between the dashed lines increases in the following order: $\boldsymbol{c_1}$ up<$\boldsymbol{c_1}$ down<$\boldsymbol{c_2}$ up<$\boldsymbol{c_2}$ down.

Across all three *m* values, an increase in *c* shifts the maximum purity up, and a decrease in *c* drives the maximum purity down. This observation can be explained as a higher *c* value contributes to higher purity values by allowing the corresponding species to become more concentrated in one phase. At *m*=2, it can be seen that neither the "c_2 up" nor the "c_2 down" variations alter the max purity of species 2. To summarize, we find that changes of c_1 do not impact the boundary purity determined by the properties of species 2 and vice versa. This phenomenon is consistent with our observation for *a* variations in the previous section. At *m*=0.02, the max purity lines decrease with increasing volume ratios for species 1 and stay close to 1 regardless of volume

ratios for species 2. At *m*=200, the roles of species 1 and 2 are reversed when compared to the situations at *m*=0.02. At *m*=2, both species have a range of surfactant concentrations that satisfy the separation threshold at any volume ratio.

As mentioned earlier, the maximum yield is also changed due to variations in the *c* value. We plot max yield as a function of volume ratios for all five *c* variations in Figure 5.11. Because yield is not a function of *m,* there is no difference in yield when *m* differs.

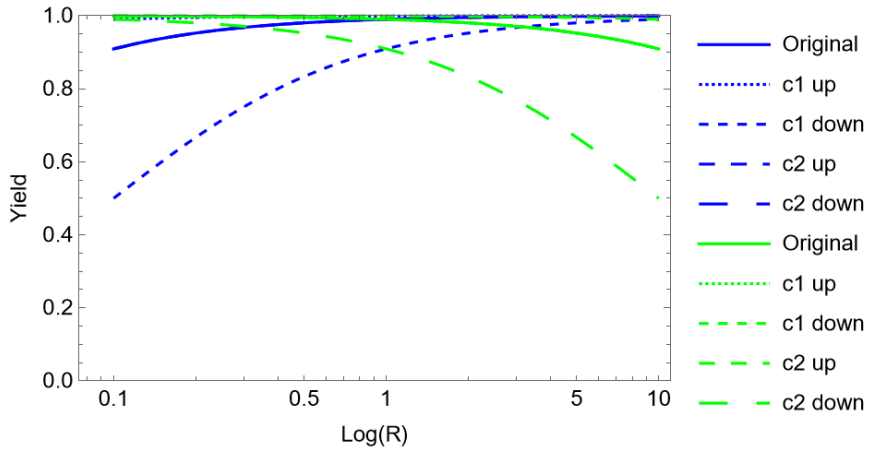

Figure 5. 11. Maximum of yield is plotted as function of volume ratios.

The general trends of max yield curves in Figure 5.11 are similar to the max purity curves in Figure 5.10. Changes on c_1 modify the max yield of species 1, but do not affect the max yield of species 2. In contrast, changes on c_1 only impact species 2, leaving the max yield of species 1 the same as the original example. An increase in *c* value also raises the max yield, while a decrease in *c* reduces the max yield. This relation between *c* and max yield can be explained by the definition of yield. In chapter 3, yields for species 1 and 2 are defined as,

$$Y_1 = \frac{K_1 R}{K_1 R + 1} \tag{3.22}$$

$$Y_2 = \frac{1}{K_2 R + 1} \tag{3.23}$$

When the value of R is fixed, the yield of both species is a monotonic function of partition coefficient, positive proportionality for species 1, and negative proportionality for species 2. Therefore, the maximum and minimum yields are obtained at either the maximum or the minimum partition coefficients. Using Figure 5.9 we know that the max and min of K_1 and K_2 respond directly to changes in c. With a larger c, the max partition coefficient increases, and consequently, the max yield also increases, which explains the trend in Figure 5.11.

Both yield and purity have been analyzed on a macro-scale. However, on the micro-scale, variations in c also cause significant behavior changes of yield and purity. To help illustrate the influence of c, yield and purity are plotted as a function of surfactant concentration under two specific experimental conditions using species 2 as an example.

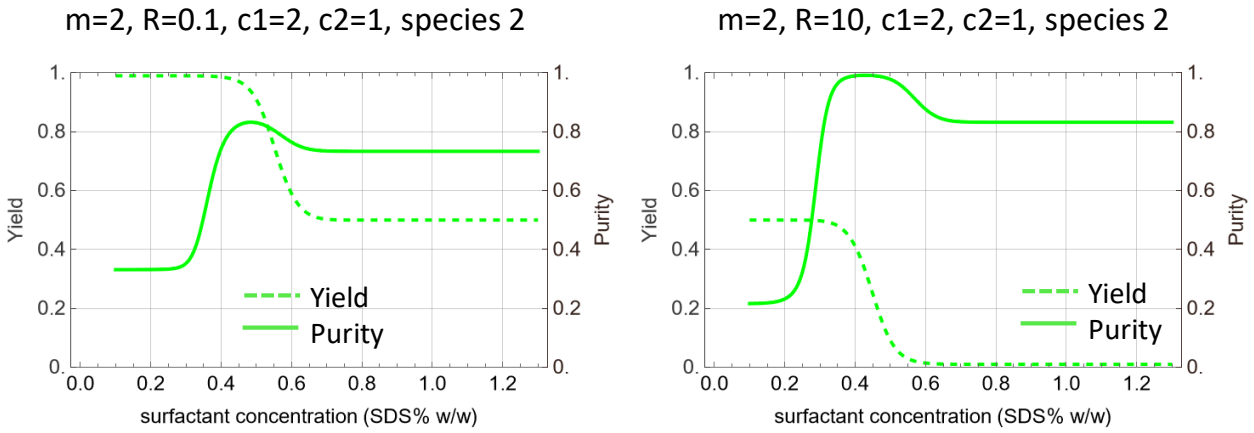

Figure 5. 12. Yield and purity are plotted as a function of surfactant concentration at two specific experimental conditions for species 2.

In Figure 5.12, there are two major differences in the shape of yield and purity curves, compared to the original example in Figure 3.2. One difference is that the max and min values of yield shift away from always being close to 1 and 0. The other difference is that the purity curves are no longer symmetric, and the purity values at the two extremes of surfactant concentrations differ. Figure 5.1 shows a subset of the "c_2 down" example. When c_2 decreases from 2 to 1, the magnitude of the max and min partition coefficients decrease for species 2. As a result, the entire

range of the partition coefficient of species 2 (K_2) shrinks. Substituting a shorter-range K_2 into Equation 3.23 causes the yield range for species 2 to shrink as well, as shown in Figure 5.12. The purity curves of one species used to have a volcano shape, returning to the same value at the two extremes of the surfactant concentration spectrum. In the original example, c_1 equals c_2. As a result, the partition coefficients for species 1 and 2 are the same at the two extremes of surfactant concentration. Plugging this relation, K_1=K_2, into Equations 3.30 and 3.31, purity becomes a function of *m* only. Thus, for the same *m* value, purity returns to the same value at the two extremes of surfactant concentrations.

$$P_1 = \frac{\frac{mK_1}{K_1R+1}}{\frac{mK_1}{K_1R+1}+\frac{K_2}{K_2R+1}} = \frac{m}{m+1}(K_1 = K_2) \tag{3.30}$$

$$P_2 = \frac{\frac{1}{K_2R+1}}{\frac{m}{K_1R+1}+\frac{1}{K_2R+1}} = \frac{1}{m+1}(K_1 = K_2) \tag{3.31}$$

However, this relation is no longer valid when *c* is changed for one species and $c_1 \neq c_2$. Thus, we see the asymmetry of purity at the two extremes of surfactant concentrations.

After examining the effect of *c* on yield and purity, we move on to study the surfactant concentration range that provides threshold-meeting yield and purity.

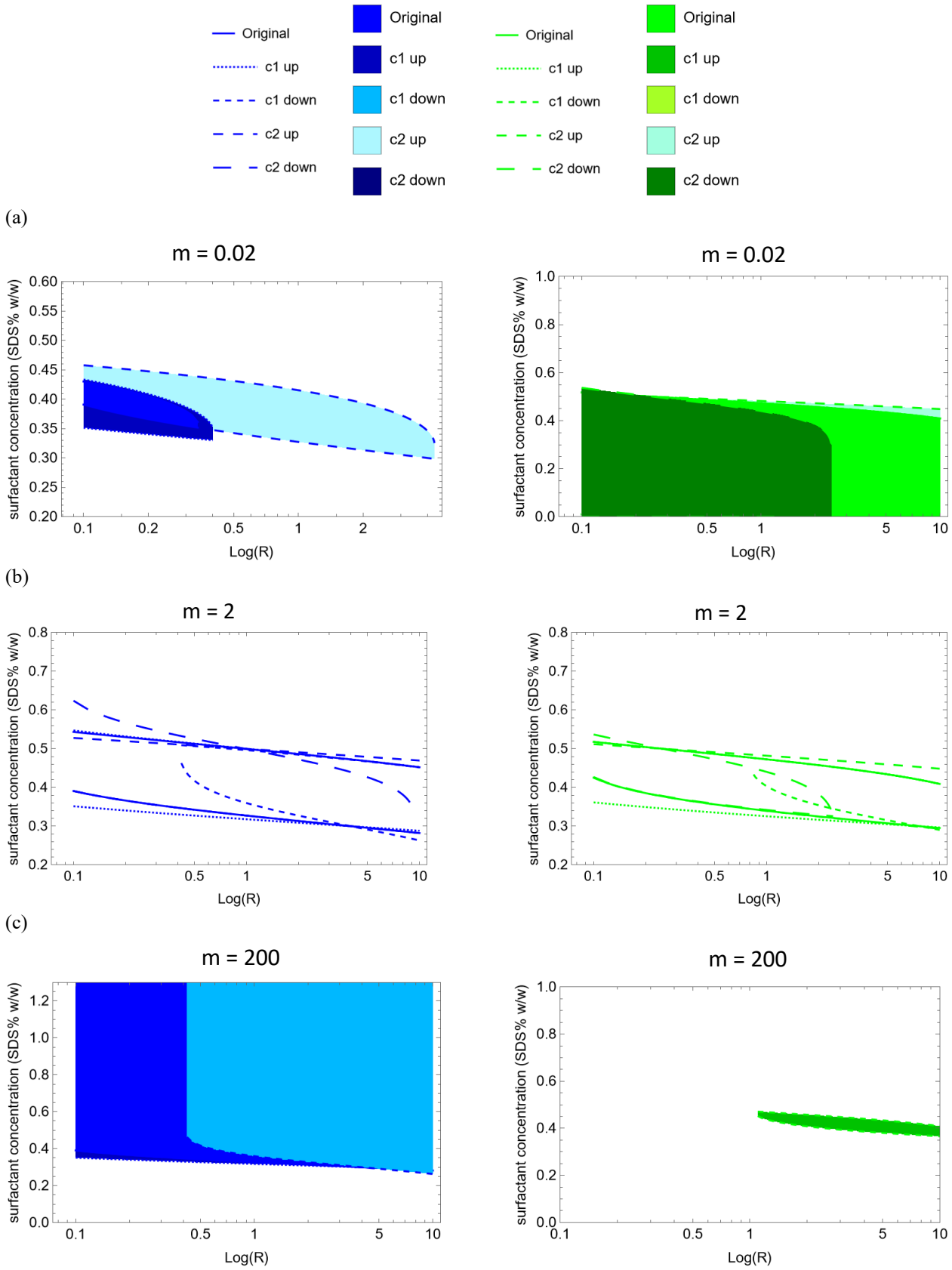
Original
c1 up
c1 down
c2 up
c2 down
Original
c1 up
c1 down
c2 up
c2 down
Original
c1 up
c1 down
c2 up
c2 down
Original
c1 up
c1 down
c2 up
c2 down
(a)
m = 0.02
surfactant concentration (SDS% w/w)
Log(R)
m = 0.02
surfactant concentration (SDS% w/w)
Log(R)
(b)
m = 2
surfactant concentration (SDS% w/w)
Log(R)
m = 2
surfactant concentration (SDS% w/w)
Log(R)
(c)
m = 200
surfactant concentration (SDS% w/w)
Log(R)
m = 200
surfactant concentration (SDS% w/w)
Log(R)

Figure 5. 13. The threshold-satisfying surfactant concentration is plotted as a function of volume ratios at three different *m* values for five different *c* variations. The color blue is used for species 1, and the color green is used for species 2. The upper and lower surfactant boundaries are outlined with dashed lines. The original situation has solid lines. For the rest, the spacing between the dashed lines increases in the following order: $\boldsymbol{c_1}$ up<$\boldsymbol{c_1}$ down<$\boldsymbol{c_2}$ up<$\boldsymbol{c_2}$ down. The intensity of the color scheme is given in the following order from the lightest to the darkest: $\boldsymbol{c_2}$ up<$\boldsymbol{c_1}$ down<original<$\boldsymbol{c_1}$ up <$\boldsymbol{c_2}$ down.

The general features of Figure 5.13 are comparable to those in Figure 5.8. An "up" type of *c* variation expands the size of the enclosed region between the lower and upper surfactant concentration boundary lines. Conversely, a "down" type *c* variation shrinks the size of the surfactant concentration region. This rule applies to changes on both c_1 and c_2. The CNT species with a larger *c* value can become more concentrated in one phase and is more sensitive to surfactant concentration. These intrinsic advantages make it easier to separate such species from other species. A similar outcome happens when the *a* value is decreased in Figure 5.8. Another shared feature between *a* and *c* variations is that a modification on one species does not affect the location of the surfactant concentration boundary set by the other species. Namely, changes on c_1 do not alter the upper surfactant concentration boundary and changes on c_2 do not alter the lower surfactant concentration boundary. This rule is valid for both species 1 and 2. After summarizing the general trends, we now examine Figure 5.13 in a more detailed fashion.

At *m*=0.02, "c_1 up" and "c_2 up" both expand the threshold-satisfying surfactant concentration range, allowing more experimental conditions to be used to achieve the same separation goal. No surfactant concentration exists that can meet the 0.8 thresholds for "c_1 down" and "c_2 down". However, it can also be understood as the "down" variations shrink the size of the surfactant concentration range to zero. For species 2, all areas below the upper surfactant boundary are threshold-complying. According to the general rules, c_1 variations do not change the location of the upper boundary. As a result, the shaded region for the original, "c_1 up", and "c_1 down"

variations are stacked on top of each other. A decrease in c_2 value shrinks the green shaded region, while a rise in c_2 expands the size of the green region slightly.

At *m*=2, no shading is added to create better visuals of the boundary lines themselves. For both species 1 and 2, only three lines are visible for the upper and the lower boundaries instead of five. This is because the upper boundary lines for "c_1 up", and "c_1 down" variations are stacked on top of the solid line for the original example. Similarly, the solid line from the original example overlaps the lower boundary lines for the "c_2 up", and "c_2 down" variations.

At *m*=200, species 1 shows three shaded surfactant concentration regions. The original and the two c_2 variations overlap with each other. An increase in c_1 shrinks the blue region, while a decrease in c_1 expands the region slightly. This scenario is a reciprocal of species 2 in Figure 5.13 (a). For species 2, only the "c_1 up" variation can produce threshold-meeting yield and purity. At the original *c* value, no surfactant concentration exists for this *m* value, which is the root cause of the discussion in chapter 4. However, since "up" type variations in *c* can expand the size of the surfactant concentration region, we expect the "c_1 up" or "c_1 up" variation might allow some surfactant concentrations to appear in Figure 5.13 (c). Only "c_1 up" is powerful enough to allow a small range of surfactant concentrations to become threshold-satisfying. Given that none of the five *a* variations creates a threshold-satisfying surfactant concentration for species 2, we deduct that variations in *c* can have more impact on the separation results than variations in *a*. This might be due to the fact that variations in *c* make a CNT species more distinguishable than other species by adjusting both the max and min and the slope of the partition coefficient curve. However, to verify this point, more investigations are needed.

5.5 Summary

In this chapter, we study the effects of three model parameters a, b, and c. Adjusting these parameters leads to a more realistic representation of different CNT species. Five types of variation are created for each parameter. For parameters a and c, their values are increased and then decreased for each CNT species, resulting in a total of four scenarios. The one discussed in chapters 3 and 4 is considered as the original example. For parameters b, b_1 and b_2 are varied as a group. The b_1-b_2 interval is shifted left and right on the surfactant concentration axis, and the width of the interval is widened and narrowed. The maximum and minimum purity and the threshold-complying surfactant concentrations are plotted for each scenario. Across all three parameters, these general trends apply. When a parameter modification makes the partition coefficient curve of a CNT species more distinguishable from other species, the purity, and the surfactant concentration ranges expand. In contrast, the ranges shrink if the modification leaves the partition coefficient curve of a CNT species more similar to other species. Moreover, in the surfactant concentration range plot, parameter changes on one species do not affect the surfactant concentration boundary determined by the other species. A dimensionless analysis is also performed for parameter b. The purity and surfactant concentration plots for the shifted-left, shifted-right, and the original scenario are compounded into one shared master plot, indicating the width of the b_1-b_2 interval has a more substantial impact on the separation result than its location. Variations in parameter c also alter the range of maximum and minimum yield, which is not seen in variations for parameters a and b.

Chapter 6: Conclusions and future works

6.1 Conclusions

The primary contribution of this thesis is the development of a model that successfully transforms the study of carbon nanotube separation from entirely experimental to primarily computational. The model considerably improves the accessibility to the vast parameter space in aqueous two-phase extractions and alleviates the experimental constraint imposed by the material shortage in highly purified CNT species. This thesis also establishes a framework to numerically quantify the separation performance with well-known criteria, yield, and purity. Thanks to the universal application of these criteria, such as in chromatography and electrophoresis[15,62,82,83], the performance of an aqueous two-phase system can be compared directly to other separation processes. The model offers enough flexibility in CNT species representation and can even mimic the partitioning behavior of species never been studied before. A large quantity of data is generated by the model. We carefully filter the data and compile the important information to present direct visualization of the appropriate operating range. We hope that the figures plotted in this thesis can be used as stand-alone reference charts. Lastly, the model is easily adaptable to other liquid-liquid extraction-based separation techniques because few assumptions made during the model-developing process are carbon nanotube specific. The potential for generalization and widespread application of this model is promising. The individual contributions from each project are stated below.

In chapter 3, we build the basic structure of the model and test its ability to simulate an entire separation process between two CNT species. We systematically vary the three key parameters, surfactant concentration x, volume ratio R, and initial mass ratio m, and discover how each of them affects the separation results. We also find out that no surfactant concentration or

volume ratio under a specific *m* value (*m*=200) can produce a separation that satisfies the imposed 0.8 thresholds using only one-step separation. This deficiency leads to the discussions in the next chapter.

In chapter 4, we use the model to approximate a multi-stage separation process between two CNT species. Besides yield and purity, other decision-making strategies are incorporated to narrow down the operational options that grow exponentially from one-stage to two-stage. For the deficiency case reported in chapter 3, we perform an analysis for two-stage separation. In the first stage, the experimental conditions that produce the best yield and purity combination are explored, and the resulted surfactant concentration and volume ratio are reported. In the second stage, two ATPS are evaluated in parallel. The calculated best operating conditions are examined against the possible values in actual experiments. The surfactant concentration has to be adjusted while the volume ratio remains unchanged. A two-stage separation process enriches both species by a substantial amount, a little less than 20 times for species 1 and almost 5000 times for species 2, validating the concentrating power of an ATPS separation process. It is also discovered that yield and purity cannot be improved simultaneously by simply performing more stages. A trade-off between these two performance metrics always exists.

In chapter 5, we study the effects of the three system-intrinsic parameters *a*, *b*, and *c*. Variations in parameter *b* reveal that the distance between the crossover surfactant concentrations of two species affects separation results. When the distance becomes further or closer, the separation performance is enhanced or diminished, respectively. Variations in *b* explores the diameter difference between CNT species. Variations in parameter *a* show that separations for species with steeper partition coefficient curves are easier to achieve and generate higher purity. According to experimental results, the metallic CNT species have steeper slopes than the

semiconducting species, and purer samples have steeper slopes than mixed samples. Thus, metallic CNT and purer samples should be extracted first compared to mixed semiconducting CNT samples. Variations in *a* is considered to represent different diameters of different CNT species. Variations in parameter *c* tell a similar story to variations in parameter *a*, except the effects are intensified because a change in *c* alters both the magnitude in max/min values and the slope of the partition coefficients curves. Variations in *c* captures a more comprehensive difference between CNT species, which includes diameter, chirality, electrical properties, and hydrophobicity.

6.2 Future works

One noticeable gap between the current status of this thesis and the simulation of an actual CNT separation process is the number of CNT species studied. In this thesis, only two CNT species are analyzed. However, in a raw CNT sample, at least dozens of species exist. Adding more CNT species into the model dramatically complicates the computation process, especially for species with unrelated *a*, *b*, and *c* values. Much more work will be required to streamline and optimize the model to process inputs from dozens of species. However, this step must be taken to make the model a more accurate representation of the real-world scenario.

In chapter 4, the analysis stops after the second stage when we realize the separation threshold can never be met simultaneously for yield and purity. However, when achieving higher purity is the priority, more stages should be performed. Especially in the case where extremely high purity is desired, the separation process might go well beyond four stages[31,59,60]. As the purity value approaches 1, the effect of one additional stage becomes less prominent. A decision has to be made weighing on the trade-off between a small sacrifice in purity and running another labor-intensive and time-consuming experiment. One way to help resolve this dilemma is to calculate the stage efficiency, which is commonly done for separation processes[78,84,85]. Reporting efficiency for a two-stage process seems redundant, but it becomes more valuable when the stage number grows large.

Another analysis we would like to run but could not due to time constraints is the economic analysis. Having access to all the raw data and the experimental settings used in the droplet-based experiments brings considerable value to the model-developing process. This great asset includes knowledge of the mass of each component in the system throughout the separation process. The pricing information can be obtained readily online. With these two types of information, we can

estimate the cost related to each separation stage. The separation outcomes can then be reported as a function of the material cost. Given that all polymers and surfactants used in the experiment are relatively cheap and commercially available, we expect the entire cost of performing CNT separation in an aqueous two-phase system is low compared to other techniques. It is a common belief that the separation process can count up to 80% of the entire downstream processing cost[53]. We believe an economic analysis can strengthen our argument for the promising future aqueous two-phase extraction has as the preferred CNT separation method.

References

1. Monthioux, M. & Kuznetsov, V. L. Who should be given the credit for the discovery of carbon nanotubes? *Carbon N. Y.* **44**, 1621–1623 (2006).

2. Baughman, R. H., Zakhidov, A. a & de Heer, W. a. Carbon nanotubes--the route toward applications. *Science* **297**, 787–92 (2002).

3. Harris, P. J. F. Carbon nanotube composites. *Int. Mater. Rev.* **49**, 31–43 (2004).

4. Franklin, A. D. *et al.* Sub-10 nm Carbon Nanotube Transistor. *Nano Lett.* **12**, 758–762 (2012).

5. Lee, N. S. *et al.* Application of carbon nanotubes to field emission displays. *Diam. Relat. Mater.* **10**, 265–270 (2001).

6. Cheng, H. M., Yang, Q. H. & Liu, C. Hydrogen storage in carbon nanotubes. *Carbon N. Y.* **39**, 1447–1454 (2001).

7. Mubarak, N. M., Abdullah, E. C., Jayakumar, N. S. & Sahu, J. N. An overview on methods for the production of carbon nanotubes. *J. Ind. Eng. Chem.* **20**, 1186–1197 (2014).

8. Belin, T. & Epron, F. Characterization methods of carbon nanotubes: A review. *Mater. Sci. Eng. B Solid-State Mater. Adv. Technol.* **119**, 105–118 (2005).

9. Arnold, M. S., Green, A. A., Hulvat, J. F., Stupp, S. I. & Hersam, M. C. Sorting carbon nanotubes by electronic structure using density differentiation. *Nat. Nanotechnol.* **1**, 60–65 (2006).

10. Tu, X., Manohar, S., Jagota, A. & Zheng, M. DNA sequence motifs for structure-specific recognition and separation of carbon nanotubes. *Nature* **460**, 250–253 (2009).

11. Khripin, C. Y. *et al.* High-resolution length fractionation of surfactant-dispersed carbon nanotubes. *Anal. Chem.* **85**, 1382–1388 (2013).

12. Tu, X., Hight Walker, A. R., Khripin, C. Y. & Zheng, M. Evolution of DNA sequences toward recognition of metallic armchair carbon nanotubes. *J. Am. Chem. Soc.* **133**, 12998–13001 (2011).

13. Silvera-Batista, C. A., Scott, D. C., McLeod, S. M. & Ziegler, K. J. A mechanistic study of the selective retention of SDS-suspended single-wall carbon nanotubes on agarose gels. *J. Phys. Chem. C* **115**, 9361–9369 (2011).

14. Liu, H., Nishide, D., Tanaka, T. & Kataura, H. Large-scale single-chirality separation of single-wall carbon nanotubes by simple gel chromatography. *Nat. Commun.* **2**, (2011).

15. Liu, H., Tanaka, T., Urabe, Y. & Kataura, H. High-efficiency single-chirality separation of carbon nanotubes using temperature-controlled gel chromatography. *Nano Lett.* **13**, 1996–2003 (2013).

16. Tvrdy, K. *et al.* A Kinetic Model for the Deterministic Prediction of Gel-Based Single Chirality Single-Walled Carbon Nanotube Separation. *ACS Nano* 1779–1789 (2013). doi:10.1021/nn305939k

17. Flavel, B. S., Kappes, M. M., Krupke, R. & Hennrich, F. Separation of single-walled carbon nanotubes by 1-dodecanol-mediated size-exclusion chromatography. *ACS Nano* **7**, 3557–3564 (2013).

18. Ghosh, S., Bachilo, S. M. & Weisman, R. B. Advanced sorting of single-walled carbon nanotubes by nonlinear density-gradient ultracentrifugation. *Nat. Nanotechnol.* **5**, 443–450 (2010).

19. Cambré, S. & Wenseleers, W. Separation and diameter-sorting of empty (end-capped) and water-filled (open) carbon nanotubes by density gradient ultracentrifugation. *Angew. Chemie - Int. Ed.* **50**, 2764–2768 (2011).

20. Green, A. A. & Hersam, M. C. Nearly single-chirality single-walled carbon nanotubes produced via

orthogonal iterative density gradient ultracentrifugation. *Adv. Mater.* **23**, 2185–2190 (2011).

21. Fagan, J. A. *et al.* Separation of empty and water-filled single-wall carbon nanotubes. *ACS Nano* **5**, 3943–3953 (2011).

22. Fagan, J. A. *et al.* Analyzing surfactant structures on length and chirality resolved (6,5) single-wall carbon nanotubes by analytical ultracentrifugation. *ACS Nano* **7**, 3373–3387 (2013).

23. Ihara, K., Endoh, H., Saito, T. & Nihey, F. Separation of metallic and semiconducting single-wall carbon nanotube solution by vertical electric field. *J. Phys. Chem. C* **115**, 22827–22832 (2011).

24. Albertsson, P. *Partition of Cell Particles and Macromolecules*. (Wiley, 1986).

25. Boris Y. Zaslavsky. *Aqueous Two-Phase Partitioning*. (Marcel Dekker, 1995).

26. Khripin, C. Y., Fagan, J. A. & Zheng, M. Spontaneous partition of carbon nanotubes in polymer-modified aqueous phases. *J. Am. Chem. Soc.* **135**, 6822–6825 (2013).

27. Zhang, M. *et al.* Single-step total fractionation of single-wall carbon nanotubes by countercurrent chromatography. *Anal. Chem.* **86**, 3980–3984 (2014).

28. Fagan, J. A. *et al.* Isolation of specific small-diameter single-wall carbon nanotube species via aqueous two-phase extraction. *Adv. Mater.* **26**, 2800–2804 (2014).

29. Subbaiyan, N. K. *et al.* Role of surfactants and salt in aqueous two-phase separation of carbon nanotubes toward simple chirality isolation. *ACS Nano* **8**, 1619–1628 (2014).

30. Fagan, J. A. *et al.* Isolation of >1 nm diameter single-wall carbon nanotube species using aqueous two-phase extraction. *ACS Nano* **9**, 5377–5390 (2015).

31. Subbaiyan, N. K. *et al.* Bench-top aqueous two-phase extraction of isolated individual single-walled carbon nanotubes. *Nano Res.* **8**, 1755–1769 (2015).

32. Gui, H. *et al.* Redox sorting of carbon nanotubes. *Nano Lett.* **15**, 1642–1646 (2015).

33. Wei, L. *et al.* (9,8) Single-Walled Carbon Nanotube Enrichment via Aqueous Two-Phase Separation and Their Thin-Film Transistor Applications. *Adv. Electron. Mater.* **1**, 1–8 (2015).

34. Yomogida, Y. *et al.* Industrial-scale separation of high-purity single-chirality single-wall carbon nanotubes for biological imaging. *Nat. Commun.* **7**, 1–8 (2016).

35. Niyogi, S., Densmore, C. G. & Doorn, S. K. Electrolyte tuning of surfactant interfacial behavior for enhanced density-based separations of single-walled carbon nanotubes. *J. Am. Chem. Soc.* **131**, 1144–1153 (2009).

36. Carvalho, E. J. F. & Dos Santos, M. C. Role of surfactants in carbon nanotubes density gradient separation. *ACS Nano* **4**, 765–770 (2010).

37. Witkowski, P. J., Smith, J. A., Fusillo, T. V. & Chiou, C. T. A review of surface-water sediment fractions and their interactions with persistent manmade organic compounds. *US Geol. Surv. Circ.* **993**, (1987).

38. Zaslavsky, B. *Aqueous Two-Phase Partitioning: Physical Chemistry and Bioanalytical Applications*. (Marcel Dekker, 1994).

39. Liu, Y., Lipowsky, R. & Dimova, R. Concentration dependence of the interfacial tension for aqueous two-phase polymer solutions of dextran and polyethylene glycol. *Langmuir* **28**, 3831–3839 (2012).

40. Forciniti, D., Hall, C. K. & Kula, M. R. Interfacial tension of polyethyleneglycol-dextran-water systems: influence of temperature and polymer molecular weight. *J. Biotechnol.* **16**, 279–296 (1990).

41. Ryden, J. & Albertsson, P. ake. Interfacial tension of dextran-polyethylene glycol-water two-phase systems. *J. Colloid Interface Sci.* **37**, 219–222 (1971).

42. Berggren, K., Wolf, A., Asenjo, J. A., Andrews, B. A. & Tjerneld, F. The surface exposed amino acid residues of monomeric proteins determine the partitioning in aqueous two-phase systems. *Biochim. Biophys. Acta - Protein Struct. Mol. Enzymol.* **1596**, 253–268 (2002).

43. Walter, H., Johansson, G. & Brooks, D. E. Partitioning in aqueous two-phase systems: recent results. *Anal. Biochem.* **197**, 1–18 (1991).

44. Huddleston, J. *et al.* The molecular basis of partitioning in aqueous two-phase systems. *Trends Biotechnol.* **9**, 381–8 (1991).

45. Abbott, N. L., Blankschtein, D. & Hatton, T. A. Protein partitioning in two-phase aqueous polymer systems. 5. Decoupling of the effects of protein concentration, salt type, and polymer molecular weight. *Macromolecules* **26**, 825–828 (1993).

46. Abbott, N. L., Blankschtein, D. & Hatton, T. A. Protein Partitioning in Two-Phase Aqueous Polymer Systems . 3 . Structure and Protein-Polymer Interactions. *Macromolecules* **25**, 3932–3941 (1992).

47. Abbott, N. L. & Hatton, T. A. Liquid-Liquid-Extraction for Protein Separations. *Chem. Eng. Prog.* **84**, 31–41 (1988).

48. Vaisman, L., Wagner, H. D. & Marom, G. The role of surfactants in dispersion of carbon nanotubes. *Adv. Colloid Interface Sci.* **128**–**130**, 37–46 (2006).

49. Arnold, M. S., Suntivich, J., Stupp, S. I. & Hersam, M. C. Hydrodynamic characterization of surfactant encapsulated carbon nanotubes using an analytical ultracentrifuge. *ACS Nano* **2**, 2291–2300 (2008).

50. Lin, S. & Blankschtein, D. Role of the bile salt surfactant sodium cholate in enhancing the aqueous dispersion stability of single-walled carbon nanotubes: A molecular dynamics simulation study. *J. Phys. Chem. B* **114**, 15616–15625 (2010).

51. Suttipong, M., Tummala, N. R., Striolo, A., Batista, C. S. & Fagan, J. Salt-specific effects in aqueous dispersions of carbon nanotubes. *Soft Matter* **9**, 3712–3719 (2013).

52. Nelson, C. W. Probing the Phase Behavior of Complex Fluids using Microliter droplet Reactors. (Carnegie Mellon University, 2016).

53. Iqbal, M. *et al.* Aqueous two-phase system (ATPS): an overview and advances in its applications. *Biol. Proced. Online* **18**, 1–18 (2016).

54. Glyk, A., Scheper, T. & Beutel, S. Influence of different phase-forming parameters on the phase diagram of several PEG − salt aqueous two-phase systems. *J. Chem. Eng. Data* **59**, 850–859 (2014).

55. Jain, R. M., Ben-Naim, M., Landry, M. P. & Strano, M. S. Competitive Binding in Mixed Surfactant Systems for Single-Walled Carbon Nanotube Separation. *J. Phys. Chem. C* **119**, 22737–22745 (2015).

56. Li, H. *et al.* Separation of Specific Single-Enantiomer Single-Wall Carbon Nanotubes in the Large-Diameter Regime. *ACS Nano* **14**, 948–963 (2020).

57. Haggenmueller, R. *et al.* Comparison of the quality of aqueous dispersions of single wall carbon nanotubes using surfactants and biomolecules. *Langmuir* **24**, 5070–5078 (2008).

58. Park, M., Park, J., Lee, J. & Ju, S. Y. Scaling of binding affinities and cooperativities of surfactants on carbon nanotubes. *Carbon N. Y.* **139**, 427–436 (2018).

59. Fagan, J. A. Aqueous two-polymer phase extraction of single-wall carbon nanotubes using surfactants. *Nanoscale Adv.* **1**, 3307–3324 (2019).

60. Tang, M. S. Y. *et al.* Metallic and semiconducting carbon nanotubes separation using an aqueous two-phase separation technique: A review. *Nanotechnology* **27**, (2016).

61. Ao, G., Khripin, C. Y. & Zheng, M. DNA-controlled partition of carbon nanotubes in polymer aqueous two-phase systems. *J. Am. Chem. Soc.* **136**, 10383–10392 (2014).

62. Janas, D. Towards monochiral carbon nanotubes: A review of progress in the sorting of single-walled carbon nanotubes. *Mater. Chem. Front.* **2**, 36–63 (2018).

63. Bati, A. S. R., Yu, L., Batmunkh, M. & Shapter, J. G. Synthesis, purification, properties and characterization of sorted single-walled carbon nanotubes. *Nanoscale* **10**, 22087–22139 (2018).

64. Asenjo, J. A. & Andrews, B. A. Aqueous two-phase systems for protein separation: Phase separation and applications. *J. Chromatogr. A* **1238**, 1–10 (2012).

65. Li, H., Gordeev, G., Garrity, O., Reich, S. & Flavel, B. S. Separation of small-diameter single-walled carbon nanotubes in one to three steps with aqueous two-phase extraction. *ACS Nano* **13**, 2567–2578 (2019).

66. Yau, Y. K. *et al.* Current applications of different type of aqueous two-phase systems. *Bioresour. Bioprocess.* **2**, 49 (2015).

67. Wei, L., Flavel, B. S., Li, W., Krupke, R. & Chen, Y. Exploring the upper limit of single-walled carbon nanotube purity by multiple-cycle aqueous two-phase separation. *Nanoscale* **9**, 11640–11646 (2017).

68. Ding, J. *et al.* Enrichment of large-diameter semiconducting SWCNTs by polyfluorene extraction for high network density thin film transistors. *Nanoscale* **6**, 2328–2339 (2014).

69. Lei, T., Pochorovski, I. & Bao, Z. Separation of Semiconducting Carbon Nanotubes for Flexible and Stretchable Electronics Using Polymer Removable Method. *Acc. Chem. Res.* **50**, 1096–1104 (2017).

70. Kenney, A. & Fowell, S. *Practical Protein Chromatography - Methods in molecular biology*. (1992).

71. de Haan, A. B. & Bosch, H. *Industrial Separation Processes*. (DE GRUYTER, 2013). doi:10.1515/9783110306729

72. NiGen. Nitrogen Gas Purity Grades for Different Industry Uses. (2021).

73. Navas, H. *et al.* Unveiling the Evolutions of Nanotube Diameter Distribution during the Growth of Single-Walled Carbon Nanotubes. *ACS Nano* **11**, 3081–3088 (2017).

74. Kanzow, H., Lenski, C. & Ding, A. Single-wall carbon nanotube diameter distributions calculated from experimental parameters. *Phys. Rev. B - Condens. Matter Mater. Phys.* **63**, 1254021–1254026 (2001).

75. Battie, Y., Jamon, D., En Naciri, A., Lauret, J. S. & Loiseau, A. Chirality distribution in single walled carbon nanotube films by spectroscopic ellipsometry. *Appl. Phys. Lett.* **102**, 1–5 (2013).

76. Blanch, A. J., Lenehan, C. E. & Quinton, J. S. Optimizing surfactant concentrations for dispersion of single-walled carbon nanotubes in aqueous solution. *J. Phys. Chem. B* **114**, 9805–9811 (2010).

77. Rastogi, R. *et al.* Comparative study of carbon nanotube dispersion using surfactants. *Journal of Colloid and Interface Science* **328**, 421–428 (2008).

78. Rosa, P. A. J. *et al.* Application of aqueous two-phase systems to antibody purification: A multi-stage approach. *J. Biotechnol.* **139**, 306–313 (2009).

79. Albertsson, P. Å. *Partition of Cell Particles and Macromolecules*. (John Wiley & Sons, 1986).

80. Benavides, J., Rito-Palomares, M. & Asenjo, J. A. Aqueous Two-Phase Systems. in *Comprehensive Biotechnology, Second Edition* **2**, 697–713 (2011).

81. Asenjo, J. A. & Andrews, B. A. Aqueous two-phase systems for protein separation: A perspective. *J. Chromatogr. A* **1218**, 8826–8835 (2011).

82. Vogg, S., Ulmer, N., Souquet, J., Broly, H. & Morbidelli, M. Experimental Evaluation of the Impact of Intrinsic Process Parameters on the Performance of a Continuous Chromatographic Polishing Unit (MCSGP). *Biotechnol. J.* **14**, 1–8 (2019).

83. Komatsu, N. & Wang, F. A comprehensive review on separation methods and techniques for single-walled

carbon nanotubes. *Materials (Basel).* **3**, 3818–3844 (2010).

84. Glyk, A., Scheper, T. & Beutel, S. PEG–salt aqueous two-phase systems: an attractive and versatile liquid–liquid extraction technology for the downstream processing of proteins and enzymes. *Appl. Microbiol. Biotechnol.* **99**, 6599–6616 (2015).

85. Sirkar, K. K. Point and Stage Efficiencies in Distillation. *Sep. Sci.* **11**, 303–315 (1976).